Grid-Connected Voltage Source Converter
— Control Principles and Wind Energy Applications

Jan Svensson

Technical Report No. 331

1998

Grid-Connected Voltage Source Converter
— Control Principles and Wind Energy Applications

by

Jan Svensson

Technical Report No. 331

Submitted to the School of Electrical and Computer Engineering
Chalmers University of Technology
in partial fulfilment of the requirements
for the degree of
Doctor of Philosophy

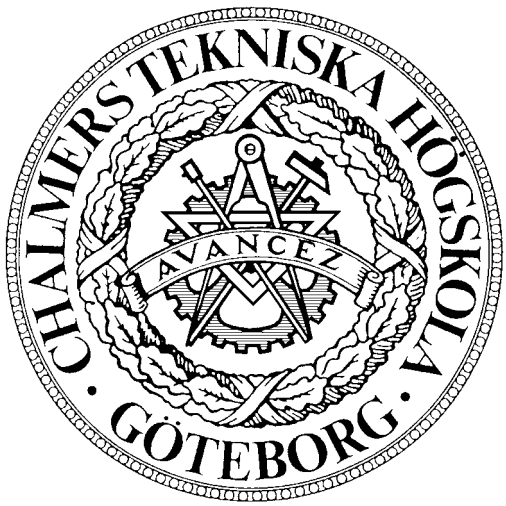

Department of Electric Power Engineering
Chalmers University of Technology
Göteborg, Sweden
Mars 1998

CHALMERS UNIVERSITY OF TECHNOLOGY
Department of Electric Power Engineering
S-412 96 Göteborg
ISBN: 91-7197-610-8
ISSN: 0346 - 718X
Chalmers Bibliotek, Reproservice
Göteborg, 1998

Abstract

The thesis focuses on a forced-commutated voltage source converter (VSC) connected to a grid in a wind energy application. The work consists of four parts. The first part addresses the type of electrical system which should be used in a wind turbine. The conclusion is to use variable-speed wind turbines, due to higher efficiency, lower noise and lower fatigue. If high power quality is demanded, a grid-connected VSC should be used instead of a grid-commutated thyristor inverter. By utilizing the high current control bandwidth of the VSC in a hybrid wind farm, consisting of wind turbines having different electrical systems, a cost-efficient solution is obtained. The VSC is used for reactive power compensation and active filtering, in addition to converting wind power. These additional features cause only a moderate increase in the VSC rating compared with only converting wind power.

In part two, an electrical system in a variable-speed wind turbine, in which the VSC uses the voltage angle control to track the reference voltage of the dc-link, is investigated. The proposed control method is based on a steady-state model of the system, which results in a low bandwidth but which is high enough to operate a wind turbine. To increase the bandwidth, the linear quadratic (LQ) control method has been introduced. Due to sensitivity to current harmonics, an extended Kalman filter has been added to the LQ-controller. Simulations show that the controller operates as expected.

A grid-connected VSC using a discrete vector current controller is investigated in the third part of the thesis. The influences of an incorrect controller tuning and grid voltage harmonics on current frequency responses at an operating point are investigated. The attenuation of low-frequency voltage harmonics decreases when their frequency increases. Furthermore, it is shown that the current controller handles parameter errors satisfactorily. It has been shown that frequency dependent losses in the grid filter affect current frequency responses at high frequencies. A compensation function has been introduced to compensate for non-ideal valves and non-ideal pulse width modulation. The function improves the small-signal current frequency response around an operating point. Also four different synchronization methods, which are adapted to digital controllers, have been investigated. A novel transformation angle detector based on a space vector filter has been introduced. The detector manages phase steps in the grid voltage, and the extended version of the detector also manages frequency changes in the grid better than the extended Kalman filtered detector, in spite of the smaller number of calculations.

The last part of the thesis deals with the current harmonics of a grid-connected VSC. By introducing a third-order LCL-filter as an alternative to an L-filter, current harmonics are decreased. Furthermore, reflections caused by high voltage derivatives are adressed.

Preface

The work presented in this thesis was carried out at the Department of Electric Power Engineering at Chalmers University of Technology. The financial support given by the Swedish National Board for Industrial and Technical Development (NUTEK), through the Wind Power Consortium, is gratefully acknowledged.

I would like to thank my supervisor, Dr. Ola Carlson, for believing in my ideas. Furthermore, many thanks to my industrial adviser Tommy Lejonberg for his support and encouraging guidance in the second half of the project. It is a great honor for me to thank my examiner Professor Jorma Luomi, who has guided me into the academic world.

In the second half of the project, I have worked together with Michael Lindgren who has been coauthor of some of the articles in the thesis. Two people working together in a group can work wonders.

Best regards to my daily sound-board, Dr. Torbjörn Thiringer, and to Kjell Siimon for keeping my computer up-to-date. Finally, I would like to thank the staff at the department.

List of Appended Papers

This thesis is based on the work contained in the following papers:

SECTION 1
Voltage Source Converters in Variable Speed Wind Turbines and Hybrid Wind Parks

1A O. Carlson, A. Grauers, J. Svensson, Å. Larsson, "A Comparison of Electrical Systems for Variable Speed Operation of Wind Turbines," *European Wind Energy Association Conference and Exhibition (EWEC'94)*, Thessaloniki, Greece, 10-14 October 1994, pp. 500-505.

1B J. Svensson, "Possibilities by using a Self-Commutated Voltage Source Inverter Connected to a Weak Grid in Wind Parks," *1996 European Union Wind Energy Conference and Exhibition*, Göteborg, Sweden, 20-24 May 1996, pp. 492-495.

1C J. Svensson, "The Rating of the Voltage Source Inverter in a Hybrid Wind Park with High Power Quality," *European Wind Energy Conference (EWEC'97)*, Dublin, Ireland, 6-9 October 1997, (in press).

SECTION 2
Voltage Angle Control of a Voltage Source Converter

2A J. Svensson, "Voltage Angle Control of a Voltage Source Inverter — Application to a Grid-Connected Wind Turbine," *6th European Conference on Power Electronics and Applications (EPE'95)*, Sevilla, Spain, 19-21 September 1995, Proceedings, Vol. 3, pp. 539-544.

2B J. Svensson, "Simulation of Power Angle Controlled Voltage Source Converter using a Linear Quadratic Method in a Wind Energy Application," *5th Workshop on Computers in Power Electronics, IEEE*, 11-14 August 1996, pp. 157-162.

SECTION 3
Vector Controlled Voltage Source Converter

3A J. Svensson, "Inclusion of Dead-Time and Parameter Variations in VSC Modelling for Predicting Responses of Grid Voltage Harmonics," *7th European Conference on Power Electronics and Applications (EPE'97)*, Trondheim, Norway, 8-10 September 1997, Proceedings, Vol. 3, pp. 216-221.

3B J. Svensson, "Synchronisation Methods for Grid Connected Voltage Source Converter," Submitted to IEE Proceedings Electric Power Applications.

3C J. Svensson, M. Lindgren, "Influence of Non-linearities on the Frequency Response of a Grid-Connected Vector-Controlled VSC," submitted to IEEE Transactions on Industrial Electronics.

SECTION 4
Connecting Fast Switching Voltage Source Converters to the Grid

4 M. Lindgren, J. Svensson, "Connecting Fast Switching Voltage-Source Converters to the Grid — Harmonic Distortion and its Reduction," *IEEE/Stockholm Power Tech Conference*, Stockholm, Sweden, June 18-22 1995, Proceedings, Vol. "Power Electronics," pp. 191-196.

Table of Contents

PART I

THE THESIS

1 Introduction

The utilization of wind energy is an area which is growing rapidly. In Europe, the installed wind power has increased by 36 % each year for 5 years, now. In northern Germany, wind turbine manufacture is the fastest growing industry. Furthermore, wind energy covers 7 % of Danish electricity consumption. Most countries in Europe have plans for increasing their share of energy produced by wind power. The increased share of wind power in the electric power system makes it necessary to have grid-friendly interfaces between the wind turbines and the grid in order to maintain power quality.

In addition, power electronics is undergoing a fast evolution, mainly due to two factors. The first factor is the development of fast semiconductor valves, which are capable of switching fast and handling high powers. The second factor is the control area, where the introduction of the computer as a real-time controller has made it possible to adapt advanced and complex control algorithms. These factors together make it possible to have cost-effective and grid-friendly converters connected to the grid.

The thesis focuses on a forced-commutated voltage source converter connected to a grid in a wind energy application. When the first part of the project started up, the objective was to determine the optimal electrical system for a wind turbine, in terms of efficiency, cost and performance. Another goal was to investigate the voltage angle control method and its suitability for controlling a grid-connected voltage source converter in a wind turbine system. A simple, low-cost analog controller was used for the implementation. In efforts to increase the bandwidth of the system, a linear quadratic control method was considered.

The objectives of the second part of the project were to investigate the performance of the vector current control method when parameter variations, delay times and grid voltage distortion affect the vector current controller. To reduce the non-linearities from the valves and from the blanking time, a valve compensation function was implemented in the controller. The transformation angle detector, which synchronizes the voltage source converter to the grid voltage is essential to the vector current controller. One aim was to investigate different synchronization methods which could be implemented in the control-computer. Furthermore, the presumed high current bandwidth of the vector current controller could make it possible to implement extra applications. A higher power quality for the whole hybrid wind park can result in a lower total cost for the park.

This report consists of two parts. The first part contains a short discussion of wind turbine concepts, electrical systems used in wind turbines, control principles of voltage source converters and modulation techniques. Furthermore, the contributions and comments of the included papers are presented and the conclusions are stated.

The second part of the report consists of nine papers which are divided into four sections. The first section is an introduction to wind power, wind turbines, different electrical systems and hybrid wind parks. The second section investigates a voltage source converter connected to a grid using a voltage angle controller. In the third section, the vector current controller of the grid connected voltage source converter is investigated. Furthermore, four synchronization methods adapted for digital implementation are presented. One of the presented methods is a novel transformation angle detector based

on a space vector filter. In the last section, the harmonics of the voltage source converter are investigated. Current harmonics attenuation at low and medium frequencies is compared for two grid filter types, the L-filter and the LCL-filter. Moreover, the influence of high voltage derivatives from fast switching valves is addressed.

2 Wind Turbine Configurations

The use of wind energy goes back far in history. Wind power plants have, for instance, been used as water pumps and as mills. One major difference between the earliest windmills and the new generation of wind turbines is that the mechanical transmission of power has been replaced by an electrical transmission. The oil crisis in the mid 1970s resulted in a new interest in wind energy. This attention has continued to grow as the demand for reduced polluting emissions has increased. The wind energy market today is small but growing rapidly.

2.1 Standard Fixed-speed Wind Turbine

The standard wind turbine plants of today use conventional horizontal-axis wind turbines. The turbine has two or three blades. In some designs, the blades can be pitched, to change the aerodynamic torque. The nacelle is placed on a high tower, in order to benefit from higher wind speeds high above ground. Furthermore, the low-speed turbine is connected to the generator via a gearbox, as shown in Fig. 1. The rotational speed of the generator is typically 1500 rpm and the turbine speed is 20 to 50 rpm. The induction machine is the most common generator type.

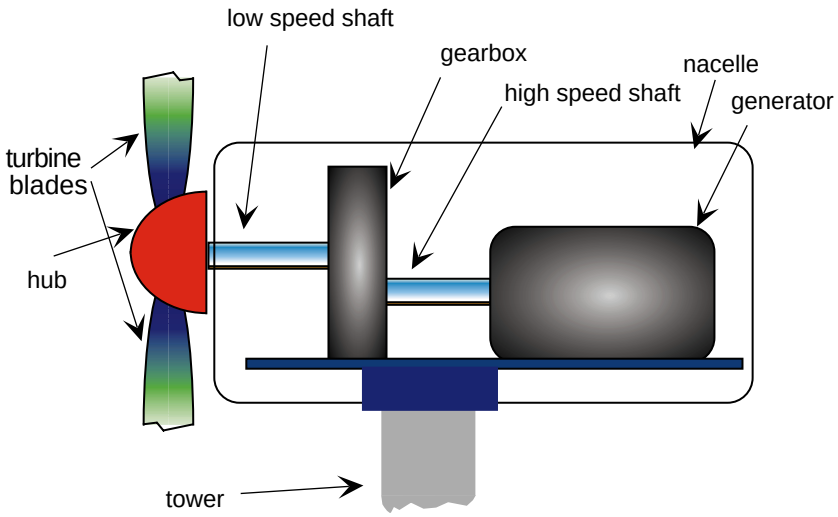

Figure 1: The parts of a wind turbine.

The kinetic power P_w of the air passing the swept turbine area A increases with the cube of the wind speed w, as

$$P_w = \frac{\rho A}{2} w^3 \tag{1}$$

where ρ is the density of air. At low wind speeds, the generated power is too low to be exploited. When the wind speed exceeds the cut-in wind speed, the wind turbine starts. The input power of the wind turbine must be reduced when the aerodynamic power becomes higher than the rated power of the wind turbine. Two common methods are used: The first method changes the pitch-angle of the blades. The second method is based on blades designed in such a way that they stall when wind speed exceeds a certain level. When wind speed reaches the cut-out speed, the wind turbine is shut down due to high

mechanical loads. The cut-out speed is approximately 25 m/s. In Fig. 2 wind power and wind turbine power are shown as a function of wind speed.

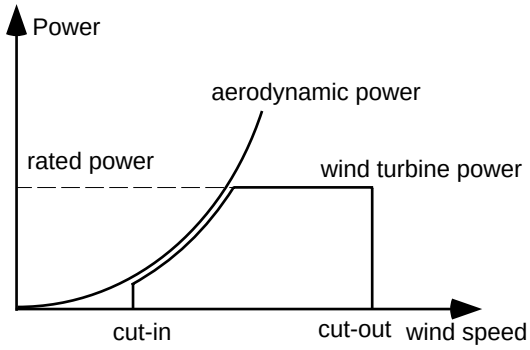

Figure 2: The ideal power curve of a wind turbine.

The probability density function of wind speed is usually described by a Weibull distribution [1]. Even if the wind turbine produces the rated power at the cut-out speed, the achieved energy capture is small at high wind speeds because the number of strong gale hours per year is few.

2.2 Variable-speed Wind Turbine

A wind turbine must run at a certain speed relative to the current wind-speed, defined by the optimal tip-speed ratio, in order to produce maximum power. For a fixed-speed concept, the efficiency will not be maximized. Losses depend on the exact design of the turbine and the wind variations at the site. An improvement of the single-speed turbine is the multiple-fixed-speed turbine (usually two speeds), provided by a generator with a changeable number of poles. An active pitch, which adjusts the pitch angle instantaneously to the wind speed, is an option to increase the energy capture. Unfortunately, the bandwidth of the active-pitch system is too small to utilize this advantage. A larger problem is wind power fluctuation at high wind speeds; the low bandwidth of the pitch control results in overloads. By introducing a variable-speed operation, it is possible to continuously adapt the rotational speed to the current wind speed, so that, ideally, the maximum obtainable power is continuously produced by the plant. Typically, this optimal mode is achieved for low to medium wind-speeds. The theoretical average efficiency of the electrical system can be increased by 5 % compared with a fixed-speed wind turbine [2]. If the plant is stall-regulated, the optimal turbine speed is proportional to the wind speed for wind speeds up to the rated speed. For higher wind speeds, turbine power is kept constant by means of a stall effect.

When using a variable-speed, stall-controlled wind turbine, the electrical system must be designed to manage a power overload. The maximum power from a stall-controlled wind turbine changes due to changes in the performance of the stall regulation. This increases the cost of the electrical system. When using both variable speed and pitch control, the electrical system can be designed to manage the rated power of the wind turbine.

3 Electrical Systems of Wind Turbines

The standard electrical system for a fixed-speed wind turbine is a squirrel-cage induction generator directly connected to a grid. To reduce the reactive power demand, a capacitor bank is installed to compensate for the no-load current of the generator. Furthermore, a thyristor-equipped, soft-starter is used to reduce the inrush current.

For variable-speed wind turbines, many different solutions of electrical systems are possible. In this report, only full-span, variable-speed systems are considered. The development of semiconductor components for use in the converters of the electrical system is progressing rapidly. The rated power of the valves increases, as a result, and the cost decreases. Furthermore, forced-commutated valves with shorter turn-on and turn-off times are introduced. In addition, the fast development of control computers has facilitated more advanced control algorithms.

A variable-speed electrical system has three main components. They are the generator, the rectifier and the inverter, shown in Fig. 3. The system can be split into two subsystems: inverter-grid and rectifier-generator. This helps when analysing one part of the system. Each sub-system has at least two different device alternatives.

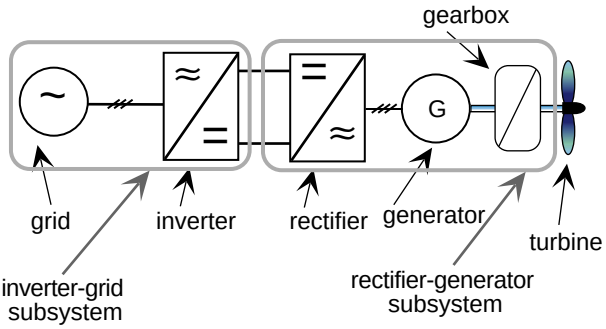

Figure 3: Overview of the electrical system for variable-speed system.

Two main types of generators are used: either the synchronous or the induction generator. The synchronous generator (SG) can use two methods of excitation: permanent magnets or field winding. A relatively new generator concept is the switched reluctance generator, which is cost-effective but, unfortunately, has a high torque ripple [3]. The common way is to use a field winding, because it has the advantage of controlling the three-phase voltage level; if the terminal voltage level is fixed, the produced reactive power can be controlled. In recent years, the costs of high performance permanent magnets have dropped and permanent magnet machines have become an interesting alternative compared with traditional machine types. When using permanent magnets, the electrical losses of the machine become smaller, which is positive. However, the voltage level is proportional to the speed. Due to the produced reactive power, the synchronous generator can be connected to a load-commutated rectifier, i.e., a diode rectifier or a thyristor rectifier. The voltage source converter (VSC), however, can be used as a rectifier. Observe that the controller of the VSC requires a minimum dc-link voltage relation to the generator voltage in order to operate properly.

The induction generator (IG) requires reactive power to operate. Consequently, the IG often uses the VSC, which produces reactive power. Another possibility is to use a diode

rectifier or a thyristor rectifier together with capacitors, which produce the required reactive power. Unfortunately, reactive power changes with speed and if the capacitance value is not correct, the performance of the system will be low.

The inverter of the system is connected to the grid. Here, the grid-commutated inverter, also called the thyristor inverter, and the VSC can be used. The VSC requires a minimum dc-link voltage in order to operate, and in some cases a step-up converter (DC/DC) must be introduced to increase the voltage level for the VSC. The VSC can act both as a rectifier and as an inverter: the power direction is set by the controller.

To give an overview of the different electrical system combinations, Fig. 4 has been introduced. Observe that the combinations are primarily for systems which use a gearbox between the generator and the turbine.

A rather new concept is to use a directly-driven permanent magnet generator, which is directly connected to the turbine without a gearbox. Depending on the optimization of the rectifier-generator subsystem, the rated power can be increased by 50 % when using a VSC, instead of a diode rectifier or a thyristor inverter [4].

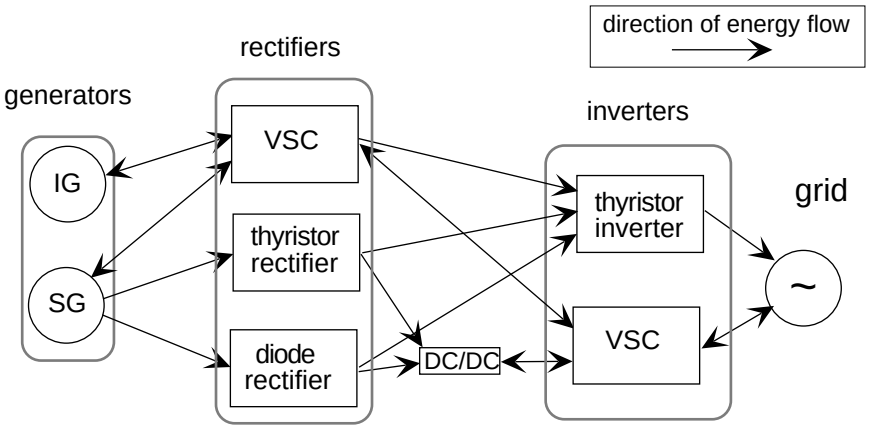

Figure 4: Diagram of different electrical system alternatives for variable speed.

4 Locations and Power Quality of Wind Turbines

Wind turbines are often located on coastal shores in rural areas, due to high wind speeds and sparse population. The grids connecting these areas are often weak, i.e., have a non-negligible, short-circuit impedance. This results in power quality problems when connecting wind turbines, which are not adapted to weak grids.

The most common electrical system of commercial wind turbines is the induction generator directly connected to the grid. A major drawback is that the reactive power flow and, thus, the grid voltage level cannot be controlled. Another drawback associated with a fixed-speed system is that the blade rotation causes power variations and, thereby, voltage fluctuations of a frequency of 1 to 2 Hz in the grid [5]. This fluctuation problem is not solved by using several turbines; on the contrary, if several identical wind turbines are installed in a wind park, the rotors can synchronize with each other and the power fluctuations will be superimposed in phase [6]. Furthermore, induction generator dynamics has resonance peaks around 10 Hz [7], where the sensitivity to flicker is high.

For the variable speed system, the inverter connected to the grid is a thyristor inverter or a VSC. Depending on the generator-rectifier sub-system, the thyristor inverter can be controlled in different ways. If a diode or thyristor rectifier and a synchronous generator are used, the dc-link voltage level will be proportional to the turbine speed, resulting in a reactive power transfer from the grid, and the reactive power will change with the active power delivered from the wind turbine, due to the varying firing angle of the thyristors. Another drawback of using a thyristor inverter is low-frequency current harmonics. If a thyristor inverter is connected to a weak grid, current harmonics will cause low-frequency voltage distortion from about 200 Hz to 1 kHz. Current harmonics can be reduced significantly by using tuned passive filters. Unfortunately, the filter size becomes large when removing low-frequency harmonics.

An alternative to a thyristor inverter is the VSC. If nothing else is mentioned, the valves of the voltage source converter are of the Insulated Gate Bipolar Transistor (IGBT) type. A VSC connected to the grid has several advantages in comparison with a thyristor inverter: The reactive power can be chosen freely, often set to zero to obtain the unity power factor. Grid currents become sinusoidal with no low-frequency harmonics, at least if a proper controller is used [8]. By using advanced control techniques, the power quality of the grid can be improved. Unfortunately a VSC has a few drawbacks: The efficiency is slightly lower in comparison with a thyristor inverter. Rated power has been a limit, but the fast development of valves has improved rated power. Also the voltage level has increased resulting in lower losses in other parts of the variable-speed electrical system.

The ability to control the turn-on and the turn-off characteristics of the IGBT has made it possible to parallel [9] and to series [10] connect several IGBT-valves, and, thus, increase the rated power of the converter. When comparing the cost of a thyristor inverter with a VSC, the thyristor inverter has a lower price, because it is a mature product and it has lower losses resulting in less cooling material. But when all the equipment around the inverters is included, the total system cost difference is levelled out.

In energy project plans for the future, it is understood that alternative energy is to be increased; the best way to increase the energy production from wind energy is to build large wind farms. To gain acceptance from the population, wind farms have been proposed to be installed offshore. This can lead to new solutions, such as high voltage direct current transmission of energy from the wind farm to a grid ashore.

5 Grid-connected VSC

The main purpose of this section is to introduce the reader to different aspects of a VSC connected to a grid. The main circuit configuration of the VSC is presented so the variables and their symbols can be defined and will be used henceforth. Furthermore, different types of grid filters and modulation techniques will be presented. Two control principles will be introduced, the voltage angle control and the vector current control principle. Finally, the modelling of the system will be described.

5.1 Main Circuit of VSC

A scheme of the main circuit of the VSC is shown in Fig. 5. The valves are of the IGBT-type. The VSC is connected to a symmetric three-phase load, which has the impedance $R + \mathrm{j}\omega L$ and the emfs $e_1(t)$, $e_2(t)$ and $e_3(t)$. The neutral point of the star-connected load has the potential $v_0(t)$, due to a floating ground. The phase potentials of the VSC are denoted as $v_1(t)$, $v_2(t)$ and $v_3(t)$. The phase voltages of the VSC are denoted as $u_1(t)$, $u_2(t)$ and $u_3(t)$. The current flowing from the dc-link to the converter is denoted as $i_v(t)$, the dc-link current is denoted as $i_{dc}(t)$ and the dc-link voltage across the dc-link capacitor is denoted as $u_{dc}(t)$.

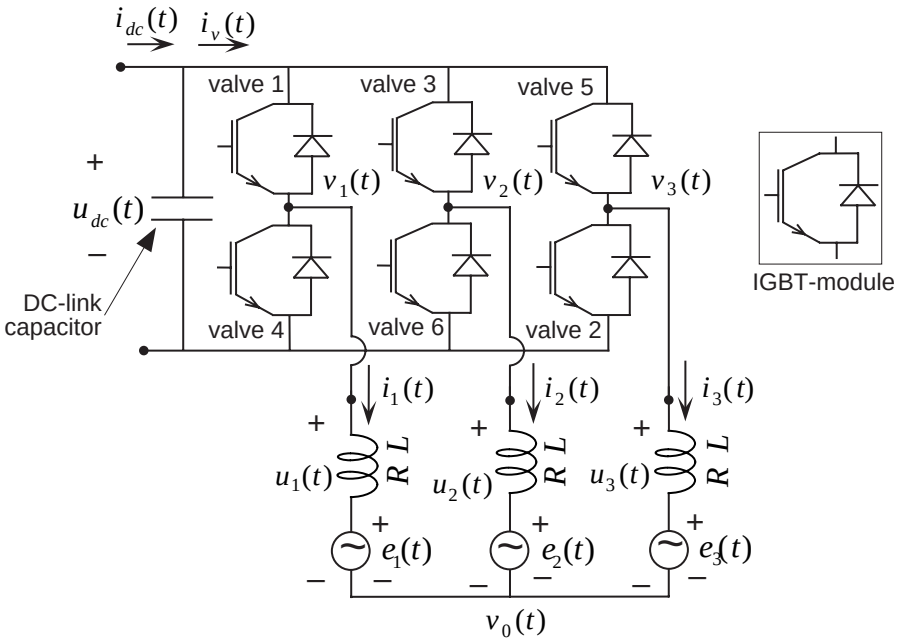

Figure 5: The main circuit of the VSC.

5.2 Grid Filters

When connecting a VSC to a grid, an inductor must be mounted between the VSC, which is operating as a stiff voltage source, and the grid, which also operates as a stiff voltage source [11]. The simplest and most common grid filter is the L-filter, which has three series connected inductors, one in each phase.

The LC-filter has the same series inductors, one in each phase, as the L-filter. In addition, the LC-filter has three parallel coupled capacitors. This filter type has often been

investigated for systems which are used in autonomous grids as an uninterruptible power supply and in most investigations, the load consists of resistors, one in each phase [12]. When connecting a system with the LC-filter to a public grid, problems can occur due to resonances. The resonance frequency depends on the capacitor value of the filter and the inductance value of the grid, which varies over time. It is difficult to reduce the resonance, because resonance frequency changes with grid inductance and, in addition, the harmonic distortion spectrum of the grid changes with time.

The resonance problem can be reduced by using an LCL-filter [13]. The main advantages of using an LCL-filter are low grid current distortion and reactive power production. The resonance frequency can be determined almost independently of the grid configuration. The disadvantage is a more complicated system to control. The L-filter attenuation is a 20 dB/decade and the LCL-filter attenuation is a 60 dB/decade for frequencies over the resonance frequency of the filter. To improve the attenuation of the system when using the L-filter, a tuned shunt filter can be introduced which is tuned to the switching frequency of the VSC [14].

5.3 Modulation

One of the advantages of the VSC over the grid-commutated converter is low harmonic distortion at low frequencies, resulting in sinusoidal grid currents. This is due to the fact that by switching the valves properly only high-frequency harmonics remain. The research field of modulation techniques has been focused on reducing the number of switching instances per cycle while still obtaining low distortion due to the current ripple caused by the switching instances [15]. The simplest modulation technique is the six-pulse modulation, where each phase switches twice per cycle. The fundamental voltage amplitude becomes high but harmonics occur at low frequencies: 5th, 7th, 11th, 13th and so on. By introducing more switching instants, the current ripple will be reduced as well as the fundamental voltage amplitude. Depending on the rated power of the VSC, the switching frequency is reduced when the rated power is increased. For small adjustable-speed drive systems, the switching frequency can be as high as 20 kHz. For converters used in high power applications, the switching frequency is reduced down to approximately 1 kHz.

The most common modulation methods can be divided into two groups: either current control or voltage control. The current control method forces the valves to switch only when it is necessary to keep on tracking the reference of the current. This control principle is often called the current hysteresis control principle [16]. The second modulation type, voltage control, has as a common characteristic subcycles of constant time duration, a subcycle being defined as the total duration during which an active inverter leg assumes two consecutive switching states of opposite voltage polarity. Operation at subcycles of constant duration is reflected in the harmonic spectrum of the phase voltage by two dominating salient sidebands, centered around the switching frequency, and by additional frequency bands around integral multiples of the carrier [17]. The modulation type can be divided into two parts: a suboscillated pulse width modulation (PWM) and a space vector modulation, denoted by SVM. The latter modulation method is often used when microcontrollers are involved in the system. The suboscillation method is a classical modulation technique and employs individual

modulators in each of the three phases. It is popular due to its simple implementation and is preferable when an analog system is used.

The input to a space vector modulator is the voltage reference vector in the αβ-frame, explained in Appendix A. The sampled input vector is then approximated by a time sequence of three well-defined switching state vectors. The ordinary three-phase voltage source converter has 8 switching vectors, also displayed in Appendix A. The modulation algorithm ensures that the time average of the switching state vectors over a sampling interval is equal to the reference vector [18]. Compared with the sub-oscillating PWM method, the SVM method can be modified to reduce the number of valve switchings during each sample interval or to change the switching valve pattern. The SVM has the following advantages: The reference voltage vector can be decomposed in a number of ways and the selected voltage vectors can be applied to different sequences. By controlling the SVM in a smart way, it is possible to reduce the switching frequency while still obtaining the same sample frequency as in the sub-oscillated PWM. This is an advantage when the rated power of the VSC is increased.

If the mid-point of the star-connected load is floating, a zero-sequence component can be added to all of the three phase reference voltages to extend the output voltage range of the converter by 15.5 % without losing the linearity from the reference voltage to the output voltage [19]. A triplen deadband PWM can be introduced to reduce the effective switching frequency, which reduces switching losses up to 33 % [20]. In this method, one leg of the converter is clamped for a certain period of time in each cycle, hence resulting in a deadband region in which no switching will occur.

5.4 Control of the VSC Connected to the Grid

In this report, two control principles are investigated for a VSC connected to a grid. They are the voltage angle control and the vector current control. Both controllers use the rotating *dq*-coordinate system, explained in Appendix A. Furthermore, only the L-filter is considered for use.

The simplified circuit of a grid-connected VSC is shown in Fig. 6. The phase voltages of the VSC are modelled as three voltage sources denoted as $u_1(t)$, $u_2(t)$ and $u_3(t)$. The equivalent series inductance and resistance of the L-filter are denoted as L_S and R_S, respectively.

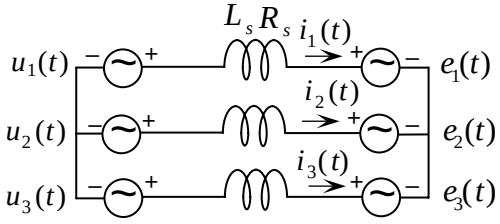

Figure 6: Schematic circuit of a grid-connected VSC, where the focus is on the L-filter.

The Kirchhoff voltage law can be applied to the circuit in Fig. 6. The equation becomes

$$\underline{u}^{(\alpha\beta)}(t) - R_s \underline{i}^{(\alpha\beta)}(t) - L_s \frac{d}{dt}\underline{i}^{(\alpha\beta)}(t) - \underline{e}^{(\alpha\beta)}(t) = 0 \qquad (2)$$

In the *dq*-coordinate system, the equation becomes

$$\underline{u}^{(dq)}(t) - R_s \underline{i}^{(dq)}(t) - L_s \frac{d}{dt}\underline{i}^{(dq)}(t) - \mathrm{j}\omega_g L_s \underline{i}^{(dq)}(t) - \underline{e}^{(dq)}(t) = 0 \quad (3)$$

where the grid angular frequency is denoted as ω_g.

5.4.1 The Voltage Angle Controller

The voltage angle controller, also called the power angle controller, is a controller based on a system model in steady-state. By setting the derivative term in Eq. (3) to zero, the steady state expression becomes

$$\underline{u}^{(dq)}(t) - \underline{e}^{(dq)}(t) = \left(R_s + \mathrm{j}\omega_g L_s\right)\underline{i}^{(dq)}(t) \quad (4)$$

By controlling the phase displacement angle between the voltage vector of the VSC and the voltage vector of the grid and by controlling the magnitude of the voltage vector of the VSC, the active and reactive power can be controlled. The phase displacement angle and the relative voltage are denoted as $\theta(t)$ and $u_x(t)$, respectively. The relative voltage is used to control the magnitude of the voltage vector of the VSC and is defined as

$$u_x(t) = \frac{\left|\underline{u}_{(1)}(t)\right|}{\left|\underline{e}(t)\right|} \quad (5)$$

where $\left|\underline{u}_{(1)}(t)\right|$ is the magnitude of the fundamental voltage vector of the VSC. In Fig. 7, the grid and VSC voltage vectors are shown in the *dq*-coordinate system. To simplify the scheme, the resistance of the grid filter coil is set to zero. Furthermore, the phase displacement angle has been scaled up, to make it easier to understand the scheme. As shown in Fig.7, the current vector is perpendicular to the difference between the converter voltage vector and the grid voltage vector.

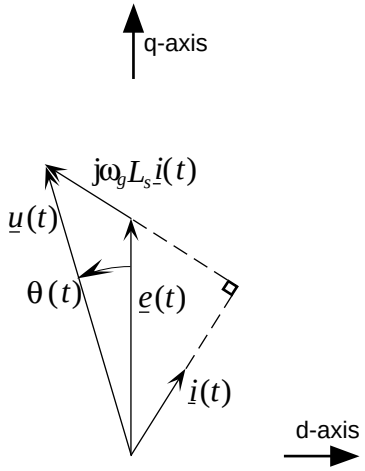

Figure 7: The principal scheme of voltage angle control.

To simplify the equations, the phase-to-phase voltage fundamental amplitudes of the VSC and the grid are denoted as U and E, respectively. If the grid and the VSC voltages are supposed to be distortion free and symmetric, the voltage vectors can be defined as

$$\underline{u}_{(1)}(t) = Ue^{\mathrm{j}\left(\theta(t)+\frac{\pi}{2}\right)} \quad (6)$$

$$\underline{e}(t) = Ee^{\mathrm{j}\frac{\pi}{2}} \quad (7)$$

The apparent power from the VSC to the grid is

$$\underline{s}(t) = \underline{u}_{(1)}(t)\bar{\underline{i}}(t) = \left(u_{d(1)}(t) + \mathrm{j}u_{q(1)}(t)\right)\left(i_d(t) - \mathrm{j}i_q(t)\right) \tag{8}$$

where the complexconjugate is denoted by a bar. By using Eqs.(4),(6),(7) and (8), the active power and the reactive power can be written as

$$P = \frac{UE}{\omega_g L_s}\theta \tag{9}$$

$$Q = \frac{E(E-U)}{\omega_g L_s} \tag{10}$$

where the resistance of the L-filter is neglected and the phase displacement angle is so small that the sine of the angle is approximately equal to the angle and the cosine of the angle is approximately equal to one. The active power is proportional to the phase displacement angle and the reactive power is proportional to the difference between the voltage amplitudes of the VSC and the grid. Investigated applications of converters using the voltage angle control are, for instance, high-voltage direct current (HVDC) converters [21,22] and static VAr compensators (SVCs) [23].

When using the voltage angle control of the VSC in a wind turbine application, the VSC connected to the grid is set to control the voltage level of the dc-link independent of the operating point of the generator-rectifier sub-system. The principle of the control scheme is shown in Fig. 8. This control has been implemented in a laboratory system [24]. The voltage vector angle $\theta_g(t)$ of the grid is obtained from an analog phase-locked loop (PLL) connected to one of the phase voltages of the grid. The amplitude of the grid voltage is obtained by low-pass (LP) filtering the rectified grid voltages through a three-phase diode rectifier. The goal of the dc-link voltage controller is to track the reference dc-link voltage $u_{dc}^{*}(t)$. The dc-link voltage is controlled by using a PI-controller, the input of which is the dc-link voltage error and the output is the phase displacement angle $\theta(t)$. The relative voltage $u_x(t)$ is determined by the reactive power controller, which has the reactive power reference $Q^{*}(t)$ and the grid voltage amplitude as inputs. The inputs to the PWM-unit are: The total voltage vector angle of the VSC, which is the sum of the phase displacement angle $\theta(t)$ and the grid voltage vector angle $\theta_g(t)$; the dc-link voltage $u_{dc}(t)$ and the relative voltage $u_x(t)$.

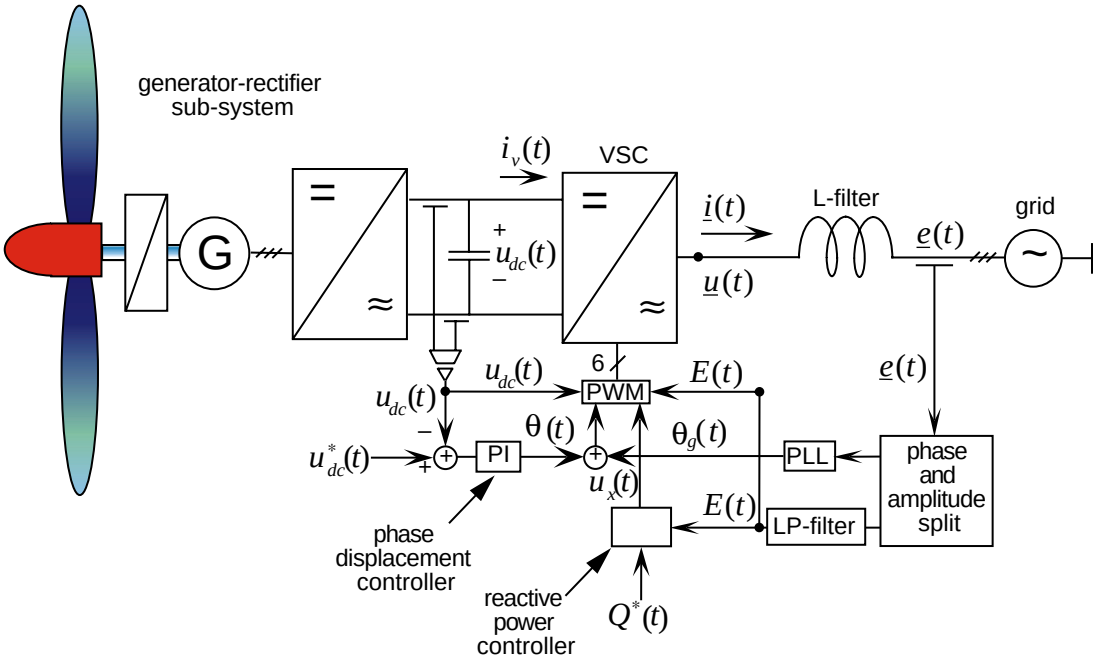

Figure 8: The principal control scheme of the voltage angle control in a variable-speed wind turbine application.

The voltage angle control is simple to implement in an analog controller or a micro-controller. However, the bandwidth of the system is low, since the controller is based on a steady-state model. The bandwidth required for controlling the wind turbine is low due to the large inertia of the turbine, which acts as an LP-filter. Furthermore, the power above 1 Hz in the wind power spectrum is small. However, it is important that the control system can damp drive train resonances actively. To do that, the bandwidth of the system must be around 10 Hz. Often the reactive power demand is set to zero to obtain a high power factor. But, if the grid is weak, the reactive power can be used to control the voltage level of the grid.

When using the voltage angle control principle, it is easy to implement an efficient PWM-generator, where the pulse pattern has been calculated off-line and stored in an EPROM. This is important if the rated power is high and the switching losses must be low. As described above, the voltage angle control principle is simple and a few simple control blocks are needed. Furthermore, grid phase currents must not to be measured to perform the control principle. The controller implementation can be made inexpensive due to the low bandwidth requirement. This indicates that the control system should be used in plants where the relative controller cost is high, i.e., low-rated power plants.

5.4.2 The Vector Current Controller

The basic principle of the vector current controlled grid-connected VSC is to control the instantaneous active and reactive grid currents independently of each other and with a high bandwidth. In this thesis, the vector current controller is implemented in a computer, the control functions are discrete and the inputs and outputs to the controller are sampled at a constant sample frequency. In the laboratory system, the sample frequency is equal to the switching frequency.

The currents and the voltages of the grid are transformed to the rotating *dq*-coordinate system. By this operation, the fundamental current and voltage components become dc-

quantities and PI-controllers can be used to reduce steady-state errors. The components of the reference voltage out from the regulator are transformed back to three-phase quantities and used as inputs to the PWM function. In Fig. 9, the principal block diagram of the system and the controller are shown.

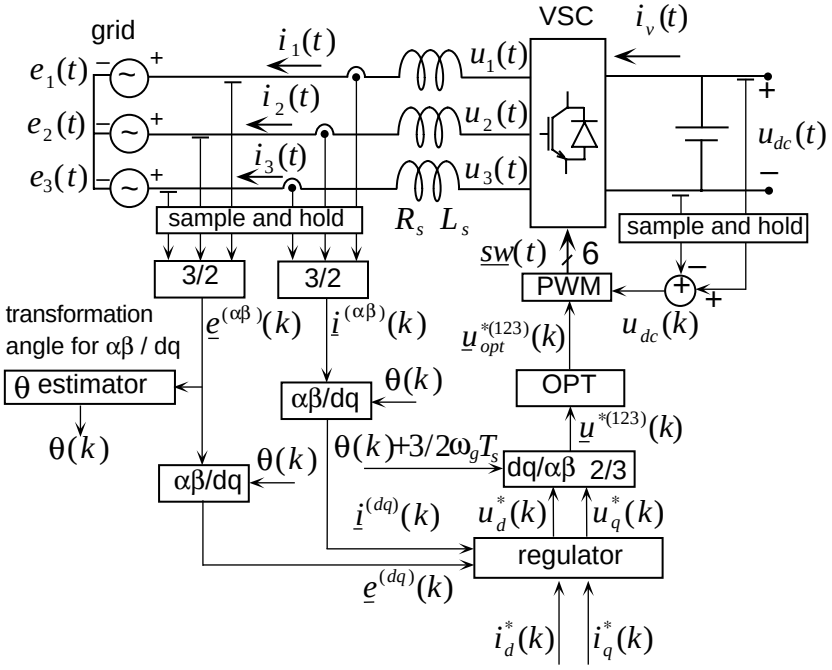

Figure 9: Principal block diagram of vector current controller.

To obtain a high bandwidth, the total system must be well-known including the influences of non-ideal components, the grid filters and the filters in the signal paths. The following items are important:

- Correct sampling instances. If the phase currents are sampled exactly at the top and bottom of the triangular wave used in the sub-oscillated PWM, the ripple of the current is zero. An error in the measured current occurs if the sample instance is delayed a few microseconds, then the error will increase if the current ripple increases.

- Overmodulation. If high gains are used, the reference voltage vector from the vector current controller will be large when trying to realize demanded current steps, and the PWM cannot realize the demanded voltage vector and an overmodulation occurs. This results in uncontrolled phase currents.

- One-sample delay in the current controller. If a discrete sampled control system is used, a delay time of one sample will occur due to the calculation time of the control-computer. If a high bandwidth is required, for instance dead-beat, high gains must be used in the current controller and the influence of the delay time must be compensated in the controller to eliminate oscillations. When not compensating for the delay time, the gain must be decreased [25].

- Valve non-linearities. In a real converter, the on-state voltage drop and the resistance of the valves of the converter influence the system negatively, such as performance of the current control and low-frequency current harmonics. A compensation function can be implemented if the non-linearities are known [26].

- Non-ideal PWM. To protect from short circuits in the phase-legs, a blanking time is introduced. The blanking time is the time between the turn-off of a valve in the phase-leg and the turn-on of the second valve in the phase-leg. This blanking time reduces the mean voltage under the sample period [26].

- Grid voltage distortion. Grid voltage distortion affects the current controller. There is a coupling between the grid voltage harmonics and current out from the converter.

- Synchronization of the transformation angle to the grid voltage. It is important that the synchronization operates effectively even if the grid has a poor power quality.

The obtained high bandwidth can be used in high-performance applications such as active filtering [27]. A cost effective solution can be obtained by reducing the component costs such as the dc-side capacitor and the grid filter; it is still possible to achieve a high power quality for applications such as rectifiers in drive systems or inverters connected to the grid in wind turbine plants.

5.5 Modelling of Control-circuit and VSC Connected to a Grid

When analysing the VSC system, a model must be created. The model should include the grid, the grid filter, the dc-link and the VSC and its controller. Two model objects are in focus: modelling the system to obtain a simulation model and creating a small-signal model of the system.

To determine proper control gains for the control loop design of the VSC system, a small-signal analysis is performed around an operating point. The small-signal model is obtained by linearizing the large-signal model of the system, which is often linear except for the discontinuity due to the pulse width modulated valves. By assuming the pulse width modulated voltage of the converter to be a constant voltage during the sample period, a linear state equation can be formed, where the states are piecewise constant under the sample period. This assumption is valid when changes in the reference voltage are slow in comparison with the switching intervals of the converter. Two common averaging methods are: the state-space averaging [28,29] and the average switch model [30].

For dc-dc converters, model accuracy can be increased by using the transient behavioural model (TBM). In this model, the first harmonic tone is added to the mean voltage during the sample period, resulting in increased performance [30]. Often, the VSC system is modelled on the rotating *dq*-coordinate system and the coordinate transformations and the valves are assumed to be ideal. For this situation, the space vector averaging method should be used, because the correct mean voltage vector is obtained during the sample period. The average switch model averages each phase individually, and if the voltages are wanted in the *dq*-coordinate system, coordinate transformations must be performed. If the ratio between the sample frequency and the grid frequency is small, the coordinate transformation together with the pulse width modulated signal can introduce errors [31].

Transfer functions of the Laplace-transformed system work well for single-input single-output (SISO) systems. But if multiple-input multiple-output (MIMO) systems are considered, the transfer function matrices become awkward to use. Furthermore, if the analysed system has time delays, which are modelled as $\exp(-sT)$, the system must be

linearized by using, e.g., the Padé approximation. Unfortunately, the polynomial degree will increase significantly. For VSC systems using discrete controllers, the discrete state equation is preferable and an one-sample delayed variable results in only one more variable in the state vector. To obtain the discrete closed-loop state equation, the grid voltage and the L-filter must be discretized. A major advantage of using discrete models in comparison with continuous models, including the switching instances, is the reduced simulation time.

6 Contributions, Comments, Conclusions and Future Research

The field of power electronics has been growing rapidly since the evolution of semiconductors. Computers and semiconductor valves increase their performance at high speed. As a result of this development, the high-performance devices of yesterday have become today's mediocre devices and, of course, published articles have also become out-of-date.

The outline of this chapter is as follows. In Section 6.1, the contributions and comments of the included papers are given. In Section 6.2, the author's conclusions are stated. Lastly, suggestions for future research are given.

6.1 Contributions and Comments of Included Papers

Paper 1A

Paper 1A acts as an introduction and also gives an overview of different electrical systems for variable-speed wind turbines. The proposed electrical system to be used in a variable-speed wind turbine consists of a synchronous generator, a diode rectifier and a grid-connected thyristor inverter, if the grid is strong. If the grid is weak, an IGBT chopper together with a forced-commutated voltage source converter is recommended, instead of the thyristor inverter. The background material about losses and converter prices originates from a study made in 1993. Due to the fast development of components and price changes for the devices, the cost results given in the paper are not valid any more. The losses in the grid filter are roughly estimated. New types of slowly-rotating permanent-magnet generators have been introduced after the publication of the paper; they result in a system without a gearbox and are of great interest today. If the new type of generator is used, a forced-commutated rectifier should be used to increase the efficiency and the rated power of the system, and the proposed IGBT chopper can be terminated.

Paper 1B

Paper 1B investigates a hybrid wind park, which is connected to a weak grid. The amplitude of the grid voltage at the point of common connection is focussed on. A grid-connected voltage source converter injects reactive power into the grid and affects the voltage level. The size of the voltage source converter for different electrical system combinations is analysed. It turns out that the increase in the rated power of the voltage source converter, when both delivering active power from the wind turbine and injecting reactive power to the grid, is moderate in comparison with only delivering active power. The results depend strongly on the short-circuit impedance ratio and the short-circuit ratio of the grid. In the paper, all converters and their control systems are assumed to be ideal.

Paper 1C

Paper 1C is an extension of the work presented in Paper 1B. The increase in the rated size of the voltage source converter is investigated for different combinations of electrical systems in the hybrid wind park. Furthermore, the effect of cancelling reactive power as well as harmonic currents from the hybrid wind park on the rated size of the voltage source converter is presented. The grid is assumed to have an infinite short-circuit power

and the voltage source converter together with its control system is supposed to operate ideally. Only harmonics up to the 13th order are considered, which is partially due to the moderate sampling frequency of the inverter. When using the voltage source converter simultaneously as an active power transmitter, a reactive power compensator and as a current harmonic canceller, the switching frequency should be moderate to keep down the losses in the converter. This results in a low current bandwidth and also restricts the highest frequency of the harmonics which can be cancelled. It turns out that the rating of the voltage source converter only needs to be increased moderately to fulfil the requirement for high power quality at the point of common connection.

Paper 2A

Paper 2A introduces an electrical system in a variable-speed wind turbine, in which the voltage source converter uses the voltage angle control principle to track the reference voltage of the dc-link independently of the delivered power from the generator-rectifier subsystem. An analog controller is used and, in the frequency analysis, the dc-link voltage fluctuation is neglected when calculating the current in the dc-link. The result of the investigation is that a voltage angle control can be used in a wind power application. Furthermore, the bandwidth of the inverter system is around 20 to 30 Hz depending on the parameter values of the system.

Paper 2B

Paper 2B introduces the linear quadratic (LQ) control method into the voltage angle controlled voltage source converter in a wind energy application. The LQ-control method is used to increase the bandwidth of the voltage angle controlled converter system; simulations show that the control method operates as expected. An analog implementation of the LQ-controller is used, since the paper is a continuation of Paper 2A, in which an analog controller was used. The system is non-linear and to get a high-performance controller, gain scheduling is used. The phase displacement angle is used to determine which gain should be used. One disadvantage of using the LQ-controller is the low attenuation of noise at frequencies near the model excitation frequencies. Therefore, an extended Kalman estimator was introduced to decrease the influence of current harmonics near the switching frequency. If a discrete LQ-controller had been used instead of the analog one, and if a proper sampling of the variables had been done, the performance of the system would probably have been improved.

Paper 3A

In Paper 3A, a grid-connected voltage source converter using a discrete vector current controller is investigated. A discrete state equation model of the grid-connected voltage source converter and its controller is derived both for a "fast computer" and for a one-sample delayed controller. The used controller inductance and resistance parameters of the grid filter inductor are changed to simulate an incorrect controller tuning. The mistuned controller is used in the model of the system for predicting responses of grid voltage harmonics. It is assumed that the sampling of the system variables, as well as the valves and the pulse width modulation, are ideal. The delay time of one sample in the discrete controller, due to the calculation time of the computer, results in a higher cross-coupling gain from the reference *d*- and *q*-currents to the *q*- and *d*-currents. Moreover the phase lag becomes larger. The delay time results in a coupling between grid voltage harmonics and

the three-phase currents of the converter, and the gain increases with frequency. The investigated errors in the controller parameters show that the vector current controller can handle inductance variations of ± 25 % and resistance variations of ± 50 %. To increase reference current tracking capacity, a modified delay time compensator, based on the Smith predictor, could be used instead of the one presented in the paper, which cannot handle overmodulations properly.

Paper 3B

In Paper 3B different synchronization methods for grid-connected voltage source converters are proposed. The methods are adapted to be used in digital controllers. A novel synchronization method based on a space vector filter (SVF), which properly handles phase jumps in grid voltage, is presented. In addition, an extended variant of the SVF is presented; this variant handles both phase jumps in grid voltage and grid frequency changes. This method has an even higher performance than the extended Kalman filter method, in spite of the smaller number of calculations that must be performed. In the paper, the three-phase grid voltage is assumed to be symmetric.

Paper 3C

Paper 3C extends the work of Paper 3A to involve experimental results of a vector current controlled VSC connected to the grid. The focus is on the frequency response from the reference current to the current in the *dq*-frame at an operating point. The grid filter inductor influences the current controller due to high losses when the frequency is increased. A valve compensation function is introduced to reduce the influence of the non-linearites of the valves and the blanking time of the pulse width modulation. In this paper, the influence of the valve compensation function and the integration term in the current controller are analysed in a small-signal scheme. The integration term does not influence the small-signal performance. However, the valve compensation function improves the performance of the current controller. The influences of the non-perfect sampling due to delays, the accuracy in the measurements and grid voltage harmonics are not considered when comparing the measurement results with the analytical ones.

Paper 4

One disadvantage of voltage source converters is generated voltage harmonics due to the valve switching of the converter. When using the sub-oscillated pulse width modulation, the harmonics occur around the switching frequency and multiples of it. The voltage harmonics from the converter result in grid current harmonics depending on the grid filter. Paper 4 focuses on low- and medium-frequency harmonics and in harmonic distortion above 100 kHz. The L-filter is compared with the third-order LCL-filter; the outcome is that the LCL-filter is proposed due to the better attenuation of low- and medium-frequency current harmonics. The fast-switched valves result in high voltage derivatives. This produces insulation stresses in the transformer or the grid filter connected to the converter. If long cables are used, the insulation stresses are further increased due to reflections. In the experiments, large reflections occurred at a cable length of 20 meters.

6.2 Conclusions

In the thesis, different types of electrical system configurations for variable-speed wind turbines have been investigated. Furthermore, different control principles used on the voltage source converter connected to a three-phase grid have been focused on.

The electrical system which is recommended consists of a voltage source converter connected to the grid if high power quality is needed. The alternative is a thyristor inverter. The directly-driven permanent magnet generator with a voltage source converter used as a rectifier has become a promising alternative to the ordinary synchronous generator and the diode rectifier. The simple and low-cost voltage angle control method has been shown to manage a wind turbine application. The extended version of the voltage angle control, which uses a linear quadratic controller, has a higher performance and operates as expected.

The vector current controlled voltage source converter has a high bandwidth in comparison with the voltage angle control method. The controller handles parameter variations well. The valve compensation function decreases the current error in steady-state, and frequency responses show that the small-signal performance increases. The L-filter inductors applied, decrease the performance at high frequencies. A novel synchronization method based on a space vector filter handles both phase jumps in the grid and grid frequency changes.

To increase the power quality in a hybrid wind park, the voltage source inverter is proposed to act both as a reactive power compensator and as an active filter, at the same time delivering active power into the grid. It is shown that the rated power of the voltage source converter increases moderately in comparison with delivering only active power.

6.3 Future Research

The performance of control computers will continue to grow. This emphasizes the need for implementing better control functions and models, while still obtaining real-time control. Moreover, the performance of valves will increase continuously. A large step will be taken when transistor valves using silicon-carbide become available on the market. The performance of converters will increase, and new applications for power electronic devices will be introduced.

A proper continuation of this work is to apply an efficient control algorithm to restrain the influence of poor power quality. In other words, it should be possible to design a controller to suppress low-frequency voltage harmonics, swells, dips, unbalance as well as phase jumps due to short-circuits in the surroundings.

When the rated power of the converter increases, the short-circuit power ratio between the short-circuit power of the grid and the rated power of the converter connected to the grid will decrease. If a high performance is to be obtained, the shrinking short circuit ratio must be regarded. By improving the algorithms of the vector current controller and the converter synchronization to the grid, a high bandwidth can be obtained for the VSC connected to a weak grid.

7 References

[1] G. L. Johnson *Wind Energy Systems*. Prentice-Hall, Inc., Englewood Cliffs, New Jersey, 1985. 360 p.

[2] A. Grauers, "Higher Electrical Efficiency with Variable Speed," *European Community Wind Energy Conference*, Lübeck-Travemünde, Germany, 8-12 March 1993, pp. 656-658.

[3] R. Cardenas, W. F. Ray, G. M. Asher, "Transputer-Based Control of a Switched Reluctance Generator for Wind Energy Application," *6th European Conference on Power Electronics and Applications (EPE'95)*, Sevilla, Spain, 19-21 September 1995. Proceedings, Vol. 3, pp. 539-544.

[4] A. Grauers, "Design of Direct-driven Permanent-magnet Generators for Wind Turbines," Doctoral Thesis, Technical Report No. 292, Chalmers University of Technology, Göteborg, Sweden, 1996.

[5] F. Santjer, G. Gerdes, "Netzrückwirkungen, verursacht durch den Betrieb von Windkraftanlagen am Netz," *DEWI Magazin*, August 1994, pp. 35-41.

[6] A. Stampa, F. Santjer, "Synchronisation von netzgekoppelten Windenergie anlagen in einem Windpark," *DEWI Magazin*, August 1995, pp. 80-86.

[7] T. Thiringer, "Measurement and Modelling of Low-frequency Disturbances in Induction Machines," Doctoral Thesis, Technical Report No. 293, Chalmers University of Technology, Göteborg, Sweden, 1996.

[8] J. Berding, G. Santjer, "Netzrückwirkungen von Windenergieanlagen in Windparks," *DEWI Magazin*, Nr. 9, August 1996, pp. 30-36.

[9] P. Hofer, N. Karrer, C. Gerster, "Paralleling Intelligent IGBT Power Modules with Active Gate-Controlled Current Balancing," *Power Electronics Specialists Conference (PESC'96)*, Baveno, Italy, 23-27 June, 1996, pp. 1312-1316.

[10] C. Gerster, P. Hofer, N. Karrer, "Gate-Control Strategies for Snubberless Operation of Series Connected IGBTs," *Power Electronics Specialists Conference (PESC'96)*, Baveno, Italy, 23-27 June, 1996, pp. 1739-1742.

[11] K. Thorborg, *Power Electronics — in Theory and Practice*. Lund, Sweden, Studentlitteratur, 1993.

[12] Y. Ito, S. Kawauchi, "Microprocessor-based Robust Digital Control for UPS with Three-Phase PWM Inverter," *IEEE Transactions on Power Electronics*, Vol. 10, No. 2, March 1995, pp. 196-204.

[13] A. Draou, Y. Sato, T. Kataoka, "A New State Feedback-based Transient Control of PWM AC to DC Voltage Type Converters," *IEEE Transactions on Power Electronics*, Vol. 10, No. 6, March 1995, pp. 716-724.

[14] S. Bhattacharya, T. M. Frank, D. M. Divan, B. Banerjee, "Parallel Active Filter System Implementation and Design Issues for Utility Interface of Adjustable Speed

Drive Systems," *IEEE Industry Applications Society 31st IAS Annual Meeting*, San Diego, California, USA, October 6-10,1996, Vol. 2, pp 1032-1039.

[15] J. Holtz, "Pulsewidth Modulation for Electronic Power Conversion," *Proceedings of the IEEE*, Vol. 82, No. 8, August 1994, pp. 1194-1214.

[16] L. J. Borle, C. V. Nayar, "Zero Average Current Error Controlled Power Flow for AC-DC Power Converters," *IEEE Transactions on Power Electronics*, Vol. 10, No. 6, November 1995, pp. 725-732.

[17] K. Taniguchi, Y. Ogino, H. Irie, "PWM Technique for Power MOSFET Inverter," *IEEE Transactions on Power Electronics*, Vol. 3, No. 3, July 1988.

[18] J. Holtz, E. Bube, "Field-Oriented Asynchronous Pulse-Width Modulation for High-Performance AC Machine Drives Operating at Low Switching Frequency," *IEEE Transactions on Industry Applications*, Vol. 27, No. 3, May/June 1991, pp 574-581.

[19] V. Kaura, V. Blasko, "Operation of a Voltage Source Converter at Increased Utility Voltage," *IEEE Transactions on Power Electronics*, Vol. 12, No. 1, January 1997, pp. 132-137.

[20] M. F. M. Mohd Siam, B. W. Williams, S. J. Finney, "Improved Active Power Filter With Triplen Deadband PWM," *Power Electronics Specialists Conference (PESC'96)*, Baveno, Italy, 23-27 June, 1996, pp. 1899-1905.

[21] Å. Ekström, "Calculation of Transfer Functions for a Forced-commutated Voltage-source Converter," *Power Electronics Specialists Conference (PESC'91)*, Boston, USA, June, 1991, pp. 314-322.

[22] B. T. Ooi, X. Wang, "Voltage Angle Lock Loop Control of the Boost Type PWM Converter for HVDC Application," *IEEE Transactions on Power Electronics*, Vol. 5, No. 2, April 1990, pp. 229-234.

[23] G. Joos, L. Morán, P. Ziogas, "Performance Analysis of a PWM Inverter VAR Compensator," *IEEE Transactions on Power Electronics*, Vol. 6, No. 3, July 1991, pp. 380-391.

[24] J. Svensson, "Power Angle Control of Grid-connected Voltage Source Converter in a Wind Energy Application," Technical Report No. 218L, Chalmers University of Technology, Göteborg, Sweden, 1995.

[25] V. Blasko, V. Kaura, "A New Mathematical Model and Control of a Three-phase AC-DC Voltage Source Converter," *IEEE Transactions on Power Electronics*, Vol. 12, No. 1, Januariy 1997, pp. 116-123.

[26] J. K. Pedersen, F. Blaabjerg, J. W. Jensen, P. Thogersen, "An Ideal PWM-VSI Inverter with Feedforward and Feedback Compensation," *5th European Conference on Power Electronics and Applications (EPE'93)*, Brighton, England, 13-16 September 1993, pp. 501-507.

[27] H. Akagi, "Trends in Active Power Line Conditioner," *IEEE Transactions on Power Electronics*, Vol. 9, No. 3, May 1994, pp. 263-268.

[28] S. R. Sanders, J. M. Noworolski, X. Z. Liu, G. C. Verghese, "Generalized Averaging Method for Power Conversion Circuits," *IEEE Transactions on Power Electronics*, Vol. 6, No. 2, April 1991, pp. 251-259.

[29] B. Lehman, R. M. Bass, "Extensions of Averaging Theory for Power Electronics System," *IEEE Transactions on Power Electronics*, Vol. 11, No. 4, July 1996, pp. 542-553.

[30] R. Kagalwala, S. S. Venkata, P. O. Lauritzen, A. Sundaram, R. Adapa, "A Transient Behavioral Model (TBM) for Power Converters," *IEEE 5th Workshop on Computers in Power Electronics, Portland*, USA, August 11-14, 1996, pp. 18-24.

[31] S. Hiti, D. Boroyevich, "Small-signal Modeling of Three-phase PWM Modulators," *Power Electronics Specialists Conference (PESC'96)*, Baveno, Italy, 23-27 June, 1996, pp. 550-555.

Appendix A

Transformations for Three-phase Systems

The transformations in this appendix are used when analysing three-phase machines and three-phase converters dynamically [1]. The transformations ensure power invariance.

A.1 Transformations between Three-phase and αβ-system

The three phase quantities $x_1(t)$, $x_2(t)$ and $x_3(t)$ can be transformed into two vectors, positive- and negative-phase sequence vectors, in a complex reference frame, called αβ-frame

$$\underline{x}_p(t) = x_{p\alpha}(t) + \mathrm{j}x_{p\beta}(t) = \sqrt{\frac{2}{3}}\left[x_1(t) + \mathrm{e}^{\mathrm{j}\frac{2\pi}{3}}x_2(t) + \mathrm{e}^{\mathrm{j}\frac{4\pi}{3}}x_3(t)\right] \tag{A.1}$$

and

$$\underline{x}_n(t) = x_{n\alpha}(t) + \mathrm{j}x_{n\beta}(t) = \sqrt{\frac{2}{3}}\left[x_1(t) + \mathrm{e}^{\mathrm{j}\frac{4\pi}{3}}x_2(t) + \mathrm{e}^{\mathrm{j}\frac{2\pi}{3}}x_3(t)\right] \tag{A.2}$$

where the sum of the three-phase quantities will be zero when no conductor is connected to the mid-point of the three-phase system, i.e.,

$$x_1(t) + x_2(t) + x_3(t) = 0 \tag{A.3}$$

A.1.1 Positive-Phase Sequence

The normal condition of a grid is to have positive-phase sequence vectors and no negative-phase sequence vectors. Hereby, a vector in the αβ-frame without the subscript *p* denotes a positive sequence vector. Equation (A.1) can now be expressed as a matrix equation

$$\begin{bmatrix} s_\alpha(t) \\ s_\beta(t) \end{bmatrix} = \mathbf{C_{23}} \begin{bmatrix} s_1(t) \\ s_2(t) \\ s_3(t) \end{bmatrix} \tag{A.4}$$

and the inverse becomes

$$\begin{bmatrix} s_1(t) \\ s_2(t) \\ s_3(t) \end{bmatrix} = \mathbf{C_{32}} \begin{bmatrix} s_\alpha(t) \\ s_\beta(t) \end{bmatrix} \tag{A.5}$$

where

$$\mathbf{C_{23}} = \begin{bmatrix} \sqrt{\frac{3}{2}} & 0 & 0 \\ 0 & \frac{1}{\sqrt{2}} & -\frac{1}{\sqrt{2}} \end{bmatrix} \qquad \mathbf{C_{32}} = \begin{bmatrix} \sqrt{\frac{2}{3}} & 0 \\ -\frac{1}{\sqrt{6}} & \frac{1}{\sqrt{2}} \\ -\frac{1}{\sqrt{6}} & -\frac{1}{\sqrt{2}} \end{bmatrix}$$

A.2 Currents and Voltages of Voltage Source Converter

The three-phase voltages of the voltage source converter can be represented in state-space vectors by the phase voltages $u_1(t)$, $u_2(t)$ and $u_3(t)$. The voltage vector in the complex αβ-frame becomes

$$\underline{u}(t) = u_\alpha(t) + \mathrm{j}u_\beta(t) \tag{A.6}$$

From now on, the valves of the voltage source converter are replaced by ideal switches. The switches sw_1, sw_2 and sw_3 of the converter can have a total of eight different combinations. For each state of the total number of combinations of switches, a state-space vector $\underline{sw}$ can be written as

$$\underline{sw}(t) = \sqrt{\frac{2}{3}}\left(sw_1(t) + \mathrm{e}^{\mathrm{j}\frac{2\pi}{3}} sw_2(t) + \mathrm{e}^{\mathrm{j}\frac{4\pi}{3}} sw_3(t) \right) = sw_\alpha(t) + \mathrm{j}sw_\beta(t) \tag{A.7}$$

In Table A.1, the eight different switch combinations and the state-space vectors of the switch values are shown. In Fig. A.1, the different switch states are presented in the form of state-space vectors.

TABLE A.1
SWITCH COMBINATIONS

sw_1	sw_2	sw_3	$\underline{sw}$
1	–1	–1	$\sqrt{\frac{8}{3}}\mathrm{e}^{\mathrm{j}\frac{0\pi}{3}}$
1	1	–1	$\sqrt{\frac{8}{3}}\mathrm{e}^{\mathrm{j}\frac{1\pi}{3}}$
–1	1	–1	$\sqrt{\frac{8}{3}}\mathrm{e}^{\mathrm{j}\frac{2\pi}{3}}$
–1	1	1	$\sqrt{\frac{8}{3}}\mathrm{e}^{\mathrm{j}\frac{3\pi}{3}}$
–1	–1	1	$\sqrt{\frac{8}{3}}\mathrm{e}^{\mathrm{j}\frac{4\pi}{3}}$
1	–1	1	$\sqrt{\frac{8}{3}}\mathrm{e}^{\mathrm{j}\frac{5\pi}{3}}$
1	1	1	0
–1	–1	–1	0

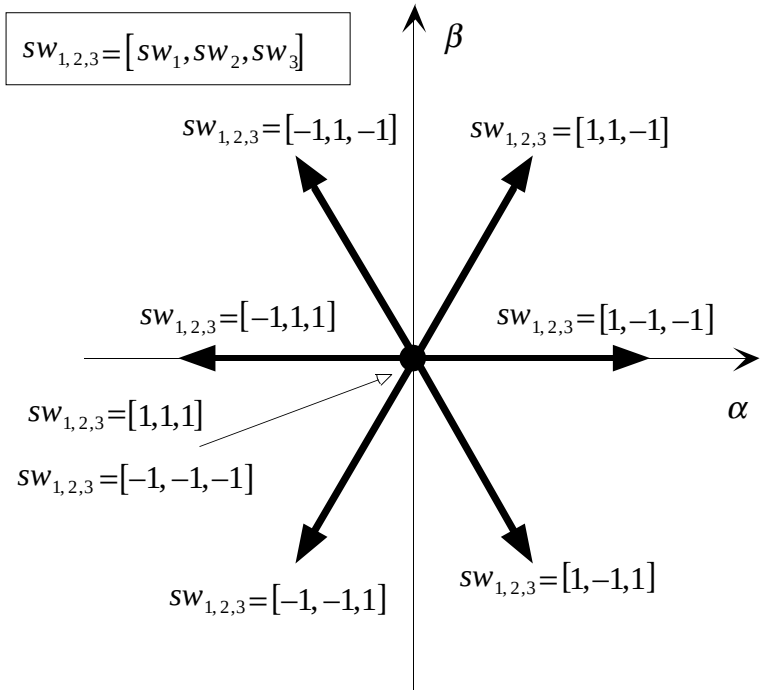

Figure A.1: State-space vector representation of the voltage vectors for the voltage source converter.

The output voltages of the voltage source converter can now be written as a state-space vector

$$\underline{u}(t)=\frac{u_{dc}}{2}\underline{sw}(t) \tag{A.8}$$

In a similar fashion, the three phase currents $i_1(t)$, $i_2(t)$ and $i_3(t)$ can be expressed as a state-space vector

$$\underline{i}(t)=\sqrt{\frac{2}{3}}\left(i_1(t)+\mathrm{e}^{\mathrm{j}\frac{2\pi}{3}}i_2(t)+\mathrm{e}^{\mathrm{j}\frac{4\pi}{3}}i_3(t)\right)=i_\alpha(t)+\mathrm{j}i_\beta(t) \tag{A.9}$$

The sum of the three-phase currents is always zero. The DC-link current $i_V(t)$ between the dc-link capacitor and the voltage source converter can be written as

$$i_V(t)=sw_1(t)i_1(t)+sw_2(t)i_2(t)+sw_3(t)i_3(t)=\mathrm{Re}\left[\underline{i}(t)\,\mathrm{conj}(\underline{sw}(t))\right] \tag{A.10}$$

A.3 The Connection between the αβ– and the *dq*-system

Let the vectors $\underline{v}(t)$ and $\underline{w}(t)$ rotate with the angular frequency ω and ω_g in the αβ-frame, respectively. The vector $\underline{v}(t)$ becomes a fixed vector in the *dq*-frame if the vector $\underline{w}(t)$ forms the *d*-axis in the *dq*-frame and the angular frequencies ω and ω_g are equal, as illustrated in Fig. A.2.

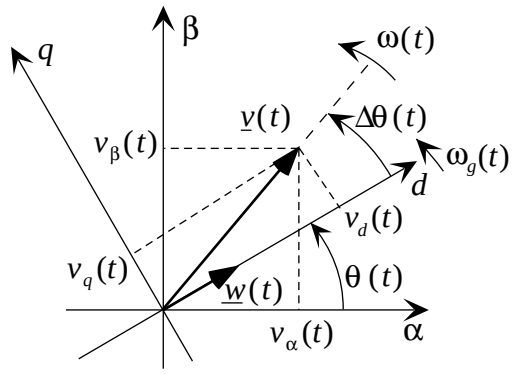

Figure A.2: The relation between the αβ-frame and the dq-frame.

The angles $\theta(t)$ and $\Delta\theta(t)$ in Fig. A.2 are given by

$$\theta(t) = \int_0^t \omega_g(\tau) d\tau \tag{A.11}$$

$$\Delta\theta(t) = \int_0^t \left[\omega(\tau) - \omega_g(\tau)\right] d\tau \tag{A.12}$$

The components in the *dq*-frame can be determined from Fig. A.2. The transformation equation from the αβ-frame to the *dq*-frame becomes, in matrix form

$$\begin{bmatrix} v_d(t) \\ v_q(t) \end{bmatrix} = \mathbf{R}(-\theta(t)) \begin{bmatrix} v_\alpha(t) \\ v_\beta(t) \end{bmatrix} \tag{A.13}$$

and the inverse becomes

$$\begin{bmatrix} v_\alpha(t) \\ v_\beta(t) \end{bmatrix} = \mathbf{R}(\theta(t)) \begin{bmatrix} v_d(t) \\ v_q(t) \end{bmatrix} \tag{A.14}$$

where the projection matrix is

$$\mathbf{R}(\theta) = \begin{bmatrix} \cos(\theta) & -\sin(\theta) \\ \sin(\theta) & \cos(\theta) \end{bmatrix} \tag{A.15}$$

The transformation Eq. (A.13) can be written in vector form

$$\underline{v}^{(dq)}(t) = \mathrm{e}^{-\mathrm{j}\theta(t)} \underline{v}^{(\alpha\beta)}(t) \tag{A.16}$$

and the inverse Eq. (A.14) becomes

$$\underline{v}^{(\alpha\beta)}(t) = \mathrm{e}^{\mathrm{j}\theta(t)} \underline{v}^{(dq)}(t) \tag{A.17}$$

Some useful projection matrix translations are

$$\begin{aligned} &\mathbf{R}^T(\theta) = \mathbf{R}(-\theta) \\ &\mathbf{R}(\theta)\mathbf{R}(\theta) = \mathbf{R}(2\theta) \end{aligned} \qquad \begin{aligned} &\mathbf{R}^T(\theta)\mathbf{R}(\theta) = \begin{bmatrix} 1 & 0 \\ 0 & 1 \end{bmatrix} \\ &\mathbf{R}(-\theta)\mathbf{R}(-\theta) = \mathbf{R}(-2\theta) \end{aligned} \tag{A.18}$$

A.4 Voltage and Current Vectors in αβ– and *dq*-systems

Suppose that a symmetrical sinusoidal three-phase voltage, with the angular frequency ω_g, is transformed into a vector $\underline{u}(t) = u_\alpha(t) + \mathrm{j}u_\beta(t)$ in the αβ-frame. Define the *q*-axis

in the *dq*-frame as parallel to the voltage vector $\underline{u}(t)$. This definition orginates from a flux vector parallel to the *d*-axis in the *dq*-frame. The voltage vector is proportional to the time derivative of the flux vector. As a consequence of the chosen reference vector, the voltage vector $\underline{u}(t)$ will only contain a *q*-component in the *dq*-frame. The transformation equation for a current vector from the αβ-frame to the *dq*-frame becomes, in matrix form

$$\begin{bmatrix} i_d(t) \\ i_q(t) \end{bmatrix} = \mathbf{R}\left(-\left(\omega_g t - \frac{\pi}{2}\right)\right)\begin{bmatrix} i_\alpha(t) \\ i_\beta(t) \end{bmatrix} \tag{A.19}$$

and the inverse

$$\begin{bmatrix} i_\alpha(t) \\ i_\beta(t) \end{bmatrix} = \mathbf{R}\left(\omega_g t - \frac{\pi}{2}\right)\begin{bmatrix} i_d(t) \\ i_q(t) \end{bmatrix} \tag{A.20}$$

Of course the voltage vector transformations from the αβ-frame to the *dq*-frame will be the same as those for the current vectors.

A.5 Positive-, Negative- and Zero-phase Sequence Harmonics

Harmonics in a three-phase system transformed to the αβ-frame will rotate in different directions depending on the harmonic number. For instance, the fundamental current will rotate counter-clockwise; the 5th harmonic currents will rotate clockwise and the 7th harmonic current will rotate counter-clockwise. The three voltage vectors in the αβ-frame are shown in Fig. A.3. The rotation directions of the different sequence harmonics are marked.

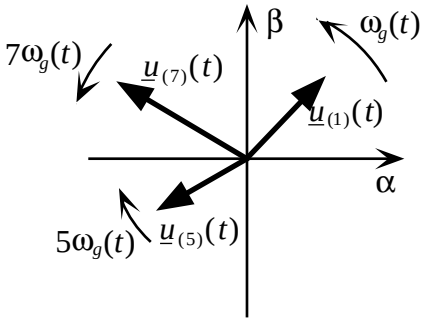

Figure A.3: The direction of different harmonics in the αβ-frame.

Harmonics of the orders $n = 3k, \quad k = 1,2,3,\ldots$ are of a zero sequence. In the αβ-frame this harmonic vector will not rotate. In a three-phase grid without a neutral conductor, no zero-sequence harmonics will occur.

Harmonics of the order $n = 6k + 1, \quad k = 1,2,3,\ldots$ are of a positive sequence. Thus, the harmonic vector in the αβ-frame will rotate counter-clockwise. For the lowest-order frequencies, the positive-sequence harmonics are the 7th, 13th and 19th.

Harmonics of the order $n = 6k - 1, \quad k = 1,2,3,\ldots$ are of a negative sequence and the harmonic vector rotates clockwise in the αβ-frame. For the lowest-order frequencies, the negative-sequence harmonics are the 5th, 11th and 17th.

A.5.1 Harmonics in the *dq*-frame

When transforming vectors from the αβ-frame to the *dq*-frame, a counter-clockwise rotation of the αβ-frame with fundamental angular frequency will occur. The current vector $\underline{i}^{(\alpha\beta)}$ is transformed using

$$\underline{i}^{(dq)} = \mathrm{e}^{-\mathrm{j}\left(\omega_g t-\pi/2\right)}\underline{i}^{(\alpha\beta)} \tag{A.21}$$

The fundamental current vector in the αβ-frame will be transformed to a stationary vector in the *dq*-frame. Positive-sequence harmonics will rotate slower in the *dq*-frame. For negative-sequence harmonics, the vectors in the αβ-frame will rotate faster in the *dq*-frame. The harmonics transformation from the αβ-frame to the *dq*-frame are shown in Table A.2.

TABLE A.2

HARMONICS TRANSFORMATION FROM αβ-FRAME TO *DQ*-FRAME.

Harmonic type	Harmonic number *n*	αβ-frame	*dq*-frame
fundamental	n=1	$\underline{i}_{(1)}^{(\alpha\beta)}(t) = \hat{\underline{i}}_{(1)}\mathrm{e}^{\mathrm{j}\left(\omega_g t-\pi/2\right)}$	$\underline{i}_{(1)}^{(\alpha\beta)}(t) = \hat{\underline{i}}_{(1)}$
positive sequence	$n = 6k+1,$ $k = 1,2,3,\ldots$	$\underline{i}_{(n)}^{(\alpha\beta)}(t) = \hat{\underline{i}}_{(1)}\mathrm{e}^{\mathrm{j}n\left(\omega_g t-\pi/2\right)}$	$\underline{i}_{(n)}^{(dq)}(t) = \hat{\underline{i}}_{(n)}\mathrm{e}^{\mathrm{j}(n-1)\left(\omega_g t-\pi/2\right)}$
negative sequence	$n = 6k-1,$ $k = 1,2,3,\ldots$	$\underline{i}_{(n)}^{(\alpha\beta)}(t) = \hat{\underline{i}}_{(n)}\mathrm{e}^{-\mathrm{j}n\left(\omega_g t-\pi/2\right)}$	$\underline{i}_{(n)}^{(dq)}(t) = \hat{\underline{i}}_{(n)}\mathrm{e}^{-\mathrm{j}(n+1)\left(\omega_g t-\pi/2\right)}$

A.6 References

[1] M. P. Kazmierkowski, H. Tunia, *Automatic Control of Converter-Fed Drives*, PWN–Polish Scientific Publishers, Warszawa Polen, 1994, p. 559.

PART II

INCLUDED PAPERS

SECTION 1
Voltage Source Converters in Variable Speed Wind Turbines and Hybrid Wind Parks

SECTION 2
Voltage Angle Control of a Voltage Source Converter

SECTION 3
Vector Controlled Voltage Source Converter

SECTION 4
Connecting Fast Switching Voltage Source Converters to the Grid

PAPER 1A

O. Carlson, A. Grauers, J. Svensson, Å. Larsson, "A Comparison of Electrical Systems for Variable Speed Operation of Wind Turbines," *European Wind Energy Association Conference and Exhibition (EWEC'94)*, Thessaloniki, Greece, 10-14 October 1994, pp. 500-505.

A Comparision Between Electrical Systems for Variable Speed Operation of Wind Turbines

O. Carlson, A. Grauers, J. Svensson, Å. Larsson

Chalmers University of Technology
Sweden

Abstract: The aim of this paper is to compare variable speed electrical systems for a wide speed range. Synchronous as well as induction generators are investigated. Line-commutated thyristor converters are compared with force-commutated transistor converters. The system characteristics are investigated regarding power quality, capability of damping resonance, losses and price. The rated power of the investigated systems is 400 kW. The investigation shows clearly that the synchronous generator with a diode rectifier is the best choice of generator systems. The force-commutated IGBT converter is the preferable inverter.

I. INTRODUCTION

During the last decade researchers and wind turbine manufacturers have been working on electrical systems for variable speed wind turbines. The well-known advantages of wind turbines with variable speed are reduction of noise, optimal C_p–λ operation, a well controlled torque in the drive train and thereby the possibility to damp resonance and avoid speeds causing resonance.

Several different electrical systems have been developed both for a broad and a narrow speed range. For the narrow speed range rotor cascades of the induction generator are the most common. The German wind turbine, Growian, and the US. Mod 5B have a cycloconverter connected to the rotor. The Spanish AWEC-60 has a Kramer cascade. This type of cascade has also been investigated by Hylander [1].

For the wide speed range the synchronous generator with a rectifier and a thyristor inverter is the most common system. In the Netherlands, a wind farm with this system was erected in the mid eighties. Several German machines are also equipped with this kind of system. Another interesting system is the induction generator with force-commutated transistor converters. This system has been developed for wind turbine operation, by US Windpower, and today it is in production for a rated power of 300 kW.

Earlier, it has often been said that the losses in the frequency converter of a variable-speed system are a drawback. Grauers [2] has, however, shown that the total energy losses do not have to increase because of the frequency converter. The generator and gear losses can be reduced when the converter is used, and this reduction is large enough to compensate for the losses in an efficient converter. This means that the total energy losses of a variable-speed generator system can be as low as those of a constant-speed system.

II. ELECTRICAL SYSTEMS

The different parts of an electrical generating system for variable speed operation are described, evaluated and compared to select the optimal system, see also Svensson et al.

[3]. The aim of the investigation is to find the best commercially available 400 kW variable speed system for a wide speed range. In this article only the two most interesting generators, rectifiers and inverters are presented.

The choice of electrical system can be divided into two almost independent choices. The generator and rectifier must be chosen as a combination and the inverter can be chosen almost independently of the generator and rectifier used.

A. Generators

The usual generator in wind turbines is the induction generator. In a few wind turbines the brushless synchronous generator has been used.

The advantages of the induction generator are mechanical simplicity, robustness and closed cooling (IP54). The major disadvantage is that the stator needs reactive magnetizing current, preferably from the rectifier.

The synchronous generator is mechanically more complicated than the induction generator. It has more parts and it is normally cooled with ambient air internally (IP23). The only clear advantage it has, compared with the induction generator, is that it can be directly connected to the simple diode rectifier.

B. Rectifiers

The diode rectifier is a good rectifier alternative because of its simplicity, low cost and low losses. But it generates non sinusoidal generator currents and can not control the generator voltage or current. Therefore, it must be used with a generator that can control the voltage and the inverter must control the current. The non sinusoidal generator current increases the generator losses a little and decreases the rating of the generator by about 5 %. Also the commutation of the diodes is a cause for derating, because it leads to a voltage drop of about 5 to 10 %. However, the stator of the synchronous generator does not need a higher apparent power rating than the stator of an induction generator for the same active power. With a diode rectifier the motor start of the turbine must be performed by a separate start equipment if necessary.

A force-commutated rectifier is an other alternative. It can be made with different types of power electronic switches, but it has been found that the insulated gate bipolar transistor, IGBT, will be the best choice in the near future. A force-commutated rectifier can control both the generator voltage and the generator current. The disadvantages of the force-commutated rectifier, compared with the diode rectifier, are the high price and the high losses. The two main alternative combinations of a generator and rectifier are shown in Figure 1.

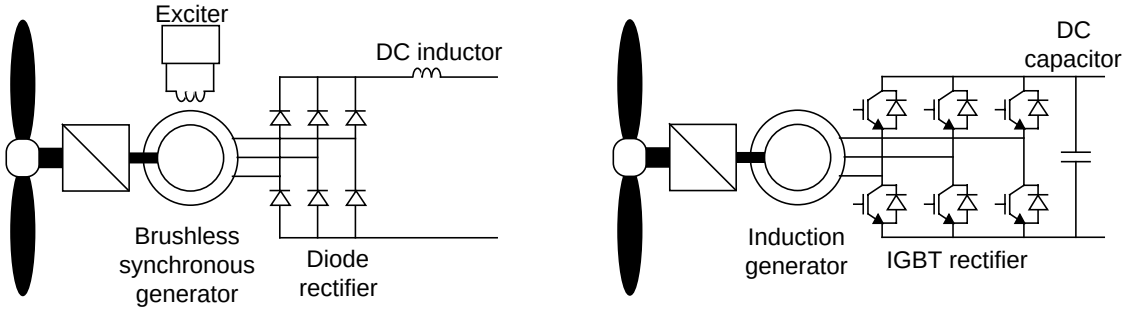

Figure 1. The two main generator and rectifier alternatives.

C. Inverter and Grid Filter

Two types of inverters are compared, line commutated inverter and force commutated voltage stiff inverter. The two types of inverters need different line filters.

Line Commutated Inverter

Another name of the line commutated inverter is thyristor inverter and it needs connection to the grid to operate. The thyristor inverter can be seen in Figure 2. The current on the grid side is proportional to the current on the DC-side of the inverter but the power factor varies with the DC-side voltage. The power factor is equal to or less than 0.9 for a line commutated inverter. It means that the thyristor inverter consumes reactive power. The line commutated inverter is well known and it is a mature product. This makes the cost of the inverter stable and it will not be dramatically reduced in the future. Thyristor valves can be overloaded without any damages. The line commutated inverter is available up to 5 MW. To protect the line commutated inverter, when the grid voltage disappears, a special break circuit needs to be installed. The line commutated inverter control has a maximum dead time of 3.3 ms and the bandwidth is approximately 20 Hz.

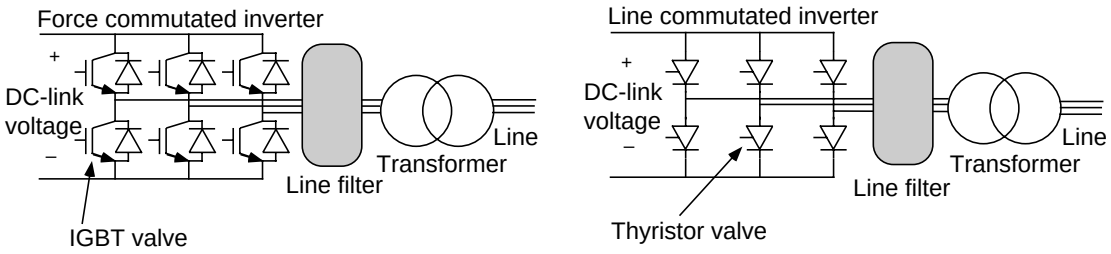

Figure 2.Schematic figures of a line commutated inverter and a force commutated inverter.

Grid Filter to Line Commutated Inverters

The line commutated inverter produces not only fundamental current but also harmonic current that turns to voltage harmonics on the grid. By using grid filter the harmonic voltage can be minimized. The line commutated inverter produces harmonic current with low frequency content. Low frequency harmonic contains more energy than the harmonic of high frequency. To eliminate the low frequency harmonics large grid filter must be used. To eliminate all harmonics is not realistic because then a huge filter is required. Often it is enough to eliminate the harmonic of the fifth and seventh orders. One side-effect when using a grid filter is that the filter produces reactive power. This increases the power factor for the whole inverter system.

Force Commutated Inverter

By force commutate means that the converter freely can choose when to turn on and when to turn off its valves. This means that the force commutated inverter can create its own three-phase voltage system and if the inverter is connected to the grid, the inverter can freely choose which power factor to use and in which direction the power should flow. Often the power factor is chosen as high as possible. By the use of pulse width modulation technique (PWM) the low frequency harmonics will be eliminated and the first harmonics have their frequency around the switching frequency of the inverter. Usually the switching frequency is about 5 to 10 kHz when insulated gate bipolar

transistors (IGBT) are used. For older components, for instance gate turn off (GTO) thyristors, the maximum switching frequency is about one kHz.

The advantage of the GTO thyristor is that it can handle more power than the IGBT. The disadvantages of the GTO inverter is that the inverter needs more complicated circuits to control its valves and that it has lower efficiency. Manufacturers choose IGBT instead of GTO if the power is possible to handle with IGBT valves. The evolution of IGBT goes on fast. The power rates are increasing very fast and the prices are falling. The component ratings have been doubled every second year. Now the manufacturers offer IGBT components which make it possible to handle 600 kVA with a single six-pulse inverter. In a near future the development of the IGBT will make it possible to use a single six-pulse inverter with IGBT and PWM to handle power in the MVA range. In Figure 2 the force commutated inverter is shown.

The control capacity depends on which sort of control the inverter is equipped with. The fastest control method is the vector control and the bandwidth is approximately 100 Hz. Of course faster controller can be installed to eliminate current harmonics on the grid, but the disadvantage is that the cost increases with higher inverter bandwidth.

Grid Filter to Force Commutated Inverters

The voltage stiff force commutated inverter needs an inductance between the inverter and the grid in order to operate. The harmonics of low frequencies are cancelled by using the PWM technique. A smaller grid filter can be used to eliminate the high order harmonics. This makes the grid filter smaller than the grid filters for line commutated inverters.

III. POWER QUALITY

A. Definition

Perfect power quality means that the voltage is continuous and virtually purely sinusoidal, with a constant amplitude and frequency. In practice, it is physically impossible to maintain perfect "stability" of the voltage and its frequency at the user's terminal.

The quality of the power which depends on the interaction between grid and source can be expressed in terms of the physical characteristics and properties of the electricity. It is most often described by:

- Voltage stability
- Frequency stability
- Phase balance
- Electromagnetic interference effects
- Telephone interference factors

The electromagnetic interference effects and the telephone interference factors will not be discussed in this paper. The frequency of larger power systems is normally very stable and it is hence no problem. When the penetration of wind power plants increases, the fluctuating output from these may cause an unstable frequency. But, that would demand a large amount of wind turbines and we are for the moment far from that level. Moreover, under normal conditions when only three-phase loads are connected to the grid there would be no phase unbalance. Consequently, the most important among the mentioned

characteristics and properties above, especially when converters are used, is the voltage stability.

It is obvious that bad power quality from a wind turbine will affect the grid, but it is worth pointing out that the reversed case is also valid. In other words, bad power quality on the grid will affect the wind turbine.

B. Relevant Standards of Voltage Stability

Definitions and information regarding the characteristics of the irregularities are normally given in national or international standards. The present standards in Europe are, however, not easy to use. For example, only the maximum allowed voltage distortion in the network is stated. There are no specifications regarding the level of the highest allowed harmonic current from a single source. The voltage harmonics follow Ohm's law:

$$\underline{U}_n = \underline{I}_n \underline{Z}_n \tag{1}$$

where $\underline{U}_n$ is the harmonic phase voltage, $\underline{I}_n$ is the harmonic current and $\underline{Z}_n$ is the phase impedance of the grid for harmonic number n. The harmonic current generated from a converter is easy to predict, but to determine the exact value of the impedance of the grid is both difficult and time-consuming, especially since the impedance has different values for each harmonic. As a consequence, the voltage harmonics are very hard to predict.

Voltage stability can be subdivided into slow voltage variations, rapid voltage fluctuations (flicker), harmonic voltage distortion and voltage dips. These voltage irregularities will be discussed in detail, moreover, Table 1 shows a short summary of the different voltage irregularities together with a specification of the Swedish standard SS 421 18 11. In the same table there are some different reasons for these irregularities listed, and the way they will cause disturbances.

Slow Voltage Variations

Slow voltage variations can be defined as changes in the RMS value of the voltage occurring in a time span of minutes or more. National standards often state allowable variations in nominal voltage over an extended period, for instance 24 hours. IEC Publication 38 recommends 230/400 V to be the standard voltage for 50 Hz systems. Under these conditions the voltage at the user's terminal must not differ more than ±10 % from the normal voltage.

Flicker

Due to the historical association with effects on lighting, rapid voltage fluctuations have come to be commonly termed voltage flicker. Rapid voltage fluctuations or flicker are a series of changes with intervals shorter than approximately one minute, and they are defined in IEC Publication 555-3. Maximum permitted voltage changes as a function of the possible fluctuation rate are given in this standard.

Harmonic Voltage Distortions

Harmonic voltage distortions can be caused by the flow of harmonic currents in the system. The harmonic distortion can be quantified by several different methods. One of the most common methods is the total harmonic distortion (THD). An other method for quantifying harmonics is individual harmonic distortion. The maximum total harmonic

distortion allowed, according to the Swedish standard SS 421 18 11, is 6 %. Maximum permitted value of any odd individual component is 4 %.

Voltage Dips

Voltage dips are sudden reductions of the supply voltage with a magnitude between 10 % and 100 % of the supply voltage followed by a voltage recover after a short period. The duration of a voltage dip is conventionally between 10 ms and 1 minute.

C. Power Quality Applied on Wind Turbines

When it comes to power quality from wind turbines only some specific voltage irregularities are of interest. A conventional wind turbine, equipped with an induction generator connected directly to the grid, gives a fluctuating active power output and has a reactive power demand. This may lead to slow voltage variations. The design criteria for the local grid is based on the slow voltage variation standard. Voltage flicker may be of interest only when wind turbines are connected to a weak grid. As mentioned earlier, inverters do inject harmonic currents into the grid and will, due to the grid impedance, cause harmonic voltages. As a result, voltage harmonics are the most interesting type of irregularity when converters are used. A simple converter may, due to current harmonic content and reactive power demand, make the power quality worse. Using an advanced converter makes it possible to control the reactive power. An advanced converter can also operate as an active filter, Akagi [4]. These two characteristics make it possible to even improve the power quality at the point of common connection.

TABLE 1
VOLTAGE IRREGULARITIES ON LOW VOLTAGE SYSTEMS ACCORDING TO THE SWEDISH STANDARD SS 421 1811.

Voltage	Specification	Reason	Causes
Slow voltage variation	+ 6 % - 10 %	Load variations	
Sudden changes in the rms of the voltage Voltage fluctuation	"Flicker curve"	Switching loads Utility switching Motor starting	Flicker Computer system crashes
Harmonics	Odd ≤ 4 % Even ≤ 1 % THD ≤ 6 % (n = 2 - 40)	Non-linear loads Motor speed controllers Inverters	Additional losses in generators and transformers Increasing current in capacitors
Inter harmonics	≤ 3 %	Frequency converters	Unstable operation of sensitive electronic equipment

IV. COMPARISION OF SYSTEMS

In this section the alternative systems are compared regarding price, cost of losses and performance. The comparison of generator and rectifier is summarized in Table 2 and the comparison of inverters is summarized in Table 3. The prices and costs are all related to the price of a 400 kW induction generator, 14 000 ECU, to easily make comparisons.

A. Component Price

The prices of the different systems, presented in Tables 2 and 3, are only the component prices and do not include mounting and enclosure. It must also be made clear that the prices are uncertain. The generator prices vary a lot depending on who the buyer is. Also the price of the IGBT rectifier/inverter is uncertain because today only a few manufacturers have yet developed large IGBT converters. Therefore, the price of the IGBT inverter can be assumed to be reduced in the future.

B. Losses

When comparing the cost of the different systems the cost of losses must be included. Losses can be considered as a cost because they reduce the produced energy of a wind turbine and, therefore, reduce the income.

An easy way to estimate the minimum cost of the losses is to say that if the output energy of the wind turbine system is reduced by 1 % then the wind turbine will be worth 1 % less. The price of a 400 kW wind turbine is today about 350 000 ECU and if the losses reduce the output energy by 1 % that will represent a cost of 3 500 ECU. This estimation gives a lower limit to the value of losses. The value can be higher if the price of electricity is high.

The losses at rated load can not be used to calculate the cost of losses directly. The total energy losses must instead be calculated. The energy losses depend on the wind conditions at the wind turbine site and on the control of the electrical system [2].

C. Inverter Harmonics

Harmonics are an important part of the total power quality. All inverters cause harmonic currents due to their working principles. The amount of voltage harmonics on the grid is determined by how large the short-circuit inductance of the grid is. Grid filters are used to eliminate harmonics on the grid. As mentioned before line commutated inverters produce harmonics of low orders (250 and 350 Hz). Force commutated inverters using PWM and IGBT produce harmonics of high orders (larger than 5 kHz). Harmonics of high orders require smaller filter than harmonics of low orders and the cost of filter depends on the physical size. This makes filter that works with line commutated inverters larger and more expensive than the filter which works with force commutated inverters.

D. Torque Control

In the examined wind turbine all important resonance frequencies in the drive train are below 5 Hz. The bandwidth of the torque control has, therefore, been required to be at least 10 Hz. All the examined systems fulfil that requirement. A system with IGBT inverter or rectifier allows up to 100 Hz bandwidth. The slowest system is a synchronous generator with diode rectifier and thyristor inverter. The thyristor inverter controls the torque by controlling the dc current. Even that system allows a torque control bandwidth of at least 10 Hz.

E. Choice of Generator and Rectifier

The cost comparison of the two generator/rectifier alternatives is clear, see Table 2. The synchronous generator with diode rectifier has much lower total cost than the induction generator with force-commutated rectifier. The difference in total cost is large not only because of the high price of the force-commutated rectifier, but also because of its high losses. So, even if the price of the force-commutated rectifier is reduced much in the future, the synchronous generator with diode rectifier will remain the cheapest alternative. A disadvantage of the synchronous generator is that there are only a few manufacturers of enclosed synchronous generators.

There are, however, some advantages of the induction generator system. It can be used for the motor start of the turbine. There are also several manufacturers of enclosed induction generators.

The cost of generator losses is higher than the price of the generator. This shows that it is not meaningful to compare only the price of the alternative generators. It also means that it

may perhaps be interesting to make a specially designed generator that is more expensive than these standard generators if the losses can be reduced enough.

F. Choice of Inverter

The comparison of the total cost of the inverter and its losses clearly shows that the thyristor inverter is the least expensive choice, see Table 3. Even with a substantial reduction of the IGBT inverter cost the thyristor alternative will be cheaper because the difference in losses is not likely to be reduced much. However, the increasing demands on power quality may make the thyristor inverter less attractive in the long run. The higher cost of the IGBT inverter and its higher losses may very well be accepted because of its lower grid disturbance. The IGBT inverter can even improve the power quality of the grid.

TABLE 2
COMPARISON OF TOTAL COST AND SYSTEM PERFORMANCE OF
THE GENERATOR AND RECTIFIER ALTERNATIVES.

	Synchronous gen. and Diode rectifier	Induction gen. and IGBT rectifier
Motor start	needs extra equipment	possible
Generator cooling	normally open	normally enclosed
Generator price	1.2	1.0
Cost of generator losses	1.9	1.3
Rectifier price	0.1	2.0
Cost of rectifier losses	0.5	1.3
Total cost	3.6	5.6

TABLE 3
COMPARISON OF TOTAL COST AND POWER QUALITY
ASPECTS OF THE INVERTER ALTERNATIVES.

	Thyristor inv. and AC filter	IGBT inverter and AC filter
Harmonic currents	large harmonics low frequency	small harmonics high frequency
Power factor	not perfectly controllable	controllable
Filter	large tuned filters	small low pass filters
Inverter price	0.8	2.3
Cost of inverter losses	0.5	1.1
Filter price	0.3	0.2
Cost of filter losses	0.1	0.1
Total cost	1.7	3.6

V. CONCLUSION

The investigation shows clearly that the synchronous generator with a diode rectifier is the best choice of generator systems. The main reason is the possibility for the synchronous generator to use the diode rectifier with low losses and low price.

The inverter choice is the IGBT force-commutated inverter due to the low harmonic content and the possibility to control the reactive power. These advantages are important due to high power quality demands. For the system layout see Figure 3.

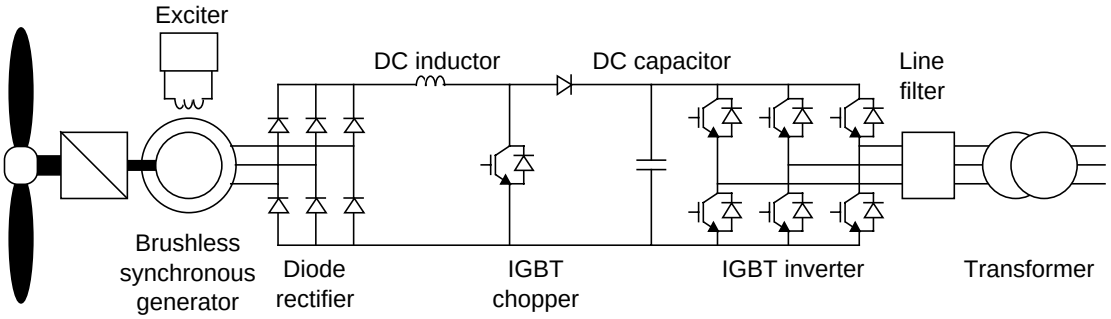

Figure 3. The proposed system for variable speed wind turbines. Synchronous generator and diode rectifier for low losses and low cost. IGBT inverter for high power quality.

VI. ACKNOWLEDGEMENT

The authors would like to express their thanks to S. Engström from Nordic Windpower AB and S. Strandberg from Oy Botnia Retail Data AB for their enthusiastic and valuable discussions and good co-operation during the work.

The financial support given by the Swedish National Board for Industrial and Technical Development and Kraftföretagens vindkraft AB is gratefully acknowledged.

VI. REFERENCES

[1] Hylander, J., ”Stator current frequency spectra and the torque pulsations in induction machines with rotor convertor cascades,” Technical report No. 163, Department of Electrical Machines and Power Electronics, Chalmers university of Technology, Göteborg, Sweden, 1986.

[2] Grauers, A., ”Synchronous generator and frequency converter in wind turbine applications: system design and efficiency,” Technical report No. 175L, Department of Electrical Machines and Power Electronics, Chalmers University of Technology, Göteborg, Sweden, 1994.

[3] Svensson, J. , Grauers, A. and Carlson, O., ”Preliminary study of an electrical system for wind power plants with variable speed,” Report nr: R–93–07, Department of Electrical Machines and Power Electronics, Chalmers University of Technology, Göteborg, Sweden, 1993.

[4] Akagi, H., ”Trends in Active Power Line Conditioner,” *IEEE Transactions on Power Electronics*, Vol. 9, No. 3, May 1994, pp. 263-268.

PAPER 1B

J. Svensson, "Possibilities by using a Self-commutated Voltage Source Inverter Connected to a Weak Grid in Wind Parks," *1996 European Union Wind Energy Conference and Exhibition*, Göteborg, Sweden, 20-24 May 1996, pp. 492-495.

Possibilities by Using a Self-Commutated Voltage Source Inverter Connected to a Weak Grid in Wind Parks

Jan Svensson M. Sc.

Department of Electric Power Engineering
Chalmers University of Technology
S-412 96 Göteborg, Sweden

Abstract: In this paper the hybrid wind farm connected to a weak grid is investigated. By combining different electrical wind power plant systems a cost-efficient solution is obtained. The point of common connection voltage level can be controlled by injecting reactive power from a phase-compensating capacitor battery and a voltage source inverter (VSI). If the short-circuit impedance ratio is lower than 1, the demanded reactive power injection to keep the voltage at nominal level is unrealistic. For short-circuit impedance ratios of 2 or higher the demanded reactive power level is acceptable. When using both induction generators and thyristor inverters the reactive power injector VSI size should be about 0.2 pu. If the hybrid farm consists of THYs, IGs and VSIs and the active power is equally shared between the systems, the VSI had to be scaled up by 5% to handle both active and reactive power.

Keywords: Electrical systems, Reactive power, Grid, Control.

1. INTRODUCTION

To successfully install wind turbines on a weak grid, a knowledge of the wind turbine impact on the grid is essential. The most common electrical system of commercial wind power plants is the induction generator (IG) directly connected to the grid. A major drawback is that the reactive power flow and thus the grid voltage level cannot be controlled. Another drawback associated with fixed speed system is that the blade rotation causes voltage fluctuations of a frequency of 1 to 2 Hz on the grid [1]. This fluctuation problem is not solved by using several turbines; on the contrary, if several identical wind turbines are installed in a wind park, the rotors can synchronize with each other and the power fluctuations are superimposed in phase [2].

With variable-speed wind turbines several advantages can be achieved compared to the directly connected IGs. Such as lower noise, increased average efficiency [3], reduced power fluctuation between the wind turbine and the grid and less dynamic stresses on the mechanical structure of the plant. However, the disadvantage is a higher cost of the electrical system [4].

Today the thyristor inverter (THY), also named grid-commutated inverters, is the cheapest solution to transmit the power into the grid. However, the grid voltage can still not be controlled since the power factor depends on the active power. If the grid is weak, voltage distortion will occur [5]. Another problem is injected current harmonics into the grid, which results in voltage distortion.

The self-commutated voltage source inverter (VSI) is a grid-friendly converter [6]. The harmonics injected into the grid are now of a much higher order and can much easier be

filtered. The reactive power can now be chosen freely. However, some drawbacks are high cost, lower efficiency than with the THY and a limited maximum size of the inverter [4].

A conventional wind park connected to a weak grid can give rise to voltage variations. Today the solution is to build a stronger grid. To equip all the wind turbine electrical systems with VSI would also be a solution, but a rather expensive one.

In this paper a solution is proposed which combines the technical and economical advantages of different systems, the hybrid wind farm. The farm consists of wind turbines with constant speed using directly connected IG as well as variable-speed electrical systems. One of the variable-speed electrical systems has a VSI connected to the grid, the others have THYs. The VSI is used to reduce harmonic distortion and voltage variations. Important factors are the short-circuit ratio, SCR, and the ratio between the reactance and the resistance of the grid, SCIR (Short-Circuit Impedance Ratio).

2. THE SYSTEM CONFIGURATION

The hybrid wind park consists of wind turbines that have directly connected IGs, variable-speed electrical systems using THYs and one or a few VSIs. In Figure 1 the hybrid wind park configuration is shown. The variable-speed system uses synchronous generators (SG) and a diode rectifier to obtain high efficiency and low cost [4]. The grid strength is governed by the grid impedance consisting of a resistance R_N and an inductance L_N. The no-load grid rms-phase voltage is denoted E_N The grid at the farm, called point of common connection (PCC), has the rms-phase voltage E. The THY DC-link voltage yields u_{dc}. The VSI rms-phase voltage is denoted U.

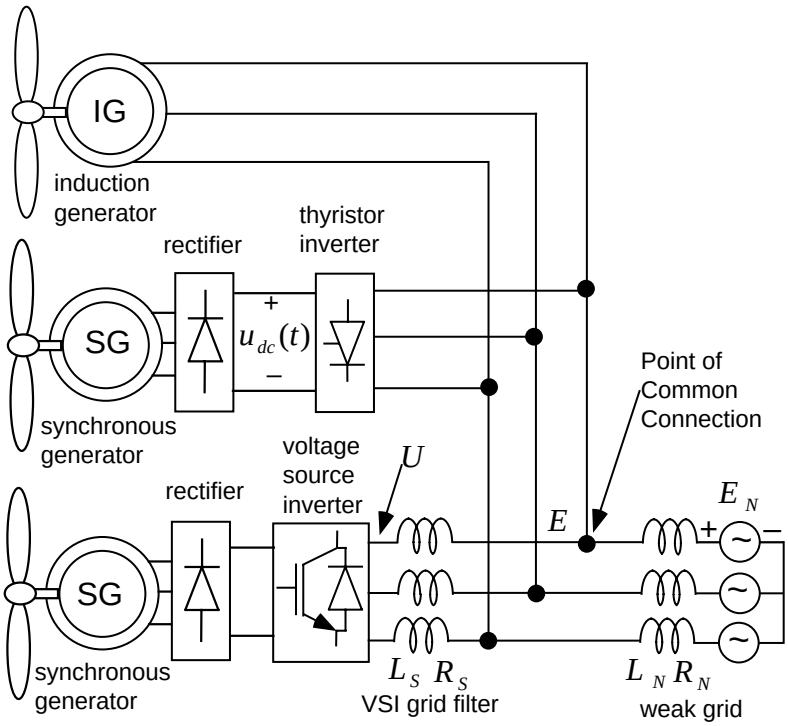

Figure 1: The hybrid wind park configuration.

For the variable-speed system with the THY, two DC-link voltage control strategies are investigated. Apart from using the conventional control strategy of constant flux (CF) in

the SG a proposed strategy is investigated. The idea is how to get optimal efficiency (OPT) for the SG [7].

3. VOLTAGE VARIATIONS DUE TO WIND VARIATION

Since the reactive power injected by IG and THY into the grid cannot be controlled, the voltage level of the PCC will vary. The two different control methods of the THY will also affect the grid voltage differently. Figure 2 shows the reactive power as a function of the active power for the IG and the THY.

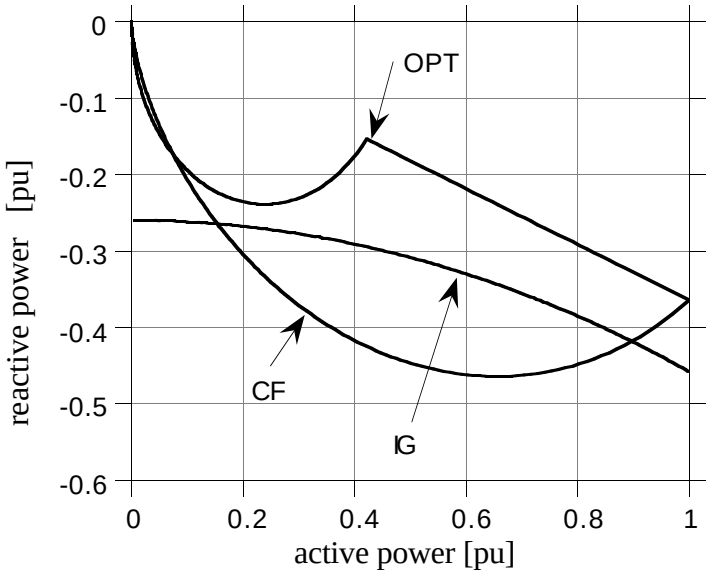

Figure 2: The reactive power as a function of the active power for the IG and the THY. The THY uses CF- and OPT-modes.

For a typical IG the reactive power varies from approximately –0.25 pu to -0.45 pu at rated active power. The reactive power of the THY goes from 0 to –0.38 pu when the advance angle is 20°. The CF-mode has the largest reactive power span, 0.45 pu. The reason for the different reactive power functions for the two types of THY controls is that the DC-link voltage is higher in the OPT-mode for median wind speeds. In Figure 3, the DC-link voltage and the resulting reactive power are plotted as a function of the wind speed.

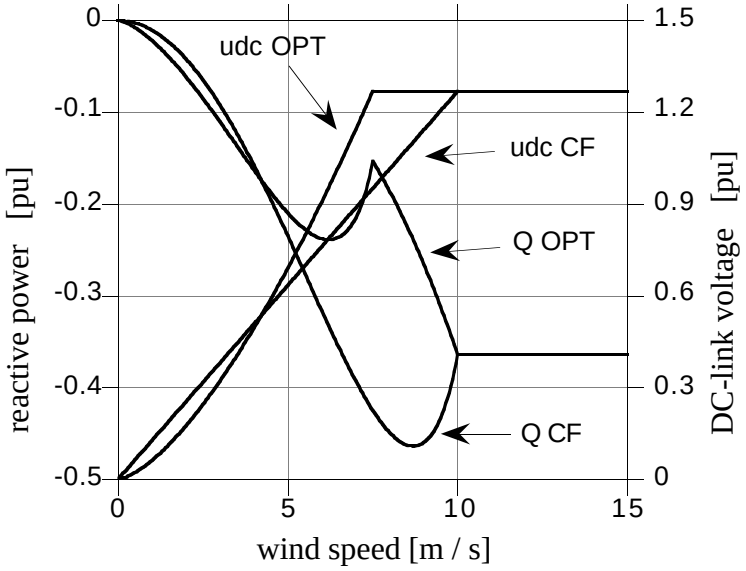

Figure 3: The THY DC-link voltage and the reactive power as a function of the wind speed and for the CF- and OPT-modes.

3.1. The Voltage Fluctuation

Here, the voltage fluctuation of the PCC with weak grid is analysed. In Figure 4 and Figure 5 the voltage fluctuation caused by the IG and the THY is presented for the SCR of 10. For a low short-circuit impedance angle (SCIA) the grid is mainly resistive and a high SCIA means that the grid is mainly inductive. As can be noted SCIA strongly governs the voltage level, especially at high active power levels. Low SCIA increases the voltage at PCC and for high SCIA the voltage at PCC decreases. The voltage fluctuation is minimized if the SCIA is about 40° to 60°.

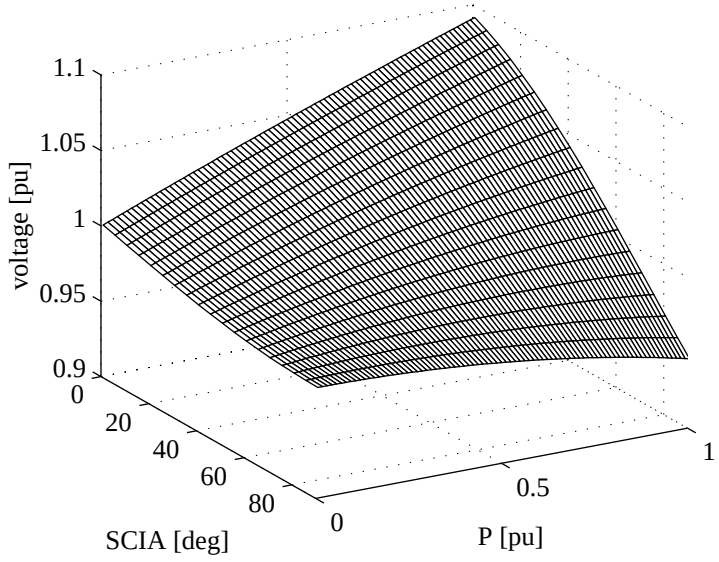

Figure 4: The PCC voltage level variation due to the SCIA and the active power from the IG. The SCR is 10.

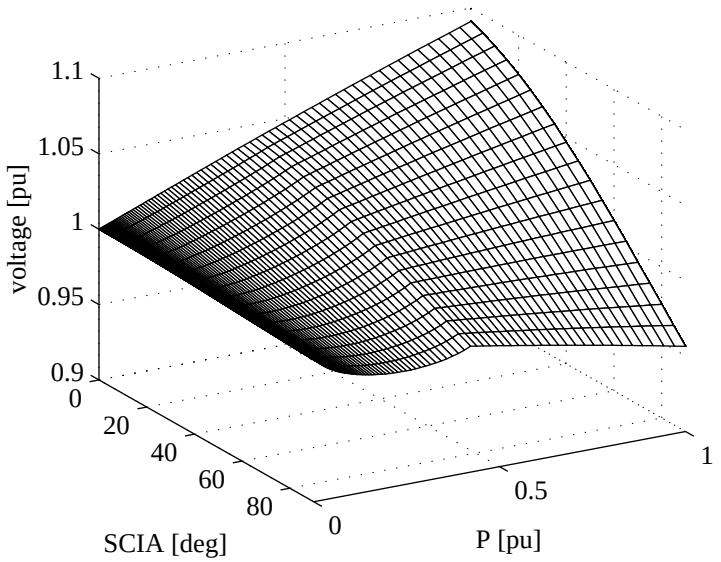

Figure 5: The PCC voltage level variation due to the SCIA and the active power from the THY. The SCR is 10 and the minimum advance angle is 20°.

4. VOLTAGE CONTROL OF THE GRID

The voltage level of the grid is used to control the reactive power injected to the grid. This can be done stepwise by a capacitor battery or continuously by controlling the reactive power from a VSI, shown in Figure 6. Usually one or two capacitor stages are used at wind turbines.

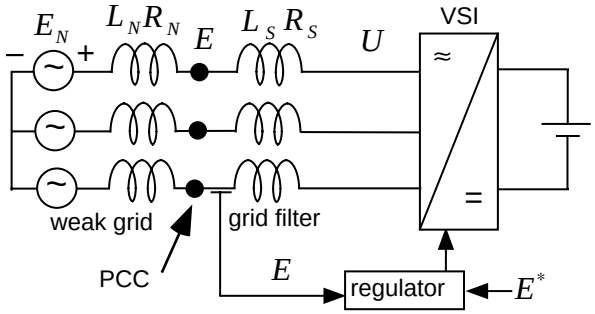

Figure 6: The method to control the voltage level of the grid.

5. REACTIVE POWER REQUIREMENTS

The reactive power, injected into the grid, needed to keep the PCC voltage at nominal level is investigated in this section. The SCR is 10 for every combination and the SCIR has the values of 0.5, 2.5, 10 and 20. The base power, 1pu of the wind farm is the total nominal active power of the wind farm. The seven variants investigated of the hybrid wind farm electrical system are presented in Table I.

TABLE I
THE DIFFERENT ELECTRICAL SYSTEM
FORMATION IN THE HYBRID WIND FARM.

Variant	Type of electrical system
A	VSI
B	IG + VSI reactive power injector
C	THY(CF) + VSI reactive power injector
D	THY(OPT) + VSI reactive power injector
E	IG+THY(CF) + VSI reactive power injector
F	IG+THY(OPT) + VSI reactive power injector
G	IG+THY(OPT)+VSI

To control the voltage at PCC all variants, A to G, have a capacitor battery, in some cases an inductor, which injects a constant value of reactive power to the grid. Furthermore, a VSI is used in every variant to actively control the voltage level at PCC by injecting reactive power. For the variants A and G the existing VSI is used. But, for the other variants, B to F, a VSI that only operates as a reactive power injector is used. In the G alternative, the VSI delivers one third of the total farm active power and also injects reactive power to the grid.

The capacitor battery is designed to deliver the mean demanded reactive power. The remaining part of the required reactive power is handled by the VSI. In this way, the VSI can be dimensioned as small as possible.

If the hybrid farm contains THYs, the capacitor battery can be designed as a tuned filter to remove harmonic currents from the grid.

The injected reactive power required for the different farm and grid configurations is shown in Figures 7 to 10. As shown, the reactive power demands changes substantially depending on the

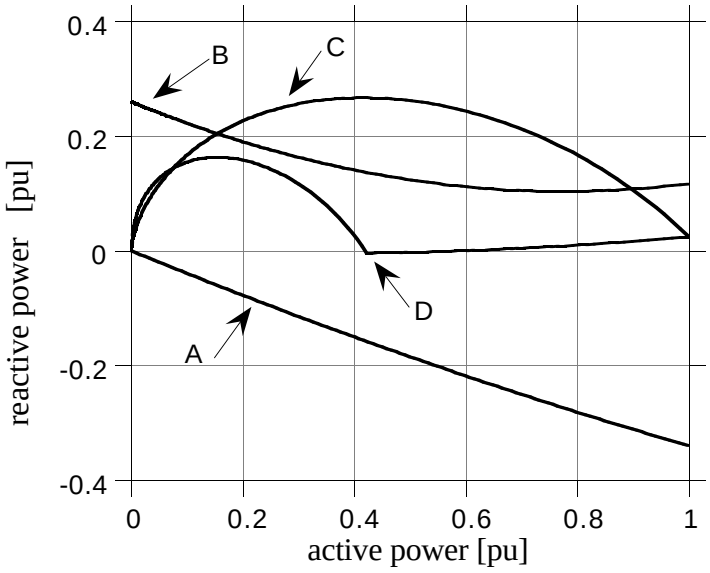

Figure 7: The injected reactive power required to maintain nominal PCC voltage. SCR is 10 and SCIR is 2.5. The electric system configurations are shown in Table I.

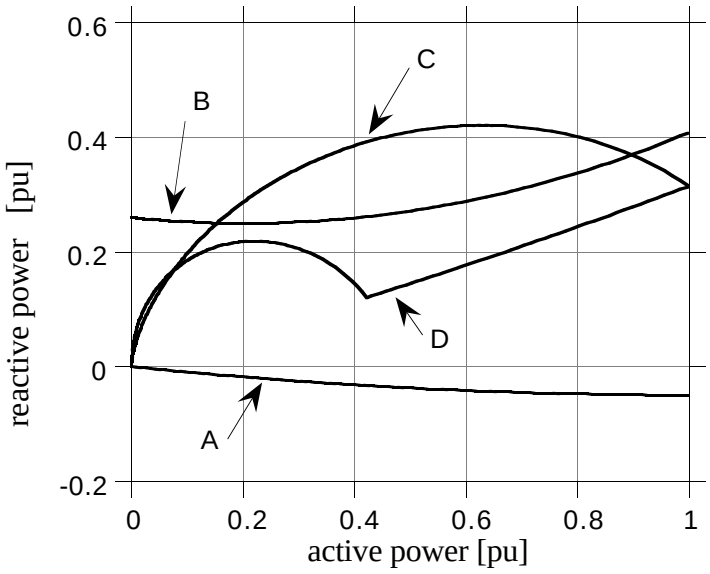

Figure 8: The injected reactive power required to maintain nominal PCC voltage. SCR is 10 and SCIR is 10. The electric system configurations are shown in Table I.

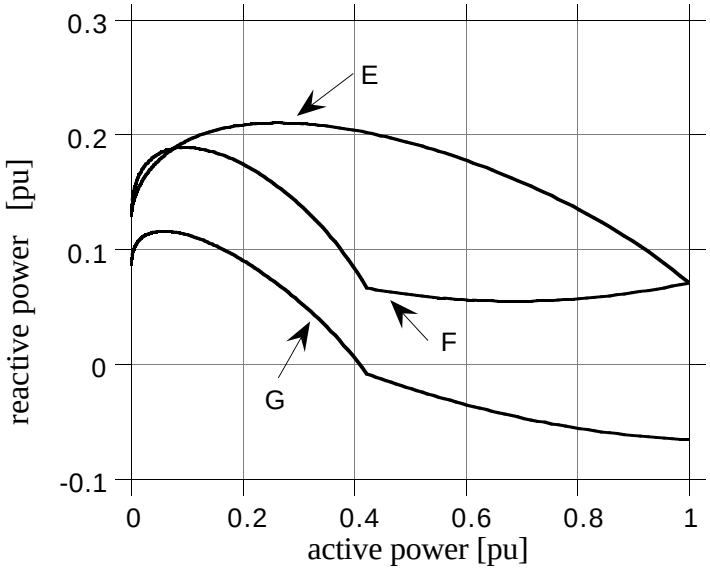

Figure 9: The injected reactive power required to maintain nominal PCC voltage. SCR is 10 and SCIR is 2.5. The electric system configurations are shown in Table I.

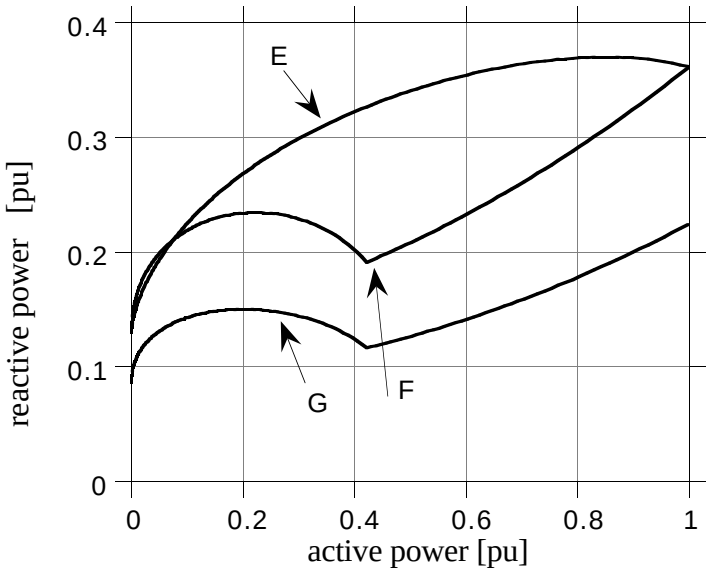

Figure 10: The injected reactive power required to maintain nominal PCC voltage. SCR is 10 and SCIR is 10. The electric system configurations are shown in Table I.

grid and the farm configuration. In some cases the demanded reactive power is inductive. The results are summarized in Table II for the different farm and grid constellations; the max and min reactive power; the size of reactive battery and the size of VSI are tabled. The VSI scale factor is also tabled, i.e. how much larger the VSI must be to handle both active and reactive power instead of only active power.

When the reactive power demand is almost constant due to active power variation, the size of the VSI can be minimized. For low values of SCIR, 0.5 and below, the required size of VSI becomes large and thus expensive. For these low SCIRs the cost of keeping a constant voltage will probably be unrealisticly high. However, the SCIR is usually high enough, at least for transmission lines with a capacity of 50 MVA or higher. The reactive power demand is approximately the same for SCIR of 10 and above. The SCIR of 10 to infinity is the same as SCIA of 84° to 90°. In Figures 4 and 5 the voltage variations at high SCIAs are almost the same. For the IG and VSI injector, variant B, and low SCIR, no capacitor battery should be used to compensate the IG reactive power if the PCC voltage level is to be controlled. Of course the grid current will increase, leading to increased transmission losses due to the increased reactive current.

When comparing the different modes of the THYs it is found that the CF-mode demands a larger VSI injector. Also the capacitor battery needs to be larger than that for the OPT-mode. But, when adding IG to the system, variants E and F, the two systems get the same characteristics, since, the reactive characteristics of the IG and the THY are smoothing each other.

The VSI injector size is maximum 0.21 pu when the VSI only is used as a reactive power injector for the hybrid farm and the SCR is 10 and the SCIA is 2.5 or higher. When the hybrid farm consists of IG, THY, VSI and each subsystem takes one third of the active farm power, case G, the VSI only needs to increase about 5% to eliminate the voltage variation. The capacitor battery is approximately 0.10 pu. If SCIR is larger than 2 it will be no problem to control the voltage at the PPC.

TABLE II
THE DEMANDED REACTIVE POWER TO MAINTAIN
THE NOMINAL VOLTAGE LEVEL AT PCC.

Variants	SCIR 0.5	SCIR 2.5	SCIR 10	SCIR 20
A: MinQ [pu]	-1.98	-0.42	-0.050	-0.0125
MaxQ [pu]	0.66	0.12	0.035	0.0196
Q(C or L) [pu]	-0.66	-0.15	-0.007	0.0035
Q(VSI) [pu]	1.32	0.27	0.042	0.016
VSI scale	66%	3.6%	≈0%	≈0%
B: MinQ [pu]	-1.1439	0.1036	0.2498	0.2574
MaxQ [pu]	0.26	0.2598	0.4079	0.4576
Q(C or L) [pu]	-0.44	0.1817	0.3289	0.3575
Q(VSI) [pu]	0.70	0.0781	0.0790	0.1001
C: MinQ [pu]	-1.2374	0	0	0
MaxQ [pu]	0.0391	0.2670	0.4206	0.4529
Q(C or L) [pu]	-0.5991	0.1335	0.21	0.2264
Q(VSI) [pu]	0.6382	0.1335	0.21	0.2264
D: MinQ [pu]	-1.2374	-0.0042	0	0
MaxQ [pu]	0.0568	0.1632	0.3145	0.3642
Q(C or L) [pu]	-0.5903	0.0795	0.1572	0.1821
Q(VSI) [pu]	0.6471	0.0837	0.1572	0.1821
E: MinQ [pu]	-1.1906	0.0709	0.1299	0.1299
MaxQ [pu]	0.1353	0.2103	0.3698	0.4139
Q(C or L) [pu]	0.5277	0.1406	0.2498	0.2719
Q(VSI) [pu]	0.6630	0.0697	0.12	0.1420
F: MinQ [pu]	-1.1906	-0.0548	0.1299	0.1299
MaxQ [pu]	0.1446	0.1888	0.3612	0.4109
Q(C or L) [pu]	-0.5230	0.1218	0.2455	0.2704
Q(VSI) [pu]	0.6676	0.067	0.1157	0.1405
G: MinQ [pu]	-1.32	-0.066	0.0866	0.0866
MaxQ [pu]	0.0932	0.1159	0.2243	0.2739
Q(C or L) [pu]	-0.6172	0.0249	0.1554	0.1803
Q(VSI) [pu]	0.7104	0.0910	0.0688	0.0937
VSI scale	138%	3.6%	2.1%	3.9%

6. CONCLUSION

In this paper a hybrid wind farm connected to a weak grid has been investigated. It is shown that the voltage can be kept constant utilizing a VSI and properly sized capacitor battery providing that SCIR is higher than approximately 2. If SCIR is lower than 1, the reactive power needed to keep the voltage constant becomes unrealistically high.

The VSI injector size is maximum 0.21 pu when the VSI only is used as a reactive power injector for the hybrid farm and the SCR is 10 and the SCIA is 2.5 or higher.

The most advantageous configuration is the variant G, where the hybrid farm consists of IG, THY, VSI and each subsystem takes one third of the active farm power. The VSI

only needs to increase about 5% to eliminate the voltage variation. The capacitor battery is approximately 0.10 pu.

7. REFERENCES

[1] F. Santjer and G. Gerdes, “Netzrückwirkungen, verursacht durch den Betrieb von Windkraftanlagen am Netz,” *DEWI Magazin*, pp. 35-41, August 1994.

[2] A. Stampa and F. Santjer, “Synchronisation von netzgekoppelten Windenergieanlagen in einem Windpark,” *DEWI Magazin*, pp. 80-86, August 1995.

[3] A. Grauers, “Higher electrical effiency with variable speed,” *presented at ECWEC'93*, pp. 656-658, Travemünde, March 1993.

[4] O. Carlson, A. Grauers, J. Svensson, and Å. Larsson, “A comparision between electrical systems for variable speed operation of wind turbines,” *presented at EWEC'94*, pp. 500-505, Thessaloniki, October 1994.

[5] K. Thorborg, *Power Electronics - in Theory and Practice*. Lund, Sweden: Studentlitteratur, 1993.

[6] J. Svensson, “Voltage Angle Control of a Voltage Source Inverter — Application to a Grid-Connected Wind Turbine,” presented at EPE'95, pp. 539-544, Sevilla, Spain, September 1995.

[7] A. Grauers, “Synchronous generator and frequency converter in wind turbine applications: system design and efficiency,” Chalmers University of Technology, School of Electrical and Computer Engineering, Göteborg, Sweden Technical Report No. 175L, May 1994.

PAPER 1C

J. Svensson, "The Rating of the Voltage Source Inverter in a Hybrid Wind Park with High Power Quality," *European Wind Energy Conference (EWEC'97)*, Dublin, Ireland, 6-9 October 1997, (in press).

The Rating of the Voltage Source Inverter in a Hybrid Wind Park with High Power Quality

Jan Svensson

Department of Electric Power Engineering
Chalmers University of Technology
S-412 96 Göteborg, Sweden

Abstract: A hybrid wind park consists of wind turbines which have different electrical systems: directly connected induction generators (IG) and variable-speed electrical systems. One of the variable-speed electrical systems has a voltage source inverter (VSI) connected to the grid, the others have grid-commutated inverters (GCI). The VSI can be used for reactive power compensation and active filtering, in addition to converting wind power. These additional features cause an increase of the VSI rating. The degree of over-rating depends on the wind park configuration. In a three-turbine wind park, consisting of an IG, a GCI and a VSI of equal rated active power, the rated current of the VSI becomes 1.33 pu for the rms-current comparison and 1.73 pu for the peak-to-peak current comparison. When a 5th-harmonic passive shunt filter is used to cancel the 5th harmonic current from the GCI and to produce the mean consumed reactive power of the wind park, the rated power of the VSI becomes 1.06 pu for the rms-current comparison and 1.2 pu for the peak-to-peak current comparison.

1. INTRODUCTION

The interest in the variable speed operation of wind turbines has increased in recent years because of the potential to improve the total wind turbine system performance. Usually, grid-commutated inverters (GCI), equipped with thyristors, are used on the grid side of the electrical system. The cost for these converters is rather low and the efficiency high. However, there are two problems associated with GCIs: low-frequency current harmonics are injected into the grid and the GCI consumes reactive power. Wind parks are often located in rural areas where the grid is often weak, i.e., the grid has a relatively low short-circuit power. A wind park connected to a weak grid will increase the voltage variations, and variable speed systems with GCI will also increase the voltage harmonic distortion. Today, these problems are solved by increasing the short-circuit power of the grid. Another solution is to equip all wind turbines with forced-commutated voltage source inverters (VSI), but the VSI costs more and has a lower efficiency than the GCI.

The benefits of all systems can be utilized by a hybrid wind park consisting of wind turbines which have different electrical systems: directly connected induction generators (IG) and variable-speed electrical systems. One of the variable-speed electrical systems has a VSI connected to the grid, the others have GCIs.

This paper deals with a hybrid configuration of a wind park, consisting of up to 3 turbines. The investigation is a continuation of [1], in which the focus was on reactive power compensation and the voltage level at the point of common connection (PCC). Here, the emphasis is on the rated current of the VSI when it converts active power and simultaneously operates as an active filter and a reactive power compensator. The rated

active powers of the VSI, the IG and the GCI are assumed to be equal, and the total reactive power to the grid is set to zero to obtain a unity power factor. The required size of the VSI in different systems and operating modes is investigated.

2. THE SYSTEM CONFIGURATION

The hybrid wind park configuration is shown in Figure 1. The variable-speed systems use synchronous generators (SG) together with rectifiers. A 5th-harmonic passive shunt filter (PSF) is connected to the PCC.

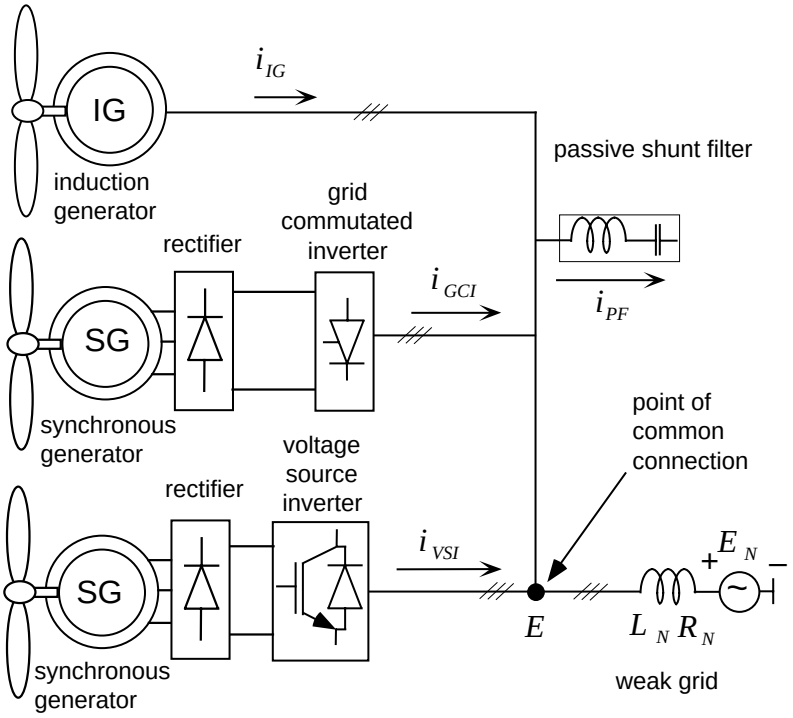

Figure 1: The hybrid wind park configuration.

For the variable-speed system with the GCI, two DC-link voltage control strategies can be used to control the SG. They are the constant flux mode (CF) and the optimal efficiency (OE) mode [1,2].

3. THE POWER QUALITY OF THE TURBINES

A. Reactive Power

Since the reactive power consumed by the IG and the GCI cannot be controlled, the voltage level of the PCC will vary if the grid is weak. The two different control methods of the GCI will also affect the grid voltage differently. Figure 2 shows the reactive power of the IG and the GCI as a function of the active power. The units are in the process of consuming reactive power and delivering active power to the grid. For a typical 400 kW IG, the reactive power varies from approximately –0.26 pu to –0.46 pu. The reactive power of the GCI goes from 0 to –0.36 pu. The CF-mode has the largest reactive power span, from 0 to –0.46 pu. The reason for the different reactive power functions for the two types of GCI control methods is that the DC-link voltage is higher in the OE mode at

intermediate wind speeds. The minimum advance angle of 20° is a trade-off between the DC-link voltage and safety margins of commutation failures.

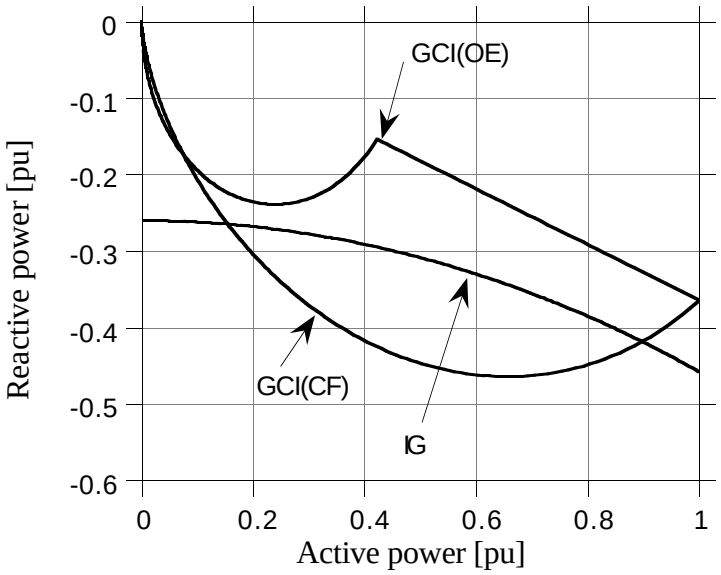

Figure 2: The reactive power (generator reference) as a function of the active power for the IG and the GCI. The GCI uses CF and OE modes.

The PSF produces a constant reactive power and is designed to deliver the mean reactive power consumed by the GCI and the IG, in the wind speed span from 0 to 1 pu. Due to the vector current controller of the VSI, the reactive power can be controlled independently of the active power.

B. Low-frequency Harmonics

The GCI produces low-frequency current harmonics with amplitudes dependent on the active power level. In the following analysis, the phase currents of the GCI will have a quasi square wave form due to a smoothing dc-link inductor [3]. Harmonics up to the 31st order are taken into consideration.

The vector-controlled VSI can act as an active shunt filter and cancel the current harmonics of the 5th, 7th 11th and 13th order. Furthermore, the VSI and its control system are assumed to operate ideally. Of course, active filters can cancel higher-order harmonics, but then the losses of the VSI increase.

4. METHOD OF ANALYSIS

The required rated power of the VSI is analysed in various cases: when the VSI acts as an energy converter, a reactive power compensator, an active filter or as a combination of these acting modes.

The current rating of the VSI can be determined either by the rms-value or the peak-to-peak value of the current. For sinusoidal currents, the two methods result in the same converter rating. If the current from the VSI is distorted, the two methods will differ. Depending on the type of valves the VSI is equipped with, one of the two methods is more appropriate to use. The rms current of the VSI is a degree of total losses in the valves. Thus, the rms-current value of the VSI for non-sinusoidal currents can be

compared with the rated sinusoidal current of a standard VSI. The peak-to-peak current value of the VSI should be used when the maximum current of the valves is the limiting factor. In this case, the peak-to-peak current of the VSI must be compared with the sinusoidal peak-to-peak current of a standard VSI. The most usual valves in medium-sized inverters are IGBTs. The IGBT does not have a maximum current limit, as the IGCT has [4], but the IGBT must be protected from overheating. Table 1 displays the maximum, minimum and the mean consumed reactive powers for different wind park configurations together with the wind speed corresponding to the mean reactive power.

TABLE 1
THE MAXIMUM, THE MINIMUM AND THE MEAN REACTIVE POWER (GENERATOR REFERENCE) FOR DIFFERENT CONFIGURATIONS. THE WIND SPEED VARIES BETWEEN 0 AND 1 PU.

Configuration	$Q_{\max}$ [pu]	$Q_{\min}$ [pu]	Q_{mean} [pu]	wind speed [pu] corresponding to Q_{mean}
IG	–0.46	–0.26	–0.36	0.89
GCI(CF)	–0.46	0	–0.23	0.50
GCI(OE)	–0.36	0	–0.18	0.44
IG + GCI(CF)	–0.84	–0.26	–0.55	0.56
IG+GCI(OE)	–0.82	–0.26	–0.54	0.84

An example of the time variation of the currents is shown in Figures 3 and 4, when the wind park consists of a VSI, an IG and a GCI. The VSI operates as a reactive power compensator and an active filter in addition to active power generation. In Figure 3, the GCI current and the grid voltage for wind speeds of 0.7 pu and 1.0 are presented together with the grid voltage. The resulting VSI current and its fundamental component are shown in Figure 4. The peak-to-peak value of the VSI current at a wind speed of 1.0 pu becomes 1.73 pu, and the fundamental current component becomes 1.3 pu. Consequently, the active filter option requires a considerable increase of the rated current of the VSI.

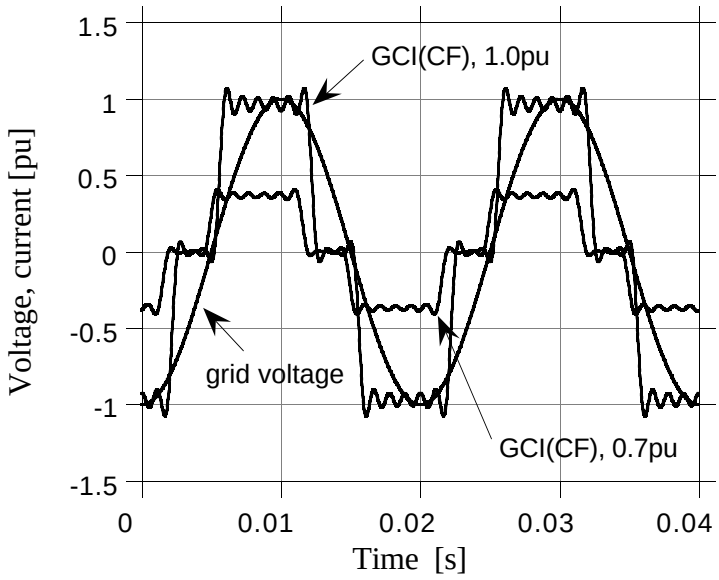

Figure 3: The GCI(CF) currents and the grid voltage for wind speeds 0.7 pu and 1.0 pu.

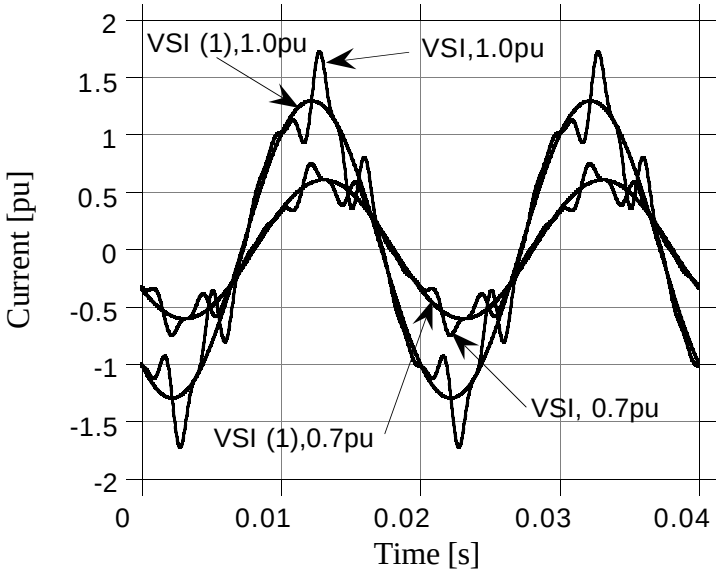

Figure 4: The VSI current and its fundamental component, VSI(1), for wind speeds 0.7 pu and 1.0 pu.

5. INVESTIGATED WIND PARK CONFIGURATION

Ten different wind park configurations were investigated as described in Table 2. Configurations A and F correspond to the active power production combined with the reactive effect compensation or active filtering. In configurations B to E, the VSI acts as an active filter and as a reactive power compensator. For the other variants (G to K), the VSI acts as an active power converter and the active filter and reactive power compensation modes alter.

TABLE 2
THE DIFFERENT WIND PARK CONFIGURATIONS THAT HAVE BEEN SIMULATED.
THE VSI COMPENSATES FOR THE ACTIVE POWER AND/OR REACTIVE POWER AND/OR CURRENT HARMONICS.

Variant (and total active power)	VSI as active power converter	Reactive power compensated by the VSI	Orders of filtered harmonics
A (3 pu)	yes	IG, GCI	
B (1 pu)	no	GCI	5, 7, 11, 13
C (1 pu)	no	PSF, GCI	7, 11, 13
D (2 pu)	no	IG, GCI	5, 7, 11, 13
E (2 pu)	no	PSF, IG, GCI	7, 11, 13
F (1 pu)	yes		5, 7, 11, 13
G (2 pu)	yes	GCI	5, 7, 11, 13
H (2 pu)	yes	PSF, GCI	7, 11, 13
J (3 pu)	yes	IG, GCI	5, 7, 11, 13
K (3 pu)	yes	PSF, IG, GCI	7, 11, 13

6. RESULT EVALUATION

Table 3 presents the maximum rated current of the VSI for wind speeds from 0 to 1 pu for the wind park configurations described in Table 2.

TABLE 3
THE MAXIMUM CURRENT OF THE VSI FOR THE WIND SPEED SPAN 0 TO 1 PU AND FOR DIFFERENT SYSTEM VARIANTS.

Variants	Maximum peak value [pu]		Maximum RMS value [pu]	
	CF-mode	OE-mode	CF-mode	OE-mode
A	1.30	1.30	1.30	1.30
B	0.74	0.73	0.52	0.47
C	0.47	0.47	0.28	0.27
D	1.13	1.12	0.88	0.87
E	0.56	0.56	0.34	0.35
F	1.10	1.10	1.04	1.04
G	1.38	1.38	1.10	1.10
H	1.17	1.18	1.03	1.04
J	1.73	1.73	1.33	1.33
K	1.20	1.20	1.06	1.06

A. The RMS-Current Comparison

In this section, the rms-current comparisons of different wind park configurations are in focus. If the wind park consists only of a GCI and a VSI which acts as an active filter and reactive power compensator (B), the rated VSI size becomes 0.52 pu for the CF mode and 0.47 pu for the OE mode. The rms-current of the VSI as a function of the wind speed is shown in Figure 5. By introducing a PSF (C), the VSI size will be reduced to 0.28 pu and 0.27 pu for the CF-mode and the OE-mode, respectively. Furthermore, the OE mode of the GCI decreases the current of the VSI below the rated wind speed, as shown in Figure 5. The current reduction is important because the mean wind speed is lower than the rated wind speed of the wind power plants, and lower rms-currents result in a greater efficiency. If an IG is added to the wind park (D, E), the consumed reactive

power is increased. It is obvious, according to Figure 6, that the use the PSF is an advantage. The rated current of the VSI is 0.87 pu without the PSF, and by using the PSF it decreases to 0.34 pu, a reduction of 61%.

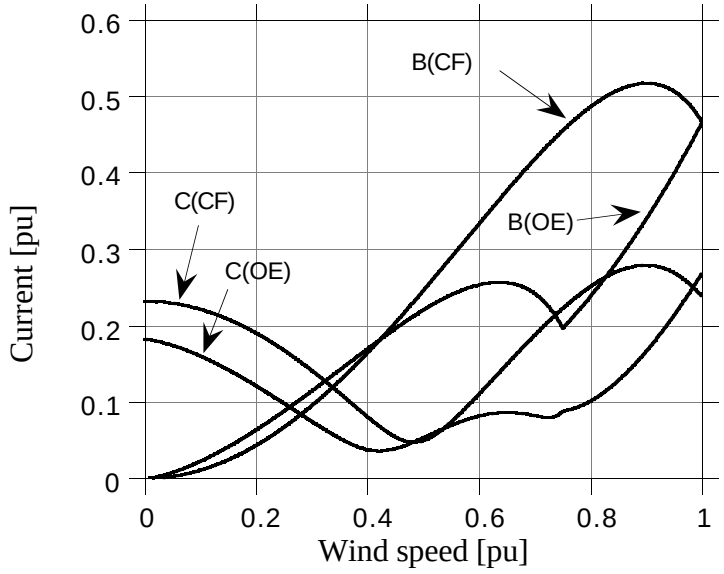

Figure 5: The rms-current of the VSI as a function of the wind speed. Wind park variants B and C are displayed.

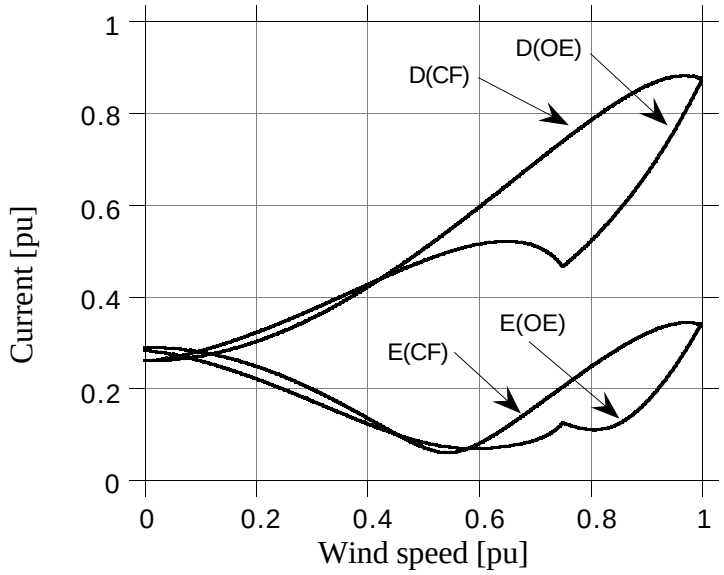

Figure 6: The rms current of the VSI as a function of the wind speed. Wind park variants D and E are displayed.

The complete wind park (variant K), consists of an IG, a GCI(OE), a PSF and a VSI. The VSI operates as an active power converter, an active filter and a reactive power compensator. The rated current of the VSI becomes 1.06 pu with and 1.33 pu without the PSF, according to Figure 7. When introducing the PSF, the VSI must consume reactive power at low wind speeds, because the IG and the GCI consume less reactive power than the reactive power produced by the PSF. The VSI current is thus higher at low wind speeds when the PSF is used. The crossing point for the VSI currents is at a

low wind speed, approximately 0.1 pu in Figure 7. At low wind speeds the captured wind power is low, resulting in a minor current, and the losses become low or the turbines are shut off.

If a PSF is used, the IG does not influence the rated current of the VSI, as demonstrated in Figures 7 and 8. The addition of an IG increases the rated current of the VSI by 21% without the PSF but only by 3% with the PSF. Because of the almost constant reactive power demand of the IG, the current increase is low.

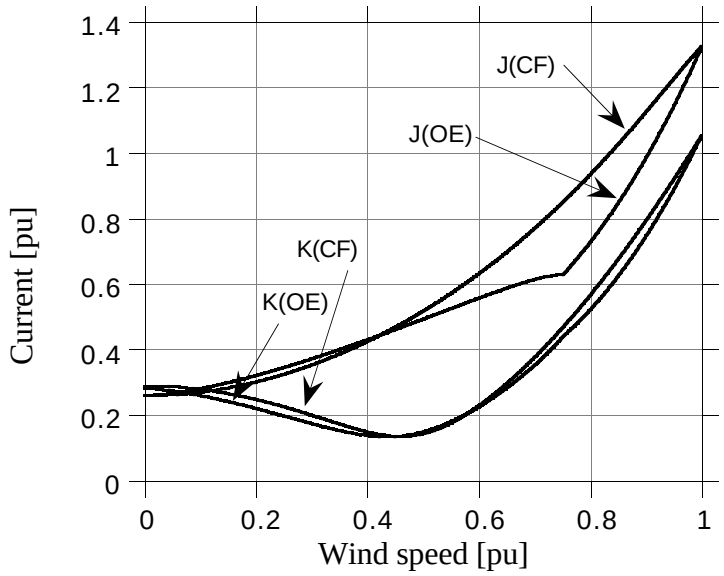

Figure 7: The rms current of the VSI as a function of the wind speed. Wind park variants J and K are displayed.

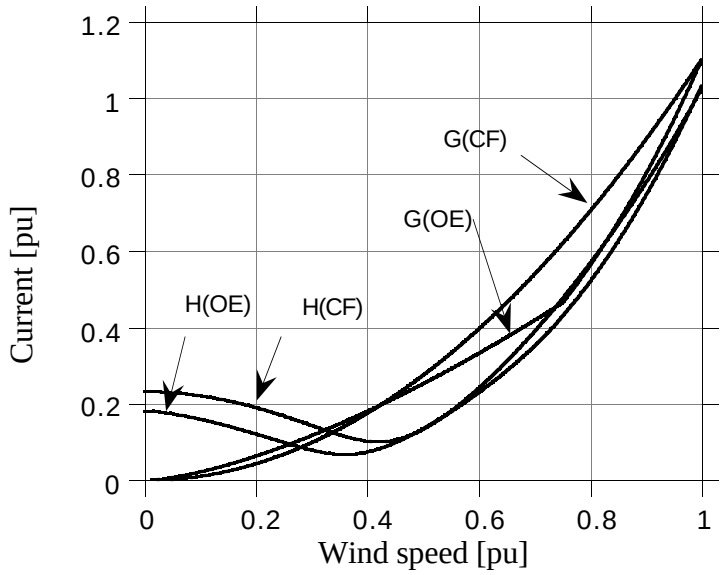

Figure 8: The rms-current of the VSI as a function of the wind speed. Wind park variants G and H are displayed.

B. The Peak-to-peak Current Comparison

The results of the peak-to-peak current demand of the VSI in the different wind park configurations have almost the same characteristics as the rms-current demand. The peak-to-peak current is scaled up compared with the rms-current in the same wind park configuration. The result of the wind park variant K is shown in Figure 9. The VSI current increases by 13% when the peak-to-peak current method is used. The largest increase is 74% for the wind park variant C. As in the rms case, the OE mode of the GCI reduces the current above 0.5 pu wind speeds, and the use of a PSF results in a lower VSI.

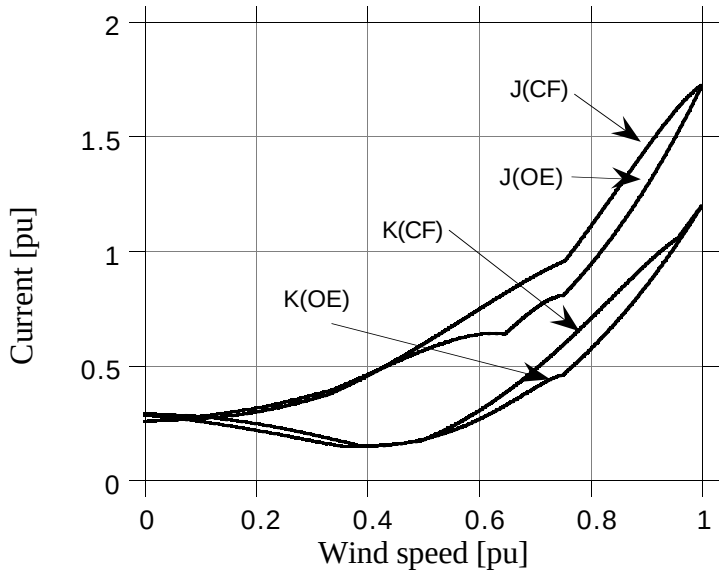

Figure 9: The peak-to-peak current of the VSI as a function of the wind speed. Wind park variants J and K are displayed.

6. CONCLUSION

In a hybrid wind park, the VSI can be used for reactive power compensation and active filtering in addition to converting wind power. These additional features cause an increase of the VSI rating. The degree of over-rating depends on the wind park configuration.

In a three-turbine wind park, consisting of an IG, a GCI and a VSI of equal rated active power, the rated current of the VSI becomes 1.33 pu for the rms-current comparison and 1.73 pu for the peak-to-peak current comparison. When a 5th-harmonic passive shunt filter is used to cancel the 5th harmonic current from the GCI and to produce the mean consumed reactive power of the wind park, the rated power of the VSI becomes 1.06 pu for the rms-current comparison and 1.2 pu for the peak-to-peak current comparison.

7. REFERENCES

[1] Svensson, J., "Possibilities by Using a Self-commutated Voltage Source Inverter Connected to a Weak Grid in Wind Parks," 1996 European Union Wind Energy Conference and Exhibition, Göteborg, Sweden, 20-24 May 1996, pp. 492-495.

[2] Grauers, A., “Synchronous Generator and Frequency Converter in Wind Turbine Applications: System Design and Efficiency,” Chalmers University of Technology,

School of Electrical and Computer Engineering, Göteborg, Sweden Technical Report No. 175L, May 1994.

[3] Thorborg, K., *Power Electronics - in Theory and Practice*. Lund, Sweden: Studentlitteratur, 1993.

[4] Gruening, H. E., Ödegard, B., "High Performance Low Cost MVA Inverters Realised with Integrated Gate Commutated Thyristors (IGCT)," 7th European Conference on Power Electronics and Applications (EPE'97), Trondheim, Norway, 8-10 September 1997. Proceedings,vol. 2, pp. 60-65.

PAPER 2A

J. Svensson, "Voltage Angle Control of a Voltage Source Inverter — Application to a Grid-Connected Wind Turbine," *6th European Conference on Power Electronics and Applications (EPE'95)*, Sevilla, Spain, 19-21 September 1995. Proceedings, Vol. 3, pp. 539-544.

Voltage Angle Control of a Voltage Source Inverter — Application to a Grid-Connected Wind Turbine

J. Svensson

Chalmers University of Technology, Sweden

Abstract: The voltage angle control of an inverter connected to the grid in a wind turbine application is presented. To analyse the system and find out the proper parameters of the controller the system is linearized at an operating point. The inverter is modelled by using only fundamental voltages. By using a PI-controller for the DC-link voltage and feedforward of the generator/rectifier current the voltage angle control can be used. The bandwidth of the inverter system is approximately 20 to 30 Hz. The parameters and the bandwidth of the system are determined by the allowed DC-link voltage fluctuation. The system can be analysed using a linearized model unless the series inductance is very large. The controller using feedforward is insensitive to series inductance variations, and the fluctuations depend on the size of the DC-link capacitor and the frequency and amplitude of the generator/rectifier current.

Keywords: PWM, GRID, INVERTER, VOLTAGE ANGLE, WIND, ENERGY

I. INTRODUCTION

Wind turbines using variable speed have many advantages in comparision with constant speed wind turbines for alternative electrical energy production. For instance, the use of variable speed improves the dynamic behaviour of the turbine and, thereby, alleviates stresses and prolongs the lifetime of the system. By decreasing the stresses on the mechanical construction of the wind turbine, it can be made lighter and, therefore, cheaper. The power production of the wind turbine can be increased by about 5 %, Grauers (1) and Leithead (2), and the noise from the wind turbines is reduced at low wind speeds, Lowson (3). The disadvantage is a more complex electrical wind turbine system which often results in a more expensive system than the electrical one for a constant speed system. There is also a risk for excitating of structural resonances, for example in the tower.

Till now, the most commonly used electrical system for a variable speed wind turbine has consisted of a synchronous generator connected to the grid over a thyristor/diode rectifier and a thyristor inverter. Due to the fast development of rapid switching valves with high power ratings, the use of forced-commutated converters is increasing in wind power application. By using forced-commutated inverters connected to the grid, current harmonics from the inverter are decreased, when compared with the grid-commutated inverter, which results in a smaller grid filter. Moreover, by using a forced-commutated inverter, any desired power factor can be obtained and the energy can flow in both directions. This can be useful when starting up the wind turbine and use the generator as a motor.

There are different methods for controlling the forced-commutated inverter connected to the grid. The most common methods for controlling the voltage source inverter use a fast

current closed-loop, see Malesani and Tomasin (4) for a survey. Another method described in Pierik et al (5) shows an electrical system for a wind turbine using current hysteres control of the inverter.

Here, the possibility of using a cheap and simple controller is investigated. The method for controlling the inverter is based on controlling the voltage angle of the inverter where the active power is proportional to the phase displacement angle, Verdelho and Marques (6). This control method is investigated for HVDC application, Ekström (7) and Ooi and Wang (8), and for a VAR compensator, Joos el al (9). Further on, suitable models for the inverter system are examined and the system performance in a wind turbine application is determined. In addition the performance sensitivity to system parameter variations is investigated.

II. THE SYSTEM CONFIGURATION

The electrical system of the wind turbine can be divided into two subsystems, the generator/rectifier system and the inverter system. The best alternative for the generator/rectifier system is to choose a synchronous generator and a diode rectifier, see Carlson et al (10). Such a choice is based on low cost and high efficiency compared with an induction generator connected to a forced-commutated rectifier. When the speed of the synchronous generator alternates, the voltage value at the DC-side of the diode rectifier will change. A voltage-stiff forced-commutated inverter utilizes a stiff DC-link voltage. A step-up chopper is used to adapt the rectifier voltage to the DC-link voltage of the inverter, see Figure 1. When the inverter system is analysed, the generator/rectifier system can be modelled as an ideal current source. The step-up chopper or the forced-commutated rectifier utilize a high switching frequency so the bandwidth of these components is much higher than the bandwidth of the generator.

The generator/rectifier current is denoted as $i_{dc}(t)$ and is independent of the value of the DC-link voltage. The capacitor of the DC-link has the value C_{dc}. The inductors at the AC-side of the inverter have the inductance L_s and the resistance R_s. The three-phase voltage system of the grid has phase voltages $e_1(t)$, $e_2(t)$ and $e_3(t)$ and the phase currents are denoted as $i_1(t)$, $i_2(t)$ and $i_3(t)$. The DC-link voltage value is denoted as $u_{dc}(t)$ and the current in the DC-link to the inverter is called $i_V(t)$.

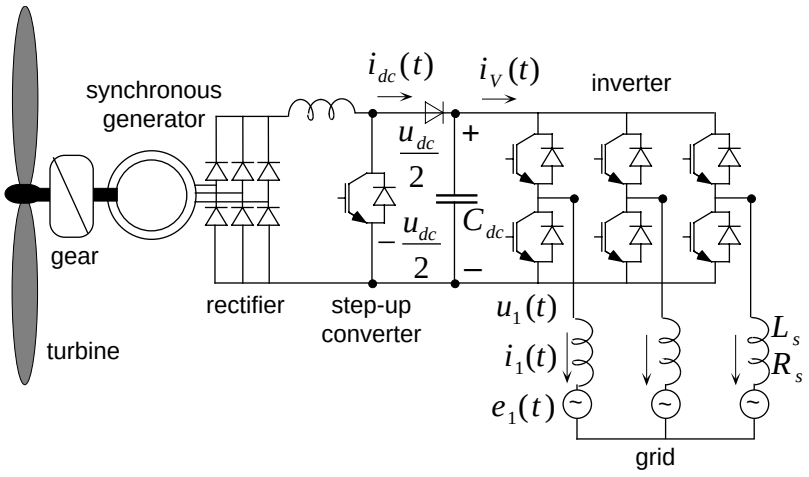

Figure 1: The system configuration.

III. THE BASIC IDEA OF VOLTAGE ANGLE CONTROL

The basic idea of voltage angle control is to vary the phase displacement angle θ between the three-phase voltage of the inverter and the three-phase voltage of the grid. The difference in voltage between the three-phase voltage of the inverter and the three-phase voltage of the grid will be placed over an inductance in each phase. The active power from the inverter to the grid is, if the inductance resistance is negligible,

$$P = \frac{EU}{\omega_N L_s}\sin(\theta) \approx \frac{EU}{\omega_N L_s}\theta \tag{1}$$

where *E* and *U* are the main rms-voltages of the inverter and the grid. The grid angular frequency is denoted as ω_N. If the phase displacement angle is small the reactive power to the grid will be

$$Q \approx \frac{E}{\omega_N L_s}(U - E) \tag{2}$$

IV. A NON-LINEAR MODEL OF THE SYSTEM

The space vector voltage of the grid is

$$\underline{e}(t) = Ee^{j\omega_N t} \tag{3}$$

and the space vector voltage of the inverter is

$$\underline{u}(t) = Ue^{j\omega t} \tag{4}$$

where ω is the angular frequency of the inverter. The phase currents in space vector form can be obtained from, see Figure 1,

$$\underline{u}(t) - \underline{i}(t)R_s - \frac{d\underline{i}(t)}{dt}L_s - \underline{e}(t) = 0 \tag{5}$$

Here, the phase displacement angle $\theta(t)$ is equal to

$$\theta(t) = \int_0^t \left(\omega(\tau) - \omega_N\right)d\tau \tag{6}$$

Equation 5 can be rewritten in component form in the *dq*-coordinate system as

$$\frac{d}{dt}i_d(t) = -\frac{1}{L_s}U\sin\left(\theta(t)\right) - \frac{R_s}{L_s}i_d(t) + \omega_N i_q(t) \tag{7}$$

$$\frac{d}{dt}i_q(t) = \frac{1}{L_s}U\cos\left(\theta(t)\right) - \frac{1}{L_s}e_q(t) - \frac{R_s}{L_s}i_q(t) - \omega_N i_d(t) \tag{8}$$

When the valves are ideal, the DC-link current $i_V(t)$ can be written as

$$i_V(t) = \frac{u_d(t)i_d(t) + u_q(t)i_q(t)}{u_{dc}(t)} \tag{9}$$

The voltage across the DC-link capacitor can be expressed as

$$u_{dc}(t) = \frac{1}{C_{dc}}\int_0^t \left(i_{dc}(\tau) - i_V(\tau)\right)d\tau \tag{10}$$

The DC-link voltage $u_{dc}(t)$ is controlled by using the amplitude of the three-phase voltage and the phase displacement angle $\theta(t)$ of the inverter.

V. THE REDUCED NON-LINEAR MODEL

In Figure 2 a reduced non-linear model, i. e. a non-harmonic model, is shown. The "*" means reference value. The control of the inverter has two input signals. They are the phase displacement angle $\theta(t)$ and the relative voltage $u_x(t)$. The grid is supposed to be constant, in other words the frequency and voltage amplitude of the grid are constant. The main rms-voltage of the inverter can be written as

$$U(t) = u_x(t)E \tag{11}$$

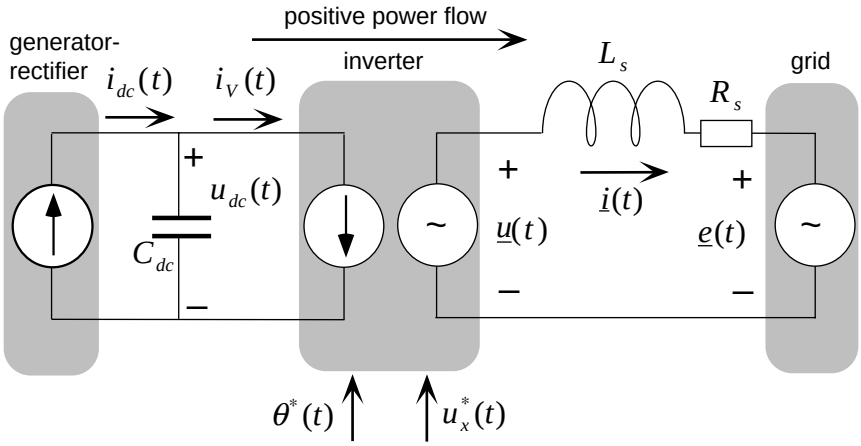

Figure 2: A reduced non-linear model of the system.

VI. THE LINEARIZATION OF THE SYSTEM AT AN OPERATING POINT

Let the operating points be denoted with the index "0" and the variables perturbation around the variable operating points be denoted with the index "Δ." The linearized currents of the inverter can be solved by means of the state equation

$$\frac{d}{dt}\begin{bmatrix}\Delta i_d(t)\\ \Delta i_q(t)\end{bmatrix} = \mathbf{A}\begin{bmatrix}\Delta i_d(t)\\ \Delta i_q(t)\end{bmatrix} + \mathbf{B}\begin{bmatrix}\Delta\theta(t)\\ \Delta u_x(t)\end{bmatrix} \tag{12}$$

and the linearized DC-link current is written as

$$\Delta i_V(t) = \mathbf{C}\begin{bmatrix}\Delta i_d(t)\\ \Delta i_q(t)\end{bmatrix} + \mathbf{D}\begin{bmatrix}\Delta\theta(t)\\ \Delta u_x(t)\end{bmatrix} \tag{13}$$

where

$$\mathbf{A}=\begin{bmatrix} -\frac{R_s}{L_s} & \omega_N \\ -\omega_N & -\frac{R_s}{L_s} \end{bmatrix} \qquad \mathbf{B}=\begin{bmatrix} -\frac{e_q}{L_s}u_{x0}\cos\theta_0 & -\frac{e_q}{L_s}\sin\theta_0 \\ -\frac{e_q}{L_s}u_{x0}\sin\theta_0 & \frac{e_q}{L_s}\cos\theta_0 \end{bmatrix}$$

$$\mathbf{C}=\frac{\begin{bmatrix} u_{d0} \\ u_{q0} \end{bmatrix}^T}{u_{dc0}}=\begin{bmatrix} \frac{u_{d0}}{u_{dc0}} & \frac{u_{q0}}{u_{dc0}} \end{bmatrix} \qquad \mathbf{D}=\frac{L}{u_{dc0}}\begin{bmatrix} i_{d0} \\ i_{q0} \end{bmatrix}^T\cdot\mathbf{B}$$

By putting the state equations 12 and 13 representing the inverter and the DC-link voltage Equation 10 together, a new state equation with three states and three inputs and one output will be achieved. The state equation becomes

$$\frac{d}{dt}\begin{bmatrix} \Delta i_d(t) \\ \Delta i_q(t) \\ \Delta u_{dc}(t) \end{bmatrix}=\mathbf{A_{VM}}\begin{bmatrix} \Delta i_d(t) \\ \Delta i_q(t) \\ \Delta u_{dc}(t) \end{bmatrix}+\mathbf{B_{VM}}\begin{bmatrix} \Delta\theta(t) \\ \Delta u_x(t) \\ \Delta i_{dc}(t) \end{bmatrix} \tag{14}$$

where $\mathbf{A_{VM}}$ and $\mathbf{B_{VM}}$ denote state equation matrices.

The Step Response of the DC-link Current

The performance of the DC-link current $\Delta i_V(t)$ is essential in order to control the whole inverter system. Here, the step responses and Bode-diagram of the DC-link current $\Delta i_V(t)$ will be analysed. The parameters of the inverter system which alternate are shown in Table 1. The constant parameters are $U=E=1$ p.u. and $u_{dc0}=1.5E=1.0$ p.u. and θ_0=5°. The AC and DC sides have separate voltage bases.

TABLE 1
DIFFERENT PARAMETERS OF THE INVERTER SYSTEM.

No	A	B	C	D
L_s [p.u.]	0.044	0.044	0.305	0.305
R_s [p.u.]	0.0028	0.0083	0.0028	0.0083
L_s / R_s [ms]	50	169	347	117

In Figure 3, the different step responses are shown. Here, the step of the DC-link current $\Delta i_V(t)$ is normalized by $\Delta i_V(\infty)$ so the step size is one. An explanation for this response is that when the value of the series inductance changes, the size of the step response will also change. The step response of the DC-link value $\Delta i_V(t)$, when the relative voltage $\Delta u_x(t)$ makes a step, is normalized by $\Delta i_V(\infty)$ which comes from the $\Delta\theta(t)$ step.

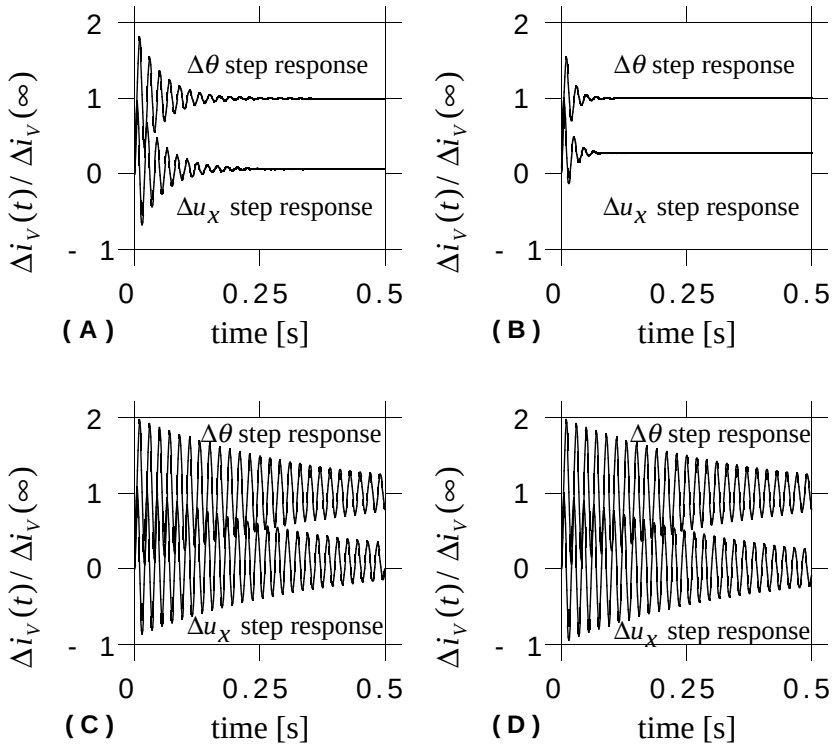

Figure 3: Step responses of $\Delta i_V(t)$ when phase displacement angle $\Delta\theta(t)$ and the relative voltage $\Delta u_x(t)$ make steps. The different Figures (A) to (D) uses parameters from Table 1.

The Bode diagram $I_V(s) / \theta(s)$ of the Equation 13 is shown in Figure 4. The parameters used come from Table 1. The Bode diagram is normalized so that the transfer functions have the same gain at low frequencies. A large resonance peak can be found at a frequency of 50 Hz. Depending on the value of the parameters of the inverter system, the resonance peak will have different amplitudes. The gain decreases by 40 dB per decade for frequencies over 50 Hz.

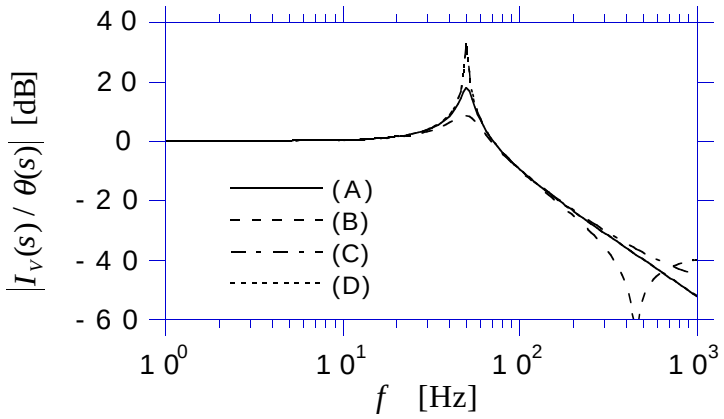

Figure 4: The Bode diagram of Equation 13. The parameters come from Table 1.

The transfer function has the damping factor of R_s / L_s. Here, $R_s / \omega_N L_s << 1$ so the resonance frequency becomes approximately $\omega_{res} \approx \omega_N$. The larger inductor resistance R_s and smaller inductor inductance L_s the smaller will the resonance peak for the Bode-

diagram in Figure 4 be and the faster will the system transients be damped out, see Figure 3. When using a large resistance R_s the losses of the system will increase and, of course, efficiency will decrease. The bandwidth of the system will be limited due to the large resonance at the resonance frequency of 50 Hz, see Figure 4. To achieve a safe system the bandwidth of the system must always be less than 50 Hz.

VII. THE REGULATORS

The regulator should control the phase angle $\theta(t)$. The relative voltage $u_x(t)$ will always have a value that will enable the amplitude of the three-phase voltage system of the inverter to be equal to the amplitude of the three-phase grid voltage, see Equation 11. Here, two regulators are analysed. The first one is a PI-regulator that feedbacks the DC-link voltage $u_{dc}(t)$. The second regulator is the same PI-regulator with a feedforward, PIFF, of the generator/rectifier current $i_{dc}(t)$. The feedforward constant is denoted as k_{FF}. The only parameter that can be changed by the user is the reference voltage value of the DC-link $u_{dc}^{*}(t)$ The PI-regulator reduces steady-state errors. $\varepsilon(t)$ is defined as the error signal, i.e. the difference between the reference value of the DC-link voltage $u_{dc}^{*}(t)$ and the value of the DC-link voltage $u_{dc}(t)$. The PI-regulator is defined as

$$\frac{\theta(t)}{\varepsilon(t)} = k_P\left(1+\frac{1}{sT_I}\right) \tag{15}$$

where k_P is the proportional gain and T_I is the integral time constant. To make it easy to implement the PI-regulator into an analogue control system, the PI-regulator will be modified to

$$\frac{\theta(t)}{\varepsilon(t)} = k_P + \frac{k_I}{1+sT_{II}} \tag{16}$$

where k_I and T_{II} are constants to the integral time constant in the modified PI-regulator. Here $T_{II} >> 1$ and

$$\frac{k_P}{T_I} \approx \frac{k_I}{T_{II}} \tag{17}$$

VIII. THE TOTAL LINEARIZED SYSTEM WITH A REGULATOR

When the regulator parameters are determined, the system can be analysed by using the state equation for the closed loop. State equation 18 represents a total linearized system with a PIFF-regulator. The state equation has three inputs; the relative voltage $\Delta u_x(t)$, the generator/rectifier current $\Delta i_{dc}(t)$ and the reference value of the DC-link voltage $\Delta u_{dc}^{*}(t)$.

$$\frac{d}{dt}\begin{bmatrix}\Delta i_d(t)\\ \Delta i_q(t)\\ \Delta u_{dc}(t)\\ \Delta\theta_I(t)\end{bmatrix} = \mathbf{A_{CLPIFF}}\begin{bmatrix}\Delta i_d(t)\\ \Delta i_q(t)\\ \Delta u_{dc}(t)\\ \Delta\theta_I(t)\end{bmatrix} + \mathbf{B_{CLPIFF}}\begin{bmatrix}\Delta u_x(t)\\ \Delta i_{dc}(t)\\ \Delta u_{dc}^{*}(t)\end{bmatrix} \tag{18}$$

where $\mathbf{A}_{\mathbf{CLPIFF}}$ and $\mathbf{B}_{\mathbf{CLPIFF}}$ denote state equation matrices. The state equation for the PI-controlled system becomes the same as Equation 18 when the feedforward term k_{FF} is set to zero.

IX. THE BODE-DIAGRAMS OF THE LINEARIZED SYSTEM

Based on the open loop state equation of the linearized system with the regulator the PI-regulator was tuned using gain margin criterion $G_m \geq 3$ and the phase margin criterion $P_m \geq 40^0$, Ollila (11) and Schmidtbauer (12). The feedforward constant is determined so that the DC-link current $\Delta i_V(t)$ has the same value as the generator/rectifier current $\Delta i_{dc}(t)$ in steady state.

Suppose that the inverter system has the parameters that are shown in Table 2, determined by an iterative approach. By using the closed loop state Equation 18, it is possible to create step responses and Bode diagrams.

TABLE 2
PARAMETERS OF THE INVERTER SYSTEM.

$U = E$	1.0 p.u.	R_{dc}	18.9 10^4 p.u.
u_{dc0}=1.5E	1.0 p.u.	k_P	1.39 10^{-4}
θ_0	5°, 10°	k_I	8.16 10^3
L_s	0.175 p.u.	T_{II}	13.9
R_s	5.6 10^{-3} p.u.	k_{FF}	2.4 10^{-3}
C_{dc}	0.10 p.u.		

Two transfer functions will be analysed here. These are the DC-link voltage as a function of the reference value of the DC-link voltage $\Delta u_{dc}^*(t)$ and the generator/rectifier current $\Delta i_{dc}(t)$. The Bode-diagram for the relative voltage and the reference value of the DC-link voltage are the same for PI- and PIFF-regulators, see Figure 5. The Bode diagrams are the same for both the PI- and the PIFF-regulators.

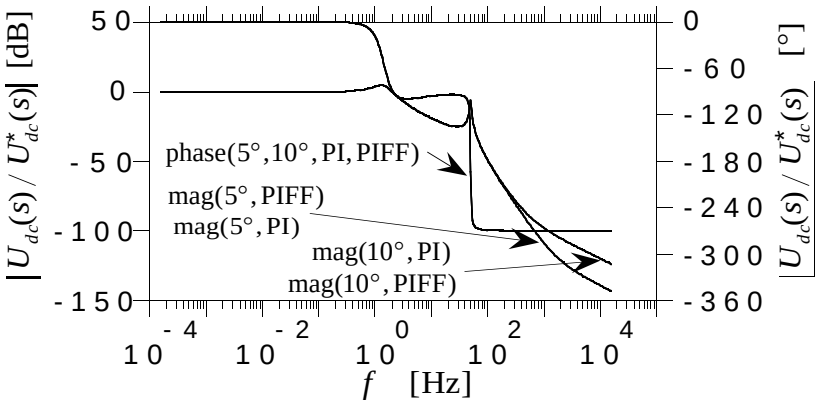

Figure 5: The Bode diagram of the DC-link voltage $\Delta u_{dc}(t)$ as a function of the reference value of the DC-link voltage $\Delta u_{dc}^*(t)$. The operating points are $\theta_0 = 5°$ and $\theta_0 = 10°$.

The step responses of the DC-link voltage $\Delta u_{dc}(t)$, when the reference value of the DC-link voltage $\Delta u_{dc}^*(t)$ makes a unity step, shows that the steady state value of $\Delta u_{dc}(t)$ is

the same as the reference value of the DC-link voltage $\Delta u_{dc}^{*}(t)$. The DC-link voltage $\Delta u_{dc}(t)$ responds with an overshoot of 38 % when the relative voltage makes a unity step, and the DC-link voltage step response returns to 0 V. The reason for this is that the active power in the system does not change.

When the generator/rectifier current $\Delta i_{dc}(t)$ varies, the DC-link voltage $\Delta u_{dc}(t)$ will behave differently when the regulator is a PI- or PIFF-controller. Figure 6 shows the Bode diagram for the DC-link voltage $\Delta u_{dc}(t)$ as a function of $\Delta i_{dc}(t)$, when the PI- and PIFF-controllers are used.

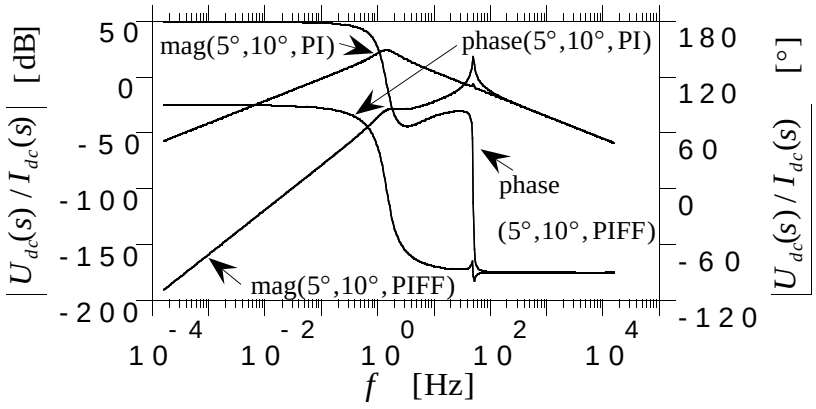

Figure 6: The Bode diagram of the DC-link voltage $\Delta u_{dc}(t)$ as a function of the generator/rectifier current $\Delta i_{dc}(t)$. The controllers are PI and PIFF. The operating points are $\theta_0 = 5°$ and $\theta_0 = 10°$.

When comparing the step responses $\Delta u_{dc}(t)$ when $\Delta i_{dc}(t)$ makes a unity step, the overshoot is reduced by approximately a factor of 20 and the settling time is reduced by approximately a factor of 2 if a PIFF-regulator is used.

The use of feedforward in the generator/rectifier current results in lower step responces of the DC-link voltage when the generator/rectifier current makes steps. The disadvantages are an increase in the cost of the controller and that the system becomes more sensitive to noise.

X. SIMULATION OF THE NON-LINEAR SYSTEM

When the regulator has been determined for the linearized system at an operating point, the total non-linear system can be simulated. By only simulating the fundamental voltage of the inverter, the simulating time is heavily decreased, by approximately a factor of 300. Here simulations both with and without harmonics are carried out. The input to the system is the generator/rectifier current $i_{dc}(t)$ and one of the most important output signals is the DC-link voltage $u_{dc}(t)$. The system is simulated in Simulink which is based on Matlab.

The total inverter system step response is here simulated when the generator/rectifier current makes steps. At the beginning of the simulation the generator/rectifier current makes a step from 0 to 0.8 p.u., at the time of 2.0 s the generator/rectifier current makes a step from 0.8 to 1.0 p.u. and at the time of 3.5 s the generator/rectifier current makes a step from 1.0 to 0.8 p.u.

Due to the different bandwidths of the two systems PI- and PIFF-regulator, the parameters of the systems must be different so the performances match each other, i. e. in the DC-link voltage fluctuation. Table 4.3 shows the parameters of the inverter systems, using two different regulators.

TABLE 3
PARAMETERS OF THE INVERTER SYSTEM.

System parameters when using the PI-controller		System parameters when using the PIFF-controller	
$U = E$	1 p.u.	$U = E$	1 p.u.
u_{dc}^{*}	1 p.u.	u_{dc}^{*}	1 p.u.
L_s	0.175 p.u.	L_s	0.175 p.u.
R_s	1.39 10^{-2} p.u.	R_s	1.67 10^{-2} p.u.
C_{dc}	3.33 10^{-2} p.u.	C_{dc}	0.10 p.u.
R_{dc}	13.9 10^{3} p.u.	R_{dc}	13.9 10^{3} p.u.
k_P	1.0 10^{-3}	k_P	4.1 10^{-4}
k_I	10	k_I	4.1
T_{II}	3.39 10^{2}	T_{II}	2.88 10^{2}
k_{FF}	0	k_{FF}	2.4 10^{-3}

The PWM-inverter system has the same parameters as in Table 3, with the exception of the switching frequency which is 5 kHz. The DC-link capacitor of the inverter system with a PI-regulator is three times larger than that of the capacitor of the inverter system with a PIFF-controller. The other parameters are the same except for the values of the regulator parameter.

Step Responses to the Generator/Rectifier Current

The system has been simulated with and without harmonics. The input to the system is the generator/rectifier current. Figures 7A and 7B show the step response of the DC-link voltage with and without harmonics, using a PI-regulator. The first step response of the DC-link voltage has a high peak, but the DC-link voltage fluctuates by approximately 2.5% with step responses at 2.0 and 3.5 s. There is no difference between the phase displacement angles in the simulations with and without harmonics.

Here the inverter system, using a PIFF-regulator, is simulated with and without harmonics. Figures 7C and 7D show the DC-link voltage both for the non-harmonics inverter and the PWM-inverter. The step responses are approximately the same. When the generator/rectifier current is 1 p.u. the phase displacement angle is 1.0 p.u. and this results in a higher fluctuation of the DC-link voltage, because the regulator parameters have been designed at the phase displacement angle of 0.5 p.u.

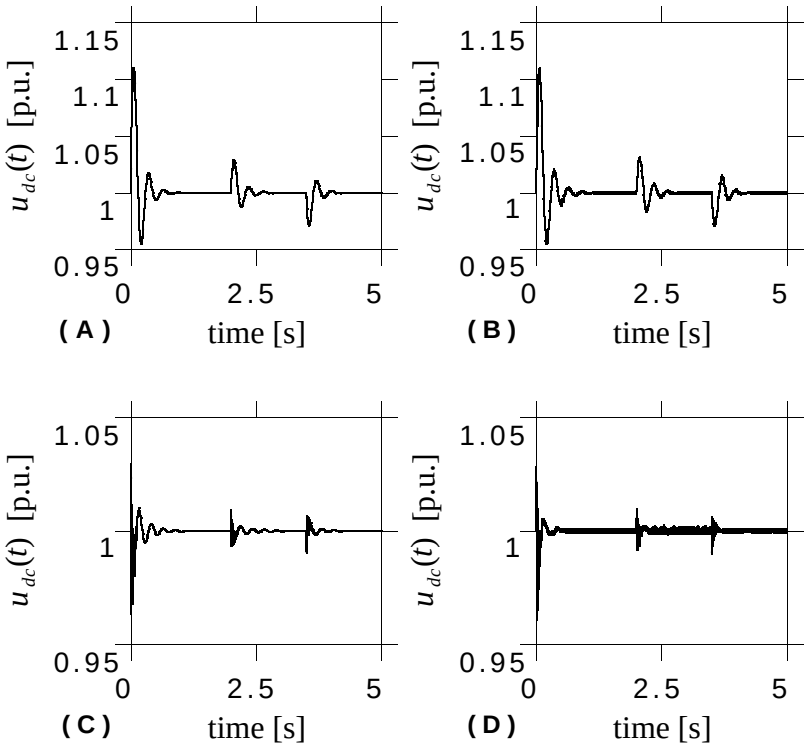

Figure 7: Step responses of the DC-link voltage when the generator/rectifier current makes steps; (A): PI-reg. and no harmonics; (B): PI-reg. and PWM; (C): PIFF-reg. and no harmonics; (D): PIFF-reg. and PWM.

The DC-link capacitor of the inverter system with a PI-regulator is three times larger than the capacitor of the inverter system with a PIFF-controller. The other parameters are the same for the two regulators with the exception of for the value of the regulator parameters. This difference clearly shows that the PIFF-controller has a better performance than the PI-controller. There are no differences between the complete inverter model which uses the PWM and harmonics and the reduced inverter model which use PWM and harmonics and the reduced inverter model which only uses the fundamental voltage of the three-phase voltage system of the inverter. The simulation time is greatly decreased if the model without harmonics is used instead of the complete harmonic model, because the simulation of the PWM-pattern in the complete model requires a small time step in the simulation program in order to maintain accuracy. Observe that the non-harmonic model is used in an application which has a low bandwidth in comparison to the switching frequency of the inverter.

XI. PARAMETER VARIATION

Due to the high inertia of the wind turbine rotor, the time constant of the wind turbine is about 1 second. The highest frequency, where essential power effects influence the wind turbine, is the drive train resonance, about 5 Hz, see Novak et al (13). This makes it possible to control the wind turbine with voltage angle control, although of cource, the system should be as cheap as possible. By minimizing the DC-link capacitor and the series inductance, the cost can be low. The value of the series inductance cannot be

chosen freely, because the inductance value partially determines the total harmonic distorsion on the grid.

The generator/rectifier current amplitude and frequency are important when determining how the parameters should be used, assuming that the DC-link voltage can fluctuate ±5 % before it affects the performance of the wind turbine. The generator/rectifier current $i_{dc}(t)$ is supposed to vary sinusoidally from zero to 1 p.u. in the simulations, i.e. with an amplitude of 0.5 p.u. and a DC-level of 0.5 p.u, at the frequency $f(i_{dc})$.

The fluctuation of the DC-link voltage can be determined by simulating the inverter system in simulink. The DC-link voltage fluctuation is calculated as a function of the frequency of the generator/rectifier current $i_{dc}(t)$ and the parameters of the inverter system. The harmonics are cancelled and the transients are damped out. Because the fluctuations of the DC-link voltage are small, the input DC-link voltage is to be set to its reference value in the inverter model.

Two methods have been used called "non-linear" and "linear." The "non-linear" method is the Simulink simulation described above and the "linear" method is used to calculate the fluctuation by means of the Linear state equation 18 and to set the operating point θ_0 / θ_n to 0.5. By stipulating the maximum DC-link voltage fluctuation to 5 %, the necessary value of the DC-link capacitor can be expressed as a function of the series inductance and the frequency of the generator/rectifier current.

DC-link Voltage Fluctuation

When comparing the simulated fluctuations "non-linear" with calculated fluctuations "linear" from the state equation 18 and by using PI-regulator, it can be seen that the fluctuations are the same for the two methods, see Figures 8A and 8B. The parameters of the system are listed in Table 4 and it is the value of the series inductance which varies, of course, along with the regulator parameters. When switching only the regulator of the system to the PIFF-type, the fluctuations become as in Figure 8C and 8D. The parameters are listed in Table 4.

TABLE 4

PARAMETERS OF THE INVERTER SYSTEMS.

	PIFF	PI
$U = E$ [p.u.]	1	1
u_{dc}^{*} [p.u.]	1	1
L_s (Fig. 8A, 8C) [p.u.]	0.087	0.087
L_s (Fig. 8B, 8D) [p.u.]	0.175	0.175
R_s [p.u.]	$1.39\ 10^{-2}$	$1.39\ 10^{-2}$
C_{dc} [p.u.]	0.10	$3.33\ 10^{-2}$
R_{dc} [p.u.]	$13.9\ 10^{3}$	$13.9\ 10^{3}$

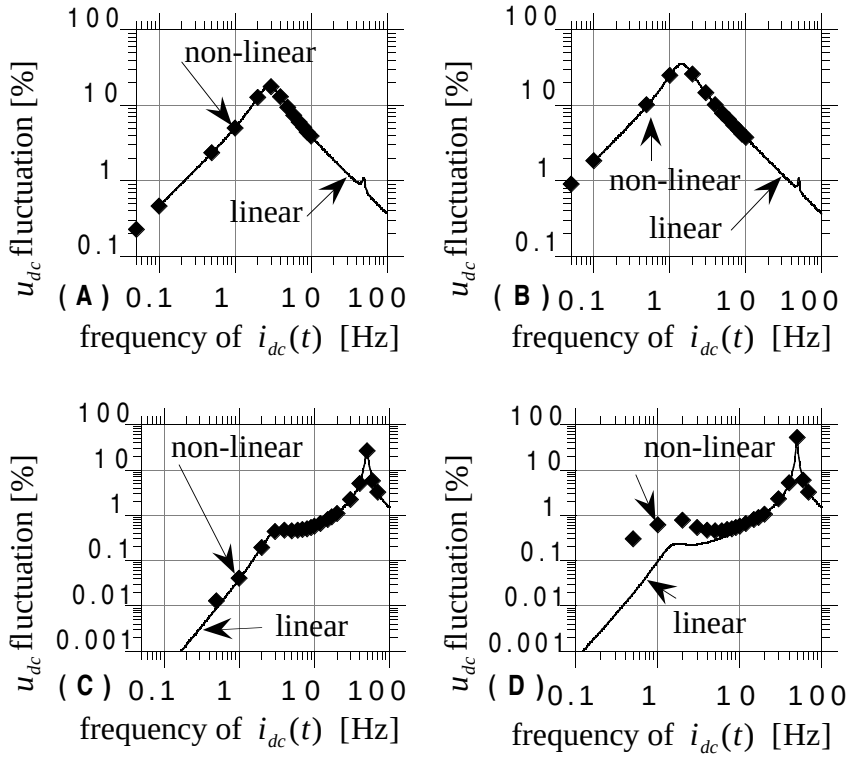

Figure 8: The DC-link voltage fluctuation in percent as a function of the frequency of the generator/rectifier current. (A): PI-reg. and L_s is 0.087 p.u.; (B): PI-reg. and L_s is 0.175 p.u.; (C): PIFF-reg. and L_s is 0.087 p.u.; (D): PIFF-reg. and L_s is 0.175 p.u.

When the value of the series inductance and the phase displacement angle is kept small then the non-linearities will also become insignificant. This results in that the linear and non-linear models agree well for small values of series inductances. When the frequency of the generator/rectifier current is around the resonance frequency of 50 Hz the difference between the linear and non-linear model is small. At approximately one Hz the non-linear model has a resonance.

The main reason for using the "linear" calculated fluctuations is that they do not require a powerful computer, which is necessary to keep down the calculation time of the calculation of the "non-linear" fluctuations. The disadvantage is that the "linear" method is not accurrate when the series inductance becomes large, see Figures 8C and 8D.

Allowed Parameter Values Variations, to Maintain the Fluctuation Below 5%

Figure 9 shows what value the DC-link capacitor must have for a specific value of series inductance and for a specific frequency of the generator/rectifier current. Both PI-and PIFF-controllers are used. The fluctuation has been calculated by using the "linear" model. A finite number of values of the DC-link capacitor, from 1 p.u. to 0.0154 p.u., has been used to calculate the fluctuation. Due to this fact, the curves in Figure 9 are discontinuous. For the same value of the DC-link capacitor and series inductance the allowed maximum frequency, until the fluctuation increases by 5 %, is increased significantly when the regulator is of a PIFF-type instead of a PI-type. The curves using PIFF-regulators have approximately the same form as those using a PI-regulator. The

maximum frequency for the PIFF-regulated system is about 20 to 30 Hz independent of the size of the series inductance and of the size of the DC-link capacitor. For the system that uses a PI-regulator the maximum frequency of generator/rectifier current is dependent on which series inductance is used and what value of the DC-link capacitor is used. The lower value of the series inductance, the higher the frequency of the generator/rectifier current can be allowed. For example, the inverter system, using PI-regulator, has a maximum DC-link voltage fluctuation of 5 % when the generator/rectifier current has a maximum frequency of 1 Hz, and when the value of the DC-link capcitor is less than 0.04 p.u. and the series inductance is 0.087 p.u.

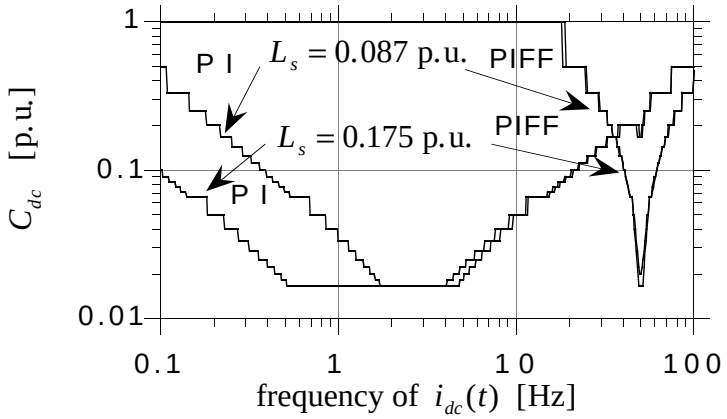

Figure 9: The relation between the values of the DC-link capacitor, series inductance and the frequency of the generator/rectifier current so the fluctuation of the DC-link voltage will be below 5 %.

XII. CONCLUSION

The control of a voltage source inverter used in a wind turbine application has been shown to operate well. By using a PI-controller for the DC-link voltage and a feedforward of the generator/rectifier current the voltage angle control can be used. The bandwidth of the inverter system is around 20 to 30 Hz if normal values of the system parameters are chosen. The wind turbine time constant is around one second and small power fluctuations can occur at 5 Hz due to the drive train resonance.

The method used to analyse the system is a non-harmonic non-linear model which was linearized at an operating point. To verify the results, a model using PWM voltages and a model using fundamental voltages are compared and no significant differences are found.

The limit of the DC-link voltage fluctuation bound the parameters of the system. At the normal size of the series inductance, due to current harmonics on the grid, the linearized model of the system can be used to determined the fluctuation. The controller using feedforward is insensitive to series inductance variation and the fluctuations depend on the size of the DC-link capacitor and the frequency and amplitude of the generator/rectifier current.

XIII. ACKNOWLEDGEMENT

The financial support given by the Swedish National Board for Industrial and Technical Development is gratefully acknowledged.

XIV. REFERENCES

[1] Grauers, A., 1993, ECWEC'93, 656-658

[2] Leithead, W. E., 1989, *Wind Engineering*, vol. 13, 302-314

[3] Lowson, M. V., 1994, *Wind Engineering*, vol. 18, 51-61

[4] Malesani, L., and Tomasin, P., 1993, IECON'93, 670-675

[5] Pierik, J. T. G., Veltman, A. T., d. Haan, S. W. H., Smith, G. A., Infield, D. G., Simmons, A. D., 1994, EWEC '94

[6] Verdelho, P., Marques, G. D., 1991, EPE,.438-443

[7] Ekström, Å., 1991, PESC'91, 314-322

[8] Ooi, B. T., Wang, X., 1990, *IEEE Trans. on Power Electronics*, vol. 5, 229-235.

[9] Joos, G., Morán, L., Ziogas, P., 1991, *IEEE Trans. on Power Electronics*, vol. 6, 380-391

[10] Carlson, O., Grauers, A., Svensson, J., Larsson, Å., 1994, EWEC'94

[11] Ollila, J., 1993, Tampere University of Technology, Finland, Tampere 111.

[12] Schmidtbauer, B., 1988, Lund, Sweden, Studentlitteratur.

[13] Novak, P., Jovik, I., and Schmidtbauer, B., 1994, IEEE 3rd Conf. on Control Applications

PAPER 2B

J. Svensson, "Simulation of Power Angle Controlled Voltage Source Converter using a Linear Quadratic Method in a Wind Energy Application," *5th Workshop on Computers in Power Electronics, IEEE,* 11-14 August 1996, pp. 157-162.

Simulation of Power Angle Controlled Voltage Source Converter Using a Linear Quadratic Method in a Wind Energy Application

Jan Svensson

Department of Electric Power Engineering
Chalmers University of Technology
S-412 96 Göteborg, Sweden

Abstract: The design, analysis and simulation of a power angle controlled voltage source inverter in a wind energy application are addressed. By controlling both the phase displacement angle and voltage amplitude, the performance of the system is improved compared with the traditional power angle control. The system becomes a multiple-input and multiple-output system preferably controlled by the linear quadratic method. To reduce harmonics and noise, a Kalman estimator is applied to the input signals of the controller. When state equations are used, the inverter system as well as the feedback and feedforward parameters are easy to handle by using the Matlab/Simulink program. The simulation results show that the proposed control method and its implementation function adequately.

I. INTRODUCTION

Several advantages can be achieved by replacing a constant-speed wind turbine by a variable-speed system consisting of a generator and power electronics [1, 2, 3]. If the inverter connected to the grid is based on forced commutation instead of on more usual grid commutation, current harmonics will be decreased, any desired power factor can be obtained and energy can flow in both directions. The inverter is often controlled by means of vector control or power angle control. The power angle control is based on the control of the voltage angle of the inverter so that the phase displacement angle is proportional to the active power [4]. This control method has been investigated in HVDC applications [5, 6] and reactive power compensators [7].

In this paper, the possibility of using a robust and easy-to-tune controller is investigated analytically and by simulations. The performance of the system is improved by controlling both the phase displacement angle and the voltage amplitude of the inverter. The system then becomes a non-linear multiple-input and multiple-output (MIMO) system. Because every output is coupled to the inputs, it is difficult or impossible to use classical control methods to analyse and design a MIMO system. Here, the linear quadratic (LQ) method will be used to control the inverter system.

II. THE SYSTEM CONFIGURATION

The electrical system of the wind turbine, see Fig. 1, can be divided into two subsystems: the generator-rectifier system and the inverter system. Concerning the generator-rectifier system, the best alternative is to choose a synchronous generator and a diode rectifier [8]. Such a choice is based on low cost and high efficiency compared with an induction generator connected to a forced-commutated rectifier. A voltage-stiff forced-commutated

inverter utilizes a stiff DC-link voltage. A step-up chopper can be used to adapt the rectifier voltage to the DC-link voltage of the inverter. The step-up chopper or the forced-commutated rectifier, if an induction generator is used, utilizes a high switching frequency so the bandwidth of these components is much higher than the bandwidth of the generator. Therefore, the generator-rectifier system can be modelled as an ideal current source when the inverter system is analysed.

The generator/rectifier current is denoted $i_{dc}(t)$ and is independent of the value of the DC-link voltage. The capacitor of the DC-link has the value of C_{dc}. The inductors at the AC-side of the inverter have the inductance L_s and the resistance R_s. The three-phase voltage system of the grid has phase voltages $e_1(t)$, $e_2(t)$ and $e_3(t)$ and the phase currents are denoted $i_1(t)$, $i_2(t)$ and $i_3(t)$. Further on, the three-phase voltage system of the inverter has phase voltages $u_1(t)$, $u_2(t)$ and $u_3(t)$. The DC-link voltage value is denoted $u_{dc}(t)$ and the DC-link current to the inverter is called $i_V(t)$.

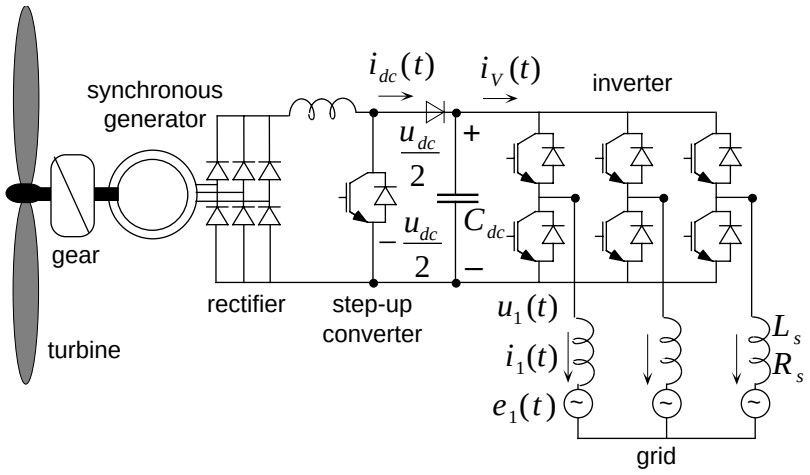

Figure 1: The system configuration.

III. A NON-LINEAR MODEL OF THE SYSTEM

The space vector voltage of the inverter and the grid is denoted $\underline{u}(t)$ and $\underline{e}(t)$, respectively. The angular frequency of the inverter is denoted ω and the grid angular frequency is called ω_N. The phase currents in component form in the *dq*-coordinate system become, see Fig. 1,

$$\frac{d}{dt}i_d(t) = -\frac{1}{L_s}U\sin(\theta(t)) - \frac{R_s}{L_s}i_d(t) + \omega_N i_q(t) \tag{1}$$

$$\frac{d}{dt}i_q(t) = \frac{1}{L_s}U\cos(\theta(t)) - \frac{1}{L_s}e_q(t) - \frac{R_s}{L_s}i_q(t) - \omega_N i_d(t) \tag{2}$$

Here, the phase displacement angle $\theta(t)$ is equal to

$$\theta(t) = \int_0^t \left(\omega(\tau) - \omega_N\right)d\tau \tag{3}$$

When the valves are ideal and no harmonics are produced, the DC-link current $i_V(t)$ can be written

$$i_V(t) = \frac{u_d(t)i_d(t) + u_q(t)i_q(t)}{u_{dc}(t)} \tag{4}$$

The voltage across the DC-link capacitor can be expressed as

$$u_{dc}(t) = \frac{1}{C_{dc}} \int_0^t \left(i_{dc}(\tau) - i_V(\tau) \right) d\tau \tag{5}$$

The DC-link voltage $u_{dc}(t)$ is controlled by using the amplitude of the three-phase voltage and the phase displacement angle $\theta(t)$ of the inverter.

IV. The Reduced Non-Linear Model

A reduced non-linear model of the system, a non-harmonic model, is shown in Fig. 2. The reference values are denoted by an asterisk (*). The control of the inverter has two input signals: the phase displacement angle $\theta(t)$ and the relative voltage $u_x(t)$. The grid is supposed to be stiff, i.e. the frequency and voltage amplitude of the grid are constant. The phase-to-phase rms voltage of the inverter can be written

$$U(t) = u_x(t)E \tag{6}$$

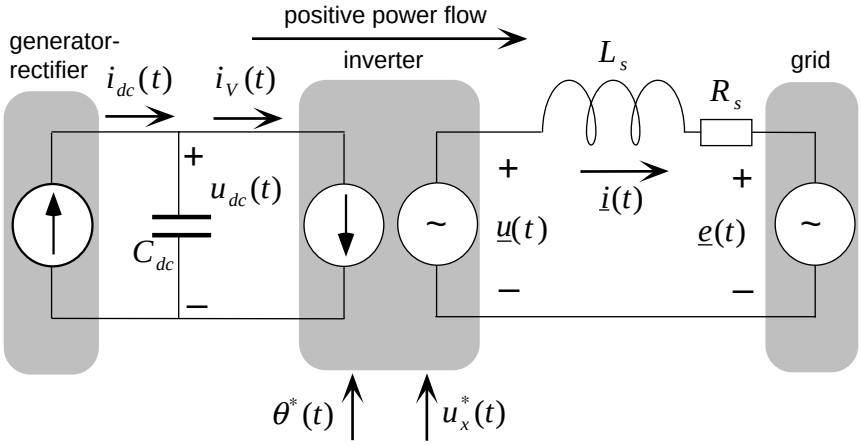

Figure 2: A reduced non-linear model of the system.

V. The Linearization of the System in an Operating Point

Let the operating points be denoted index "0" and the variable perturbation around the variable operating points be denoted index "Δ." The linearized currents and the DC-link voltage of the inverter can be obtained by means of the state equation with three states and three inputs

$$\frac{d}{dt}\begin{bmatrix} \Delta i_d(t) \\ \Delta i_q(t) \\ \Delta u_{dc}(t) \end{bmatrix} = \mathbf{A_{VM}} \begin{bmatrix} \Delta i_d(t) \\ \Delta i_q(t) \\ \Delta u_{dc}(t) \end{bmatrix} + \mathbf{B_{VM}} \begin{bmatrix} \Delta\theta(t) \\ \Delta u_x(t) \\ \Delta i_{dc}(t) \end{bmatrix} \tag{7}$$

where $\mathbf{A_{VM}}$ and $\mathbf{B_{VM}}$ are state equation matrices.

VI. THE LINEAR QUADRATIC CONTROLLER

Using linear quadratic control always results in a stable system. Unfortunately, this is only correct when the system is linear. If the system to be controlled is non-linear, it must be linearized in an operating point before the control parameters can be decided. If the system is located in one operating point but the control parameters have been designed for an other operating point, the system can become unstable. If the system becomes unstable or not, depends on how robust the system is. Every control parameter in this chapter has been designed with linearized state equations where the harmonics, which come from the pulse width modulation of the inverter, have been neglected.

In linear quadratic control [9], the control is sought that minimizes the value of a performance index J, which is of the standard form

$$J = \frac{1}{2}\int_0^\infty (x^T \mathbf{Q} x + u^T \mathbf{R} u)dt \tag{8}$$

The matrices $\mathbf{Q}$ and $\mathbf{R}$ are diagonal weighting matrices and $x^T\mathbf{Q}x$ and $u^T\mathbf{R}u$ are scalar quadratic forms which measure the performance and the cost of the control, respectively. The optimal control is a constant-gain state feedback

$$u_{opt} = -\mathbf{L}x = -\mathbf{R}^{-1}\mathbf{B}^T\mathbf{P}x \tag{9}$$

where $\mathbf{P}$ is a symmetric matrix obtained by the solution of the algebraic matrix Riccati equation

$$\mathbf{PA} + \mathbf{A}^T\mathbf{P} + \mathbf{Q} - \mathbf{PBR}^{-1}\mathbf{B}^T\mathbf{P} = 0 \tag{10}$$

The method used here can be found in [10]. The state equation of the inverter system is rewritten so the generator/rectifier current $\Delta i_{dc}(t)$ can be seen as a known process disturbance, denoted $\xi(t)$, which is separated from the other inputs of the system. The matrices of the new state equation are denoted $\mathbf{A}$, $\mathbf{B}$, $\mathbf{C}$, $\mathbf{D}$, $\mathbf{E}$ and $\mathbf{F}$. In Fig. 3 below, the system in open loop is shown.

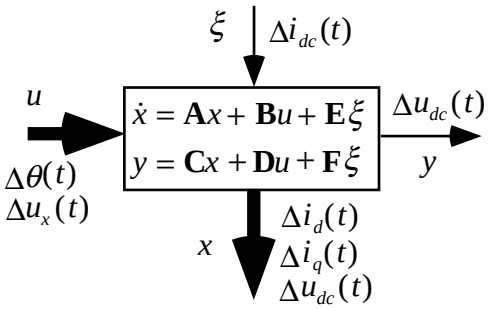

Figure 3: The linearized state equation.

By using the integral control, a stable design with no steady-state errors can be provided. With integral control a new state in the state equation of the system is created and yields $p(t)$. The reference value $y^*(t)$ of the output $y(t)$ is here defined as the reference value of the DC-link voltage Δu_{dc}^*. The state equation is written

$$\frac{d}{dt}\begin{bmatrix}\Delta i_d(t)\\ \Delta i_q(t)\\ \Delta u_{dc}(t)\\ p(t)\end{bmatrix} = \mathbf{A_I}\begin{bmatrix}\Delta i_d(t)\\ \Delta i_q(t)\\ \Delta u_{dc}(t)\\ p(t)\end{bmatrix} + \mathbf{B_I}\begin{bmatrix}\Delta\theta(t)\\ \Delta u_x(t)\end{bmatrix} + \mathbf{E_I}\begin{bmatrix}\Delta i_{dc}(t)\\ \Delta u^*_{dc}(t)\end{bmatrix} \tag{11}$$

The weighting matrix $\mathbf{Q}$, which weights the states of the state equation will be a four by four diagonal finite matrix, so the states can be weighted independent of each other. The weighting matrix $\mathbf{R}$, used to weight the inputs of the state equation, is a two by two symmetric finite matrix, so the two inputs can be weighted independently. The matrices yield

$$\mathbf{Q} = \begin{bmatrix} q_{11} & 0 & 0 & 0\\ 0 & q_{22} & 0 & 0\\ 0 & 0 & q_{33} & 0\\ 0 & 0 & 0 & q_{44}\end{bmatrix} \qquad \mathbf{R} = \begin{bmatrix} r_{11} & 0\\ 0 & r_{22}\end{bmatrix}$$

When the Riccati equation is solved by using the matrices $\mathbf{A_I}$, $\mathbf{B_I}$, $\mathbf{Q}$ and $\mathbf{R}$, the feedback gain matrix becomes $\mathbf{L}$ which can be split into two pieces,(2x3) and (2x1)

$$\mathbf{L} = \begin{bmatrix}\mathbf{L}_1 & \mathbf{L}_2\end{bmatrix} \tag{12}$$

When the generator/rectifier current $\Delta i_{dc}(t)$ is known, a feedforward can be used. The same is valid for the reference value of the DC-link voltage $\Delta u^*_{dc}(t)$. With feedforward the input vector u can be written

$$u(t) = -\mathbf{L}x(t) + \mathbf{H}\begin{bmatrix}\xi(t)\\ y^*(t)\end{bmatrix} \tag{13}$$

where

$$\mathbf{H} = \begin{bmatrix}\mathbf{H}_1 & \mathbf{H}_2\end{bmatrix} = -\begin{bmatrix}\mathbf{L_1} & I\end{bmatrix}\mathbf{G}^{-1}\mathbf{E_I} \tag{14}$$

and

$$\mathbf{G} = \begin{bmatrix}\mathbf{A} & \mathbf{B}\\ \mathbf{C} & \mathbf{D}\end{bmatrix} \tag{15}$$

A picture of the linearized system with LQ-, integrate- and feedforward controls is shown in Fig. 4.

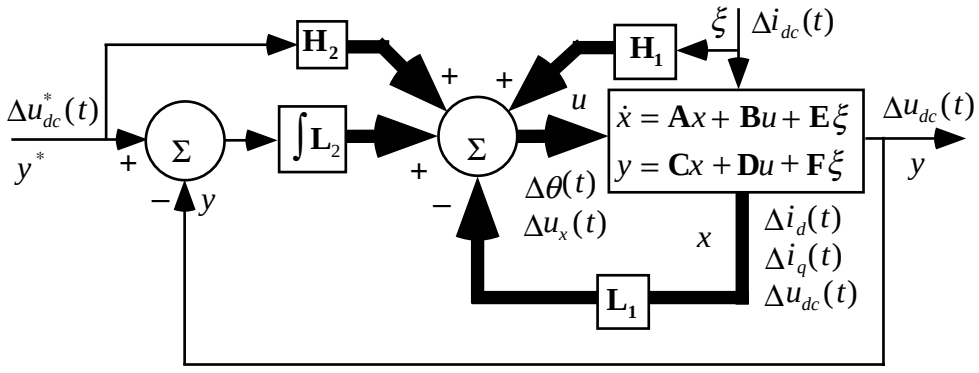

Figure 4: The linearized system with LQ-, integrate- and feedforward controls.

The linearized state equation for the closed loop system can be written

$$\frac{d}{dt}\begin{bmatrix}\Delta i_d(t)\\ \Delta i_q(t)\\ \Delta u_{dc}(t)\\ p(t)\end{bmatrix} = \mathbf{A}_{\mathbf{PIFF}}\begin{bmatrix}\Delta i_d(t)\\ \Delta i_q(t)\\ \Delta u_{dc}(t)\\ p(t)\end{bmatrix} + \mathbf{B}_{\mathbf{PIFF}}\begin{bmatrix}\Delta i_{dc}(t)\\ \Delta u^*_{dc}(t)\end{bmatrix} \tag{16}$$

and the output vector becomes

$$\begin{bmatrix}\Delta u_{dc}(t)\\ \Delta\theta(t)\\ \Delta u_x(t)\\ \Delta i_v(t)\end{bmatrix} = \mathbf{C}_{\mathbf{PIFF}}\begin{bmatrix}\Delta i_d(t)\\ \Delta i_q(t)\\ \Delta u_{dc}(t)\\ \Delta p(t)\end{bmatrix} + \mathbf{D}_{\mathbf{PIFF}}\begin{bmatrix}\Delta i_{dc}(t)\\ \Delta u^*_{dc}(t)\end{bmatrix} \tag{17}$$

where $\mathbf{A}_{\mathbf{PIFF}}$, $\mathbf{B}_{\mathbf{PIFF}}$, $\mathbf{C}_{\mathbf{PIFF}}$ and $\mathbf{D}_{\mathbf{PIFF}}$ denote state equation matrices.

A. The Controller

To simulate the inverter system a regulator is needed. The outputs of the regulator are the phase displacement angle $\theta(t)$ and the relative voltage $u_x(t)$. The inputs of the regulator are the active and reactive current components of the phase current $\underline{i}(t)$, the DC-link voltage $u_{dc}(t)$, the generator/rectifier current $i_{dc}(t)$, and the reference value of the DC-link voltage $u^*_{dc}(t)$. The parameter values of the regulator are decided for the phase displacement operating point angle θ_0 or the DC-link current $i_v(t)$. The state equation of the regulator is written

$$\dot{x}(t) = \mathbf{A}_{\mathbf{REG}}x(t) + \mathbf{B}_{\mathbf{REG}}u(t) \tag{18}$$

and the output vector becomes

$$\begin{bmatrix}\theta(t)\\ u_x(t)\end{bmatrix} = \mathbf{C}_{\mathbf{REG}}x(t) + \mathbf{D}_{\mathbf{REG}}u(t) \tag{19}$$

where

$$u(t) = \begin{bmatrix} i_d(t) & i_q(t) & u_{dc}(t) & i_{dc}(t) & u^*_{dc}(t)\end{bmatrix}^T \quad \mathbf{A}_{\mathbf{REG}} = \mathbf{0}$$

$$\mathbf{B}_{\mathbf{REG}} = \begin{bmatrix}0 & 0 & 1 & 0 & -1\end{bmatrix} \quad \mathbf{C}_{\mathbf{REG}} = -\mathbf{L}_2 \quad \mathbf{D}_{\mathbf{REG}} = \begin{bmatrix}-\mathbf{L}_1 & \mathbf{H}\end{bmatrix}$$

VII. THE KALMAN ESTIMATOR

A. The Linear Kalman Estimator

One of the disadvantages of a continuous time LQ-control is that process noise with high frequencies disturbs the regulator. For the inverter system the grid current contains harmonics due to the PWM technique. These current harmonics affect the LQ-controller. One way to eliminate the current harmonics influence is to use lowpass filter at the inputs of the regulator but then the input signals become phase-shifted and the stability of the system becomes weaker. By using an estimator, the current harmonics level is reduced without any phase shifts. Suppose that the inverter system is linearized around an operating point $\theta_0(t)$. A state equation with the matrices **A**, **B**, **C** and **D** describes the

dynamics of the inverter system. When process noise and measuring noise are added to the inverter system, the state equation becomes

$$\begin{aligned} \dot{x} &= \mathbf{A}x + \mathbf{B}u + \mathbf{G}w \\ y &= \mathbf{C}x + \mathbf{D}u + v \end{aligned} \tag{20}$$

where the process and measurement noise, means and covariances are

$$\begin{aligned} E[w] = E[v] = 0 \qquad & E\left[vv^T\right] = \mathbf{R_2} \\ E\left[ww^T\right] = \mathbf{R_1} \qquad & E\left[wv^T\right] = 0 \end{aligned} \tag{21}$$

The estimated state vector $\hat{x}$ can be obtained using the state equation

$$\dot{\hat{x}} = \mathbf{A}\hat{x} + \mathbf{B}u + \mathbf{k}\left(y - \mathbf{C}\hat{x} - \mathbf{D}u\right) \tag{22}$$

The filter gain matrix $\mathbf{k}$ comes from

$$\mathbf{k} = \mathbf{P}\mathbf{C}^{\mathbf{T}}\mathbf{R}_{\mathbf{2}}^{-\mathbf{1}} \tag{23}$$

and by solving the static Riccati equation (24) the matrix **P** will be found [11].

$$\dot{\mathbf{P}} = \mathbf{A}\mathbf{P} + \mathbf{P}\mathbf{A}^{\mathbf{T}} - \mathbf{P}\mathbf{C}^{\mathbf{T}}\mathbf{R}_{\mathbf{2}}^{-\mathbf{1}}\mathbf{C}\mathbf{P} + \mathbf{R}_{\mathbf{1}} = 0 \tag{24}$$

For the linearized inverter system the process and measurement noise covariance matrices become

$$\mathbf{R_1} = \begin{bmatrix} r_{111} & 0 & 0 \\ 0 & r_{122} & 0 \\ 0 & 0 & r_{133} \end{bmatrix} \qquad \mathbf{R_2} = \begin{bmatrix} r_{211} & 0 & 0 \\ 0 & r_{222} & 0 \\ 0 & 0 & r_{233} \end{bmatrix}$$

When the operating point of the inverter $\theta_0(t)$ is changing, the gain matrix of the estimator $\mathbf{k}\left(\theta_0(t)\right)$ must also be changed.

B. The Non-linear Kalman Estimator

When the inverter system is non-linear, the estimator should also be non-linear. The fundamental voltage of the inverter, in dq-components, can be written

$$\begin{aligned} \hat{u}_d &= -\sin\left(\theta(t)\right)u_x(t)e_q(t) \\ \hat{u}_q &= \cos\left(\theta(t)\right)u_x(t)e_q(t) \end{aligned} \tag{25}$$

and the non-linear estimator can now be

$$\begin{aligned} \frac{d}{dt}\begin{bmatrix} \hat{i}_d \\ \hat{i}_q \\ \hat{u}_{dc} \end{bmatrix} &= \begin{bmatrix} -R_s / L_s & \omega_N & 0 \\ -\omega_N & -R_s / L_s & 0 \\ -\hat{u}_d / C_{dc}\hat{u}_{dc} & -\hat{u}_q / C_{dc}\hat{u}_{dc} & -1 / R_{dc}C_{dc} \end{bmatrix}\begin{bmatrix} \hat{i}_d \\ \hat{i}_q \\ \hat{u}_{dc} \end{bmatrix} + \\ &+ \begin{bmatrix} \hat{u}_d / L_s \\ \left(\hat{u}_d - e_q\right) / L_s \\ i_{dc} / C_{dc} \end{bmatrix} + \mathbf{k}\left(\theta_0\right)\begin{bmatrix} i_d - \hat{i}_d \\ i_q - \hat{i}_q \\ u_{dc} - \hat{u}_{dc} \end{bmatrix} \end{aligned} \tag{26}$$

To determine the operating point of the system, the DC-link current $i_v(t)$ can be used. In steady-state the phase displacement angle $\theta(t)$ is proportional to the DC-link current $i_v(t)$.

VIII. Stability of the System when Using LQ-controller and Kalman Estimator

When the Kalman estimator estimates the states of the system for the LQ-controller, the system can become unstable. By adding fictitious noise to the plant input model, representing in a perhaps loose way plant variations, uncertainty, or unmodelled dynamics, there is an adjustment to the estimator design. In coping with the fictitious noise, the LQ-Kalman controller becomes more robust to gain and phase changes at the plant input. The analysed system is a MIMO-system and it is difficult to determine the stability by using analytic methods. Here two practical methods are used. By changing the parameters of the process and looking at the eigenvalues of the transfer function, the robustness of the parameter variations becomes known. The second method is to simulate by an iterative approach, the total non-linear system and to choose the parameters, weighting matrices and process and measurement noise covariances, so the system becomes stable. The weighting matrices, process and measurement noise have been determined by the last method. To verify the stability of the system, the poles of the closed system have been analysed, when the parameters have been altered. The result shows that no poles are near the imaginary axis. Thus, the system is robust due to small parameter variations.

IX. Analytic Frequency Response and Simulation of the Inverter System

A. The Parameters of the System

The parameters of the total system used in the simulations are listed in Table 1 below. The weighting matrices and the process and measuring covariance matrices have been determined using an iterative method.

TABLE 1
PARAMETERS OF THE INVERTER SYSTEM.

E	1 p.u.	q_{44}	$3\ 10^7$
u_{dc}^*	1 p.u.	r_{11}	400
L_s	0.175 p.u.	r_{22}	50
R_s	$5.6\ 10^{-3}$ p.u.	r_{111}	10
X_{Cdc}	0.1 p.u.	r_{122}	30
R_{dc}	$13.9\ 10^3$ p.u.	r_{133}	100
f_{sw}	5000 Hz	r_{211}	$5\ 10^{-6}$
q_{11}	1	r_{222}	$5\ 10^{-6}$
q_{22}	1	r_{233}	$1\ 10^{-10}$
q_{33}	100		

B. The Frequency Response of the Linearized System

Fig. 5 shows the Bode-diagram of the DC-link voltage $\Delta u_{dc}(t)$ as a function of the generator/rectifier current $\Delta i_{dc}(t)$. The regulators are both of the PI and the PIFF (PI and FeedForward) types. When the PIFF-controller is used, the system becomes a mixed phase system. Comparing the PI to the PIFF controller, the main difference is the settling time. Feedforward makes the system faster compared with using the PI-controller only, approximately 6 times, because the integration term $\mathbf{L_2}$ slows down the system. For both PI- and PIFF-controlled linearized systems the step responses have no overshoots and no ripple. Compared with the traditional power angle control [12], where only the phase displacement angle is controlled, the resonance peak at 50 Hz has disappeared. The reason is that the amplitude of the three-phase voltage inverter is now actively controlled. When feedforward is used, the DC-link voltage fluctuations are decreased, within a frequency range up to 700 Hz, and the DC-link voltage fluctuation from the system with a PI-controller becomes larger.

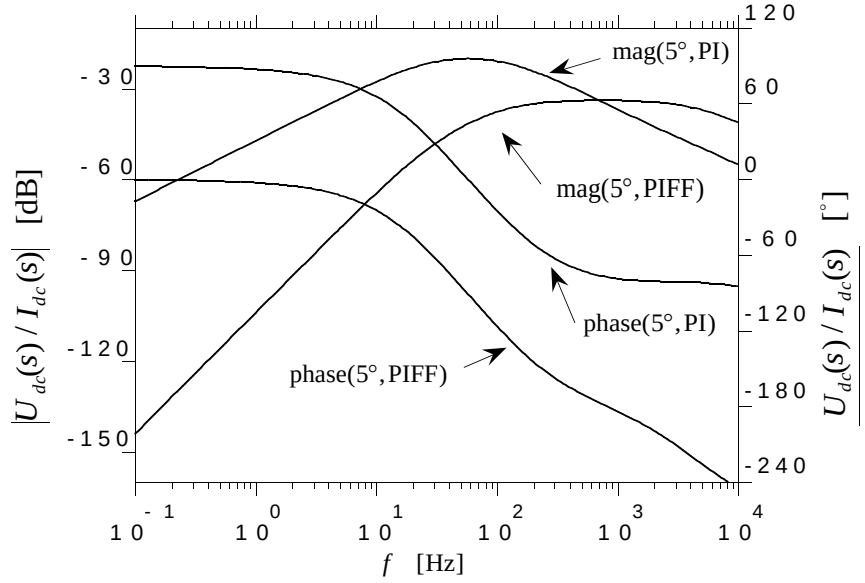

Figure 5: The Bode diagram of the DC-link voltage $\Delta u_{dc}(t)$ as a function of the generator/rectifier current $\Delta i_{dc}(t)$.

C. The Simulation Model

The inverter model consists of a PWM inverter, which has no losses and which switches ideally. Fig. 6 shows the Simulink model of the total inverter system with the estimator, the controller and the inverter system. To locate the operating point of the system, in the controller and in the estimator, the low-pass filtered DC-link current is used.

Figure 7 shows the sub-block "InvSys." From the inputs, the phase displacement angle θ and the relative voltage u_x, the reference voltages to the pulse width modulation block are determined in the sub-block "U_ref." The third harmonic injection in the block "opt" results in an increased inverter output voltage range. The inverter phase voltages, out from the sub-block "U_PWM," are used in sub-block "grid." Here, the phase currents are calculated. The momentary DC-link current i_v sub-block "iv" needs the phase

currents and the switching states of the PWM. The DC-link voltage is calculated in the sub-block "DC-link_voltage."

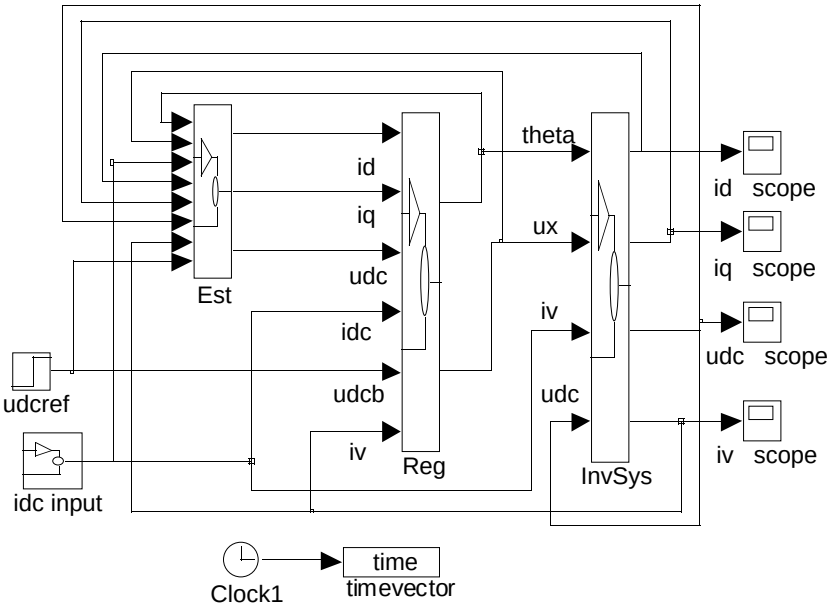

Figure 6: The Simulink model of the LQ-controlled inverter system using an estimator. Est =Kalman estimator; Reg=LQ-regulator; InvSys=inverter system using ideal PWM.

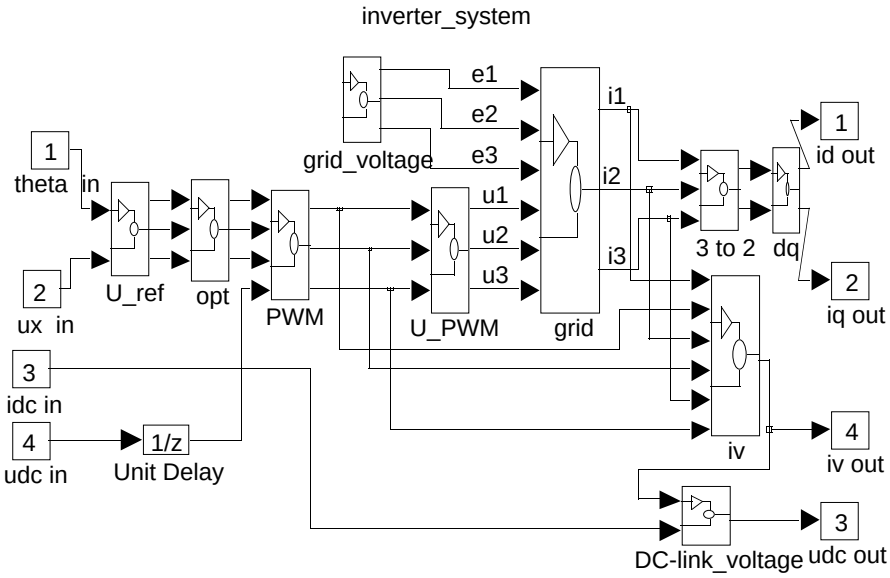

Figure 7: The sub-block "InvSys" from Fig 6.

Before the simulation can start, an m-file named "LQ_init.m" must be executed. Here, the system parameters such as the grid voltage amplitude, series inductance, series resistance, and DC-link capacitance are settled. The LQ-regulator parameters are calculated for different operating points and the gains are collected in a matrix called Lgain. The same method is used for the Kalman estimator, but here the gain matrix is called Kgain.

The LQ-regulator and the estimator are implemented in Simulink, as s-functions, due to non-linearities. The two s-functions have the same structure, see Tables 2 and 3. The gain values come from a table where the operating point angle is the table index.

TABLE 2

THE S-FUNCTION OF THE LQ-REGULATOR.

```
function  [sys,x0]=Regulator(t,x,u,flag,thetaidc,Lgain)
%   s-function LQ-regulator
%       Inputs  u(1) = id       Outputs         y(1) = theta
%               u(2) = iq                       y(2) = ux
%               u(3) = udc
%               u(4) = idc
%               u(5) = udcref
%               u(6) = iv
% operating point angle: theta = thetaidc * iv
% Lgain = matrix containing feedback and feedforward coefficients
if abs(flag)==1 % derivatives
        A=0; B=[0 0 1 0 -1]; sys=A*x+B*u(1:5);

elseif flag==3 % outputs
        theta=u(6)*thetaidc;  % operating point angle
        if theta>=30          % max operating point
                thetanr=30;
        elseif theta<=-30     % min operating point
                thetanr=-30;
        else
                thetanr=theta; % operating point number
        end
        thetanr=rem(thetanr,2);       %matrix index

        if thetanr==0; thetanr=1; end   %exclude theta=0°

        if thetanr<0; nr=thetanr+16; else;nr=thetanr+15; end

        ups=Lgain(nr,:);              % unstuff LL1, LL2 and FF
        LL1=[ups(1),ups(2),ups(3);ups(5),ups(6),ups(7)];
        LL2=[ups(4);ups(8)];
        FF=[ups(9),ups(10);ups(11),ups(12)];
        sys=-LL2*x+[-LL1   FF]*u(1:5);

elseif flag==0; sys=[1 0 2 6 0 1]; x0=0;else; sys=[]; end
```

TABLE 3

THE S-FUNCTION HEAD OF THE ESTIMATOR.

```
function  [sys,x0]=Estimator(t,x,u,flag,thetaidc,R,L,wN,Cdc,Rdc,eq,udcb,Kgain)
%
%   s-function non-linear Kalman estimator
%
%       Inputs  u(1) = theta    Outputs         y(1) = id estimated
%               u(2) = ux                       y(2) = iq estimated
%               u(3) = idc                      y(3) = udc estimated
%               u(4) = id                       y(4) = iv estimated
%               u(5) = iq
%               u(6) = udc
%               u(7) = iv
%               u(8) = udcwant
%
%       thetaidc = constant iv => theta
%       Kgain= table of gain values for different theta
```

D. Step Response of Load Steps

When the inverter system is in steady-state and the generator/rectifier current is 0.8 p.u. a positive current step of the generator/rectifier current $i_{dc}(t)$ of 0.2 p.u. is made at the

simulation time of 0.01 s. At the simulation time of 0.025 s the generator/rectifier current makes a negative step of 0.2 p.u., see Fig. 8. The step response of the DC-link voltage is small, see Fig. 9. The direct current, Fig. 10, is approximately zero except at the generator/rectifier current flanks. The current has a ripple of approximately 0.05 p.u. The quadrature current is shown in Fig. 11. The output signals of the controller, $\theta(t)$ and $u_x(t)$, make momentary spikes at the flanks of the load steps. At steady-state the phase displacement angle is proportional to the generator/rectifier current $i_{dc}(t)$ and the relative voltage is one. The DC-link current $i_v(t)$ and generator/rectifier current are plotted at the positive step of the generator/rectifier current, see Fig. 12. Because the reactance value of the DC-link capacitance is small, the ripple voltage over the DC-link capacitance is rippling. The LQ-regulator feels the voltage ripple and tries to compensate it. That is why the variables of the system have a small ripple. The phase currents of the inverter, expressed in αβ-coordinates, are shown in Fig. 13. The current ripple caused by the PWM is small and can be neglected.

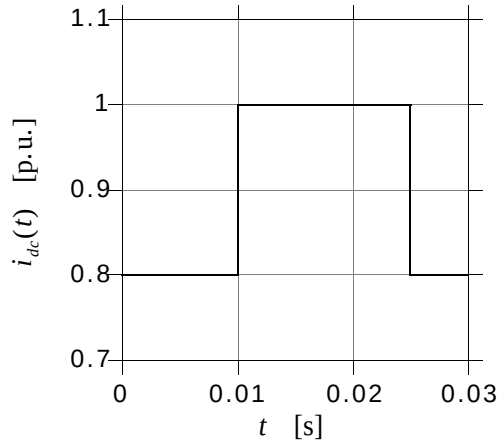

Figure 8: The generator/rectifier current.

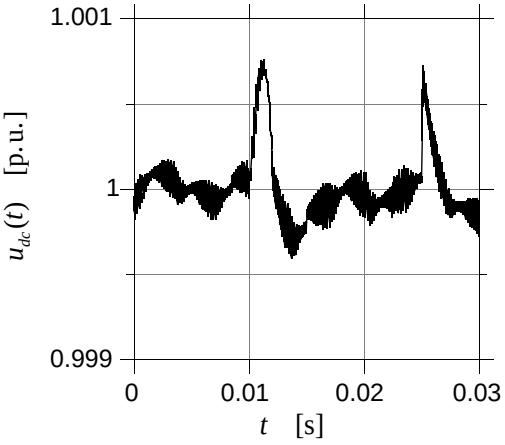

Figure 9: The DC-link voltage.

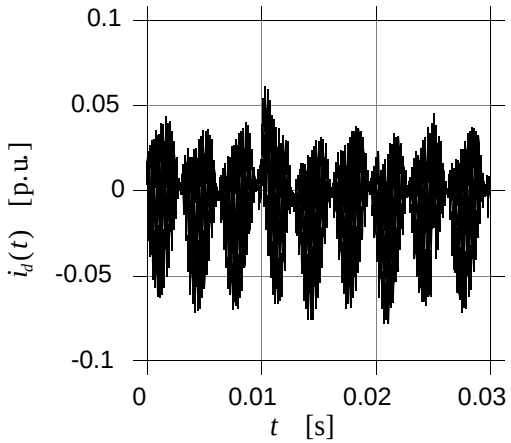

Figure 10: The direct current.

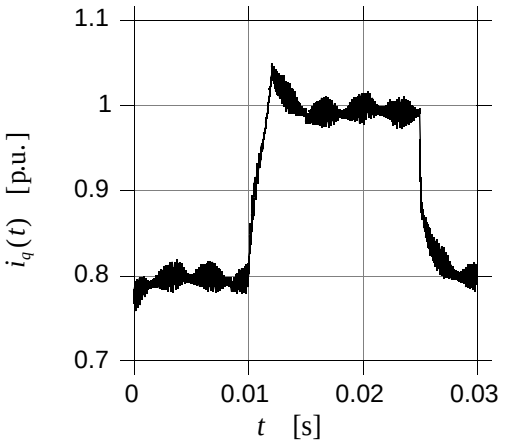

Figure 11: The quadrature current.

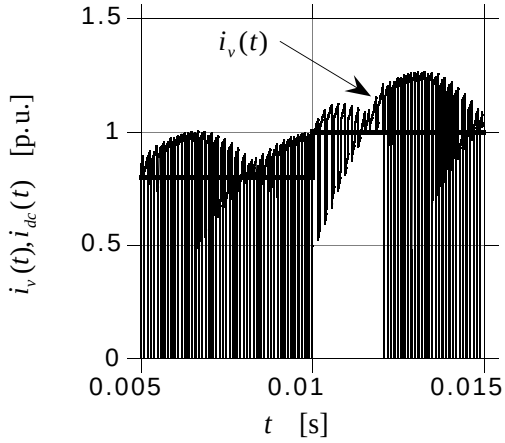

Figure 12: The DC-link current and the generator/rectifier current. Positive current step.

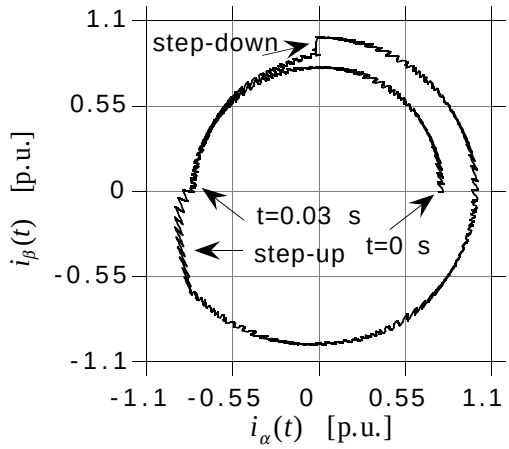

Figure 13: The phase currents in $\alpha\beta$-coordinates.

X. CONCLUSIONS

The inverter system as well as the feedback and feedforward parameters are easy to handle when state equations are used. The inputs of the MIMO system are the phase displacement angle and the relative voltage. It is easy to control the inputs by using the LQ-control. A disadvantage of the LQ-control of the power angle controlled inverter system is that the current harmonics disturb the controller. The disturbances are depressed by using a non-linear Kalman estimator to estimate the state of the non-linear inverter system. The simulation results show that the proposed methods of simulation and control function well.

XI. REFERENCES

[1] A. Grauers, "Higher electrical efficiency with variable speed," presented at ECWEC, pp. 656-658, Travemünde, 1993.

[2] W. E. Leithead, "Variable Speed Operation - Does it Have Any Advantages?," *Wind Engineering*, vol. 13, pp. 302-314, 1989.

[3] M. V. Lowson, "A New Prediction Model for Wind Turbine Noise," *Wind Engineering*, vol. 18, pp. 51-61, 1994.

[4] P. Verdelho and G. D. Marques, "Digital simulation and applications of the PWM voltage converter connected to the AC mains," presented at EPE, pp. 438-443, Firenze, 1991.

[5] Å. Ekström, "Calculation of Transfer Functions for a Forced-Commutated Voltage-Source Converter," presented at PESC'91, pp. 314-322, Boston, MA, 1991.

[6] B. T. Ooi and X. Wang, "Voltage Angle Lock Loop Control of the Boost Type PWM Converter for HVDC Application," *IEEE Trans. on Power Electronics*, vol. 5, pp. 229-235, 1990.

[7] G. Joos, L. Morán, and P. Ziogas, "Performance Analysis of a PWM Inverter VAR Compensator," *IEEE Trans. on Power Electronics*, vol. 6, pp. 380-391, 1991.

[8] O. Carlson, A. Grauers, J. Svensson, and Å. Larsson, "A comparison between electrical systems for variable speed operation of wind turbines," presented at EWEC '94, pp. 500-505, Thessaloniki, 1994.

[9] B. D. O. Anderson and J. B. Moore, *Optimal Control - linear quadratic methods*. Englewood Cliffs, NJ 07632: Prentice-Hall, Inc, 1989.

[10] J. V. D. Vegte, *FEEDBACK CONTROL SYSTEMS*. Englewood Cliffs, NJ 07632: Prentice-Hall, 1986.

[11] B. D. O. Anderson and J. B. Moore, *Optimal Filtering*. Englewood Cliffs, NJ 07632: Prentice-Hall, Inc, 1979.

[12] J. Svensson, "Voltage Angle Control of a Voltage Source Inverter, Application to a Grid-Connected Wind Turbine," presented at EPE, pp. 539-544, Sevilla, 1995.

PAPER 3A

J. Svensson, "Inclusion of Dead-Time and Parameter Variations in VSC Modelling for Predicting Responses of Grid Voltage Harmonics," *7th European Conference on Power Electronics and Applications (EPE'97)*, Trondheim, Norway, 8-10 September 1997, Proceedings, Vol. 3, pp. 216-221.

Inclusion of Dead-time and Parameter Variations in VSC Modelling for Predicting Responses of Grid Voltage Harmonics

J. Svensson

Chalmers University of Technology, Sweden

Abstract: A discrete regulator-controlled VSC connected to the grid is analysed by discrete state equations and by the use of the average switch model method. The controller takes into account the dead-time, caused by the calculation time of the controller, as well as parameter variations. All transfer functions from one voltage component (*d* or *q*) to one current component (*d* or *q*) have the same gain characteristics. The gain of the grid voltages increases when the frequency increases. The gain has a maximum at approximately 20 % of the sample frequency and decreases rapidly at higher frequencies. The maximum gain is higher for the direct coupling of *d*- and *q*-voltage to *d*- and *q*-current than for the cross coupling. The gain becomes higher when the estimated inductance is smaller than the correct inductance value. Both the *d*- and *q*-components of the voltage will fluctuate when the phase voltage harmonic components have the same amplitude in all three phases. The gain of the transfer function from the phase voltage to the grid current becomes higher than those of the *d*- and *q*-component transfer functions. The gain is still low at low frequencies resulting in a nearly sinusoidal current waveform.

Keywords: PWM, Grid, Converter, Harmonic, Dead-beat, State Equation, Dead-Time, Average Switch Model

I. INTRODUCTION

Today, Voltage Source Converters (VSC) are used in a variety of applications. The increase in the power ratings of the valves (IGBTs) results in new applications such as grid-friendly rectifiers [1] and active filters [2]. In these new applications, the dynamic performance depends on the performance of the control system.

The common procedure to analyse a suboscillated PWM VSC-system [3] is to replace the PWM-pattern during one sample period of the switching frequency with the average values of the reference value signals. The method is often called the Average Switch Model (ASM) [4]. The ASM is appropriate when the switching frequency of the PWM is much higher than the requested frequency. In addition, the PWM is not allowed to be saturated. Continuous time simulations are often used, and transfer functions in the *s*-domain are used to analyse the system in the frequency domain [5,6]. Today, the control system is implemented in a computer. The computer samples the input signals and introduces a dead-time of at least one sample period due to the calculation time. The sample frequency is constant and depends on the switching frequency of the suboscillating PWM. The sample frequency can be at most twice the switching frequency. The dead-time can be modelled by using the Padé approximation [7]. The disadvantage is the increased polynom order in the transfer function.

In this paper, a discrete regulator-controlled VSC connected to the grid is analysed by discrete state equations and by the use of the ASM. The controller takes into account the dead-time as well as parameter variations. The currents are controlled by a dead-beat controller [8], which is possible due to the switching principle of the VSC. Closed-loop models of the total system can be achieved by assembling the different current regulators and the grid model. The simplest current regulators analysed are the P-regulator and the PI-regulator which have an infinitely fast control computer. The P and PI controllers which introduce a dead-time of one sample, due to the calculation time, are called delayed controllers and denote ZP and ZPI. The performance of the closed-loop models of the different systems is analysed. The focus is on the sensitivity to grid voltage harmonics. In addition, the system responses of the active and reactive phase current components to the reference currents are of interest.

II. THE SYSTEM CONFIGURATION

The system configuration is shown in Figure 1. The scheme contains a VSC, an L-filter and a regulator. The regulator tracks the reference active current $i_q^*(t)$ and reference reactive current $i_d^*(t)$. The grid currents and grid voltages are sampled and transformed into the two-axis αβ-coordinate system and then into the rotating *dq*-coordinate system. The *d*-axis of the *dq*-frame is synchronized with the grid flux vector. The reference voltage vector from the regulator, in the *dq*-coordinate system, is transformed into the three-phase system. To take full advantage of the DC-link voltage level, denoted by $u_{dc}(t)$, third harmonics are added to the reference voltage values in the block OPT. The last step to control the VSC is to transform the reference voltages into a pulse width pattern in the block PWM. The resistance and the inductance of the series filter are denoted R_s and L_s, respectively. The three-phase voltages and currents of the grid are denoted $e_1(t)$, $e_2(t)$ and $e_3(t)$ and $i_1(t)$, $i_2(t)$ and $i_3(t)$, respectively. The three-phase voltages of the VSC are denoted $u_1(t)$, $u_2(t)$ and $u_3(t)$. The current from the DC-link to the converter is denoted $i_V(t)$.

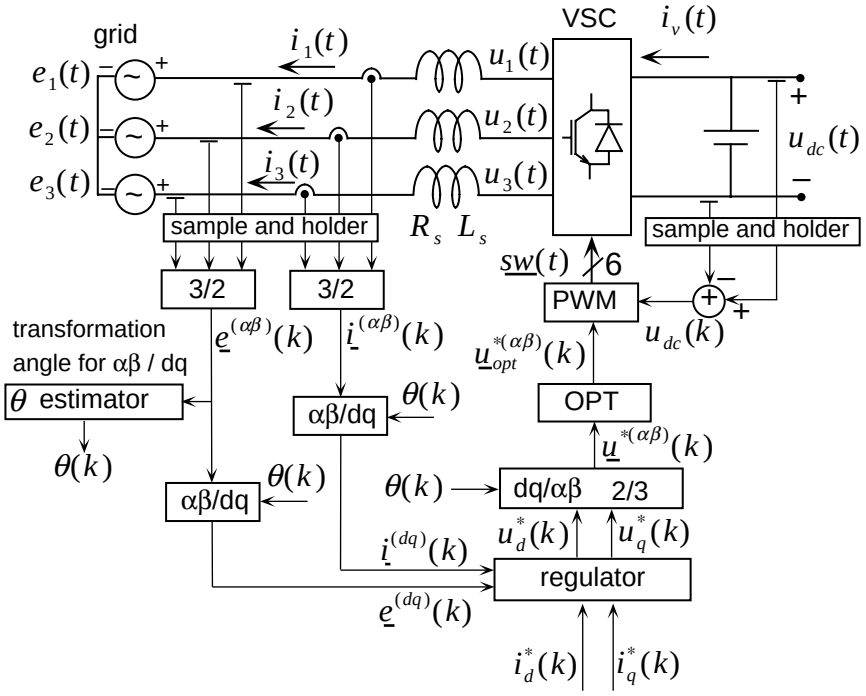

Figure 1: Overview of the system, which contains the VSC, L-filter and the regulator.

In the analysis, the VSC model is assumed to be ideal. This means that the valves switch momentaneously and have no losses, and the dead-time to prevent phase-leg short-circuit is zero. The grid filter consists of three series inductors, one in each phase. The inductors have a constant inductance and resistance. The VSC is modelled as a three-phase voltage source with sampled voltages when using the ASM method. For all models, the voltage reference values from the regulator are not allowed to be saturated and small-signal analysis is used when a state equation becomes non-linear.

III. THE GRID MODEL

The VSC and the grid are modelled as two three-phase voltage sources. The grid filter is placed between the two voltage sources. The continuous-time state space equation for the system in the dq-frame is

$$\frac{d}{dt}\begin{bmatrix} i_d(t) \\ i_q(t) \end{bmatrix} = \mathbf{A}\begin{bmatrix} i_d(t) \\ i_q(t) \end{bmatrix} + \mathbf{B_u}\begin{bmatrix} u_d(t) \\ u_q(t) \end{bmatrix} + \mathbf{B_e}\begin{bmatrix} e_d(t) \\ e_q(t) \end{bmatrix} \tag{1}$$

where the matrices are given by

$$\mathbf{A} = \begin{bmatrix} -\frac{R_s}{L_s} & \omega_N \\ -\omega_N & -\frac{R_s}{L_s} \end{bmatrix} \qquad \mathbf{B_u} = \begin{bmatrix} \frac{1}{L_s} & 0 \\ 0 & \frac{1}{L_s} \end{bmatrix} \qquad \mathbf{B_e} = \begin{bmatrix} -\frac{1}{L_s} & 0 \\ 0 & -\frac{1}{L_s} \end{bmatrix}$$

The current and voltage regulators operate in discrete time. To combine the grid model with the other models, the grid model is transformed from the continuous time into a zero-order held sampled system with the sample time T_s. The state equation becomes

$$\begin{bmatrix} i_d(k+1) \\ i_q(k+1) \end{bmatrix} = \mathbf{F}\begin{bmatrix} i_d(k) \\ i_q(k) \end{bmatrix} + \mathbf{G_u}\begin{bmatrix} u_d(k) \\ u_q(k) \end{bmatrix} + \mathbf{G_e}\begin{bmatrix} e_d(k) \\ e_q(k) \end{bmatrix} \tag{2}$$

The matrices are

$$\mathbf{F} = e^{\mathbf{A}T_S}$$
$$\mathbf{G_u} = -\mathbf{G_e} = \int_0^{T_S} e^{\mathbf{A}\tau} d\tau \mathbf{B_u} \tag{3}$$

IV. Regulator and Closed-loop System Equations

A. The P-Regulator

The P-regulator presented here has partially been taken from [9]. The application of the Kirchhoff voltage law to the grid model yields

$$u_d(t) = e_d(t) + R_r i_d(t) - \omega_N L_r i_q(t) + L_r \frac{d}{dt} i_d(t) \tag{4}$$

$$u_q(t) = e_q(t) + R_r i_q(t) + \omega_N L_r i_d(t) + L_r \frac{d}{dt} i_q(t) \tag{5}$$

where the inductance and the resistance of the series coil are denoted by subscript *r* to emphasize that the parameters of the regulator can differ from the real values. The mean voltages over the sample period *k* to *k*+1 are derived by integrating Eqs. (4) and (5) from kT_S to $(k+1)T_S$ and dividing by T_S. By assuming the dead-beat control as well as linear current variations over the interval and no changes in the grid voltage components over one sample period, the control equations can be written as

$$u_d^*(k) = e_d(k) + R_r i_d(k) - \frac{\omega_N L_r}{2} i_q(k) - \frac{\omega_N L_r}{2} i_q^*(k) + k_P\left(i_d^*(k) - i_d(k)\right) \tag{6}$$

$$u_q^*(k) = e_q(k) + R_r i_q(k) + \frac{\omega_N L_r}{2} i_d(k) + \frac{\omega_N L_r}{2} i_d^*(k) + k_P\left(i_q^*(k) - i_q(k)\right) \tag{7}$$

where the gain for the dead-beat control is

$$k_P = \frac{L_r}{T_s} + \frac{R_r}{2} \tag{8}$$

Equations (6) and (7) can be written in matrix form

$$\begin{bmatrix} u_d^*(k) \\ u_q^*(k) \end{bmatrix} = \mathbf{D_P} u_{reg}(k) \tag{9}$$

where the input vector u_{reg} to the regulator is

$$u_{reg}(k) = \left[i_d^*(k)\ i_q^*(k)\ i_d(k)\ i_q(k)\ e_d(k)\ e_q(k)\right]^T$$

and the matrix is

$$\mathbf{D_P} = \begin{bmatrix} k_P & -\frac{\omega_N L_r}{2} & R_r - k_P & -\frac{\omega_N L_r}{2} & 1 & 0 \\ \frac{\omega_N L_r}{2} & k_P & \frac{\omega_N L_r}{2} & R_r - k_P & 0 & 1 \end{bmatrix}$$

The closed-loop system can be determined by inserting Eq. (9) into Eq. (2). The state equation becomes

$$\begin{bmatrix} i_d(k+1) \\ i_q(k+1) \end{bmatrix} = \mathbf{F_{CLP}} \begin{bmatrix} i_d(k) \\ i_q(k) \end{bmatrix} + \mathbf{G_{CLP}} \begin{bmatrix} i_d^*(k) \\ i_q^*(k) \end{bmatrix} \tag{10}$$

where

$$\mathbf{F_{CLP}} = \mathbf{F} + \mathbf{G_u A_{P,reg}} \qquad \mathbf{G_{CLP}} = \mathbf{G_u B_{P,reg}}$$

and

$$\mathbf{A_{P,reg}} = \begin{bmatrix} R_r - k_P & -\frac{\omega_N L_r}{2} \\ \frac{\omega_N L_r}{2} & R_r - k_P \end{bmatrix} \qquad \mathbf{B_{P,reg}} = \begin{bmatrix} k_P & -\frac{\omega_N L_r}{2} \\ \frac{\omega_N L_r}{2} & k_P \end{bmatrix}$$

B. The PI-Regulator

The PI-regulator is introduced to remove static errors. The errors come from non-linearities, noisy measurements and non-ideal components. The regulator equations are

$$u_d^*(k) = e_d(k) + R_r i_d(k) - \frac{\omega_N L_r}{2} i_q(k) - \frac{\omega_N L_r}{2} i_q^*(k) + k_P\left(i_d^*(k) - i_d(k)\right) + \Delta u_{Id}(k) \tag{11}$$

$$u_q^*(k) = e_q(k) + R_r i_q(k) + \frac{\omega_N L_r}{2} i_d(k) + \frac{\omega_N L_r}{2} i_d^*(k) + k_P\left(i_q^*(k) - i_q(k)\right) + \Delta u_{Iq}(k) \tag{12}$$

where the integration constants come from the state equation

$$\begin{bmatrix} \Delta u_{Id}(k+1) \\ \Delta u_{Iq}(k+1) \end{bmatrix} = \begin{bmatrix} \Delta u_{Id}(k) \\ \Delta u_{Iq}(k) \end{bmatrix} + k_I \begin{bmatrix} i_d^*(k-1) \\ i_q^*(k-1) \end{bmatrix} - k_I \begin{bmatrix} i_d(k) \\ i_q(k) \end{bmatrix} \tag{13}$$

The state equation of the closed loop system using PI-regulator is

$$\begin{bmatrix} i_d(k+1) \\ i_q(k+1) \\ i_{dz}^*(k+1) \\ i_{qz}^*(k+1) \\ \Delta u_{Id}(k+1) \\ \Delta u_{Iq}(k+1) \end{bmatrix} = \mathbf{F_{CLPI}} \begin{bmatrix} i_d(k) \\ i_q(k) \\ i_{dz}^*(k) \\ i_{qz}^*(k) \\ \Delta u_{Id}(k) \\ \Delta u_{Iq}(k) \end{bmatrix} + \mathbf{G_{CLPI}} \begin{bmatrix} i_d^*(k) \\ i_q^*(k) \end{bmatrix} \tag{14}$$

C. The Delayed P-Regulator

The delayed P-regulator contains one term more than the previous P-regulator. The regulator equations, including the time delay, are

$$\begin{aligned} u_d^*(k+1) = {} & e_d(k) + R_r i_d(k) - \frac{\omega_N L_r}{2}\left(i_q^*(k) + i_q(k)\right) \\ & + k_P\left(i_d^*(k) - i_d(k)\right) - \Delta u_d(k) \end{aligned} \tag{15}$$

$$\begin{aligned} u_q^*(k+1) = {} & e_q(k) + R_r i_q(k) + \frac{\omega_N L_r}{2}\left(i_d^*(k) + i_d(kT)\right) \\ & + k_P\left(i_q^*(k) - i_q(k)\right) - \Delta u_q(k) \end{aligned} \tag{16}$$

In the present sample, the last voltage component has not affected the grid currents due to the delay time of one sample [10]. The delay time compensation must remove the voltage component due to the current error. The compensation terms become

$$\Delta u_d(k) = k_p\left(i_d^*(k-1) - i_d(k-1)\right) - \Delta u_d(k-1) \tag{17}$$

$$\Delta u_q(k) = k_p\left(i_q^*(k-1) - i_q(k-1)\right) - \Delta u_q(k-1) \tag{18}$$

The closed-loop system with the delayed P-controller becomes

$$\begin{bmatrix} i_d(k+1) \\ i_q(k+1) \\ u_d^*(k+1) \\ u_q^*(k+1) \\ \Delta u_d(k+1) \\ \Delta u_q(k+1) \end{bmatrix} = \mathbf{F_{CLZP}} \begin{bmatrix} i_d(k) \\ i_q(k) \\ u_d^*(k) \\ u_q^*(k) \\ \Delta u_d(k) \\ \Delta u_q(k) \end{bmatrix} + \mathbf{G_{CLZP}} \begin{bmatrix} i_d^*(k) \\ i_q^*(k) \\ e_d(k) \\ e_q(k) \end{bmatrix} \tag{19}$$

D. The Delayed PI-Regulator

For a delayed regulator using dead-beat control, it takes two samples before the grid currents are equal to the reference values of the current. The equations of the delayed PI-regulator become

$$\begin{aligned} u_d^*(k+1) = {} & e_d(k) + R_r i_d(k) - \frac{\omega_N L_r}{2}\left(i_q^*(k) + i_q(k)\right) + \\ & k_P\left(i_d^*(k) - i_d(k)\right) + \Delta u_{Id}(k) - \Delta u_d(k) \end{aligned} \tag{20}$$

$$\begin{aligned} u_q^*(k+1) = {} & e_q(k) + R_r i_q(k) + \frac{\omega_N L_r}{2}\left(i_d^*(k) + i_d(kT)\right) + \\ & k_P\left(i_q^*(k) - i_q(k)\right) + \Delta u_{Iq}(k) - \Delta u_q(k) \end{aligned} \tag{21}$$

The compensation terms are the same as for the P-regulator. The integration term of the PI-regulator is a sum of the current errors for all the old samples and can be written as

$$\begin{bmatrix} \Delta u_{Id}(k+1) \\ \Delta u_{Iq}(k+1) \end{bmatrix} = \begin{bmatrix} \Delta u_{Id}(k) \\ \Delta u_{Iq}(k) \end{bmatrix} + k_I \begin{bmatrix} i_d^*(k-2) \\ i_q^*(k-2) \end{bmatrix} - k_I \begin{bmatrix} i_d(k) \\ i_q(k) \end{bmatrix} \tag{22}$$

The closed-loop system with the PI-regulator and the delayed controller becomes

$$x(k+1) = \mathbf{F_{CLZPI}} x(k) + \mathbf{G_{CLZPI}}\left[i_d^*(k)\ i_q^*(k)\ e_d(k)\ e_q(k)\right]^T \tag{23}$$

where the state vector $x(k)$ has 12 states.

V. The Interaction Between the AC- and DC-Sides of the VSC

The DC-link current can be written as

$$i_v(t) = \left(u_d(t) i_d(t) + u_q(t) i_q(t)\right) / u_{dc}(t) \tag{24}$$

if the output voltage of the VSC is modelled as a smooth voltage vector $\underline{u}(t)$, the converter losses are negligible and the converter output voltages are not saturated. Due to the fact that the system is non-linear and the analysis method only works in linear

systems, the non-linear system is linearized in an operating point and the analysis only describes how the system behaves in a small region around the operating point.

A. Operating Points

The operating point of the system is determined by the reference values of the grid currents, the grid voltages and the DC-link voltage. Let the operating points be denoted by the subscript 0. Here the regulator parameters are correctly tuned, due to the real system parameters. When using a PI-regulator, the grid currents are equal to their reference values in steady state. The regulator output becomes

$$\begin{aligned} u_{d0}^{*} &= e_{d0} + R_r i_{d0} - \omega_N L_r i_{q0}^{*} \\ u_{q0}^{*} &= e_{q0} + R_r i_{q0} + \omega_N L_r i_{d0}^{*} \end{aligned} \tag{25}$$

and the output voltage of the converter is equal to the reference voltage of the converter. The steady-state grid current is

$$\begin{bmatrix} i_{d0} \\ i_{q0} \end{bmatrix} = (I - \mathbf{F})^{-1} \left(\mathbf{G_u} \begin{bmatrix} u_{d0} \\ u_{q0} \end{bmatrix} + \mathbf{G_e} \begin{bmatrix} e_{d0} \\ e_{q0} \end{bmatrix} \right) \tag{26}$$

The operating point of the DC-link current is

$$i_{v0} = \left(u_{d0} i_{d0} + u_{q0} i_{q0} \right) / u_{dc0} \tag{27}$$

B. The System Linearization

Here, the linearized system will be analysed around an operating point. Let the perturbation around the operating point be denoted by Δ. The small-signal DC-link current to the VSC becomes

$$\Delta i_v(t) = \frac{\begin{bmatrix} u_{d0} \\ u_{q0} \end{bmatrix}^T \begin{bmatrix} \Delta i_d(t) \\ \Delta i_q(t) \end{bmatrix} + \begin{bmatrix} i_{d0} \\ i_{q0} \end{bmatrix}^T \begin{bmatrix} \Delta u_d(t) \\ \Delta u_q(t) \end{bmatrix}}{u_{dc0}} - \frac{i_{v0}}{u_{dc0}} \Delta u_{dc}(t) \tag{28}$$

The other equations are linear, so the small signal equations become the same.

C. The Linearized Model of the System

In the linearized model, in contrast with the closed-loop ZPI model (23), the DC-link current is determined. The state space equation for the system with a stiff DC-link voltage can be written as

$$x(k+1) = \mathbf{A_{LIN}} x(k) + \mathbf{B_{LIN}} \left[\Delta i_d^{*}(k) \; \Delta i_q^{*}(k) \; \Delta e_d(k) \; \Delta e_q(k) \right]^T \tag{29}$$

$$\begin{bmatrix} \Delta i_d(k) \\ \Delta i_q(k) \\ \Delta u_d(k) \\ \Delta u_q(k) \\ \Delta i_v(k) \end{bmatrix} = \mathbf{C_{LIN}} x(k) + \mathbf{D_{LIN}} \begin{bmatrix} \Delta i_d^{*}(k) \\ \Delta i_q^{*}(k) \\ \Delta e_d(k) \\ \Delta e_q(k) \end{bmatrix} \tag{30}$$

where the state vector $x(k)$ has 12 states.

VI. THE FREQUENCY ANALYSIS

A number of transfer functions can be obtained from the different state equations of the closed loop systems. Here, a small number of the transfer functions will be presented. The parameters of the VSC, the grid and the regulators are given in Table 1. To make the notation of the different system and control configurations simple, the configurations are denoted by letters from A to E, as shown in Table 2.

TABLE 1
THE PARAMETERS OF THE SYSTEM INCLUDING THE REGULATORS.

E	1.0 p.u.	E_{d0}	0 p.u.
$U_{dc}^{*}=1.5E$	1.0 p.u.	E_{q0}	1.0 p.u.
L_S	0.15 p.u.	i_{d0}	0.5 p.u.
R_S	0.015 p.u.	i_{q0}	0.5 p.u.
T_S	100 μs	ω_N	100π rad/s

TABLE 2
THE SYSTEM AND CONTROL CONFIGURATIONS.

#	current regulator	State equation
A	P, without time delay	CLP
B	PI, without time delay	CLPI
C	P, with time delay	CLZP
D	PI, with time delay	CLZPI
E	PI, with time delay	LIN

A. The Coupling from the Reference Current to the Grid Current

The main reason for using the vector control is to control the active and the reactive current independently. In Figure 2, the Bode diagram of the transfer function from the reference of the *d*-current to the *d*-current is shown. The gain is approximately one for the transfer functions for the different systems. The phase shifts are larger for the regulators which have a time delay of one sample. The same characteristic is obtained for the transfer function from the reference of the *q*-current to the *q*-current. The Bode diagram of the transfer function from the reference of the *d*-current to the *q*-current is shown in Figure 3. The gain is small and can be neglected in practice. The gain for the time-delayed regulator is higher than for the regulators which do not have a time delay. The frequency response from the reference of the *q*-current to the *d*-current is identical to the previous one.

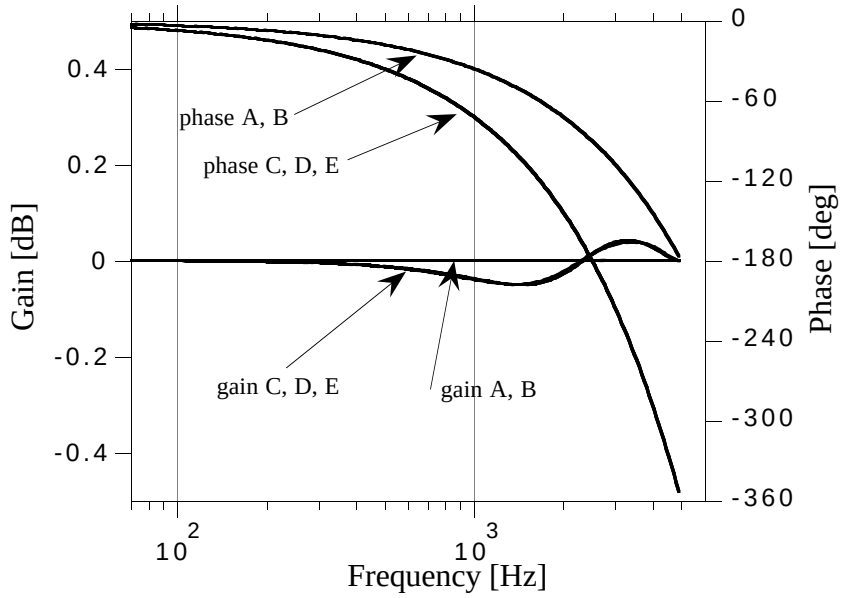

Figure 2: The Bode diagram from the reference value of the d-current Δi_d^* to the d-current Δi_d. The systems A, B, C, D and E are displayed.

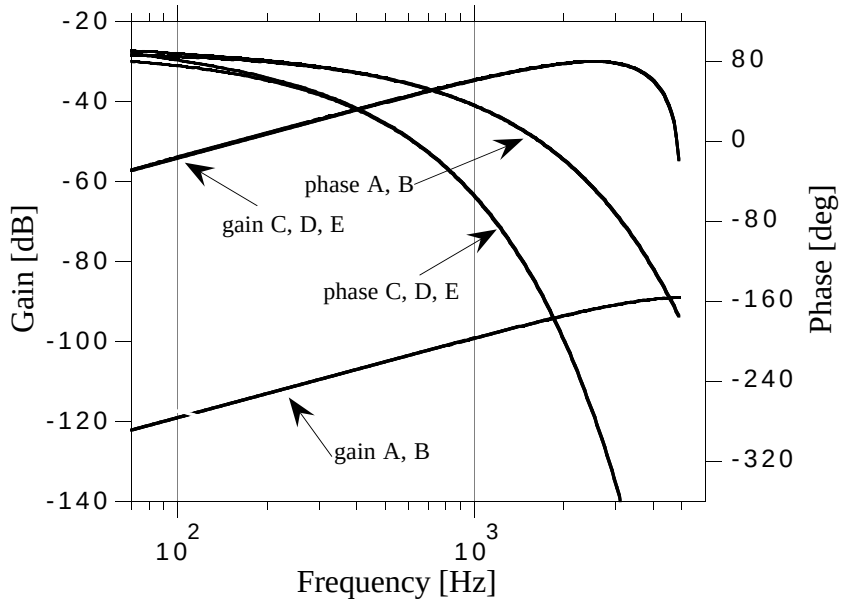

Figure 3: The Bode diagram from the reference value of the d-current Δi_d^* to the q-current Δi_q. The systems A, B, C, D and E are displayed.

B. The Grid Voltage Coupling to VSC Currents

The low-frequency voltage harmonics of the grid affect the output currents of the VSC. Figures 4 to 6 show the Bode diagrams of the transfer functions from the *d*- and *q*-grid voltages to the *d*- and *q*-grid current. The transfer functions from Δe_d to Δi_d and Δe_q to Δi_q have the same characteristics. For all transfer functions, the gain of the grid voltages increases when the frequency increases. The gain has a maximum at 2.2 kHz (i. e.,

approximately 20 % of the sample frequency) and then decreases rapidly. There is no difference between the characteristics of the time-delayed P-regulator and the time-delayed PI-regulator. But the gain differs for the different transfer functions. The gain of the transfer functions Δe_d to Δi_q and Δe_q to Δi_d are the same but the phase shifts are different. The maximum gain is larger for the direct coupling, -25 dB, than for the cross couplings, which have the maximum gain of -50 dB.

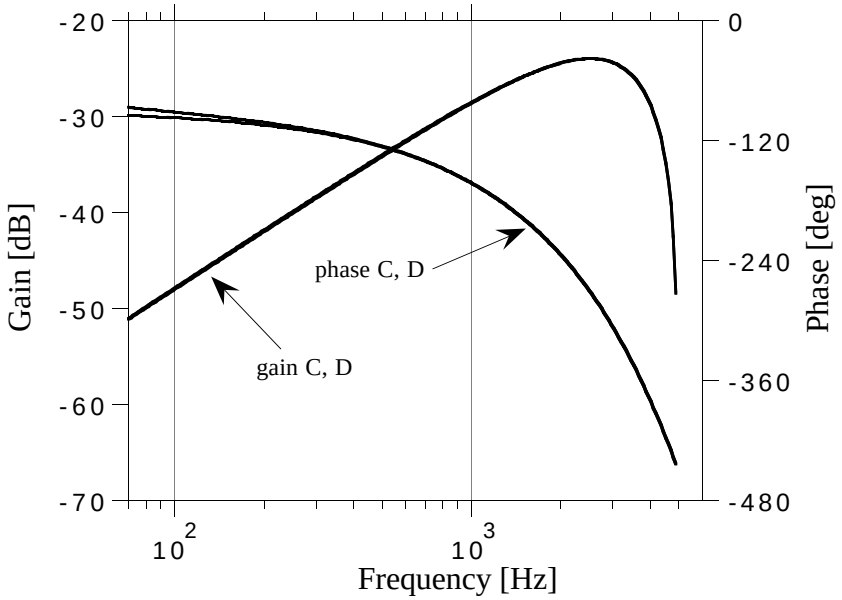

Figure 4: The Bode diagram from the d-grid voltage Δe_d to the d-current Δi_d. The systems C and D are displayed.

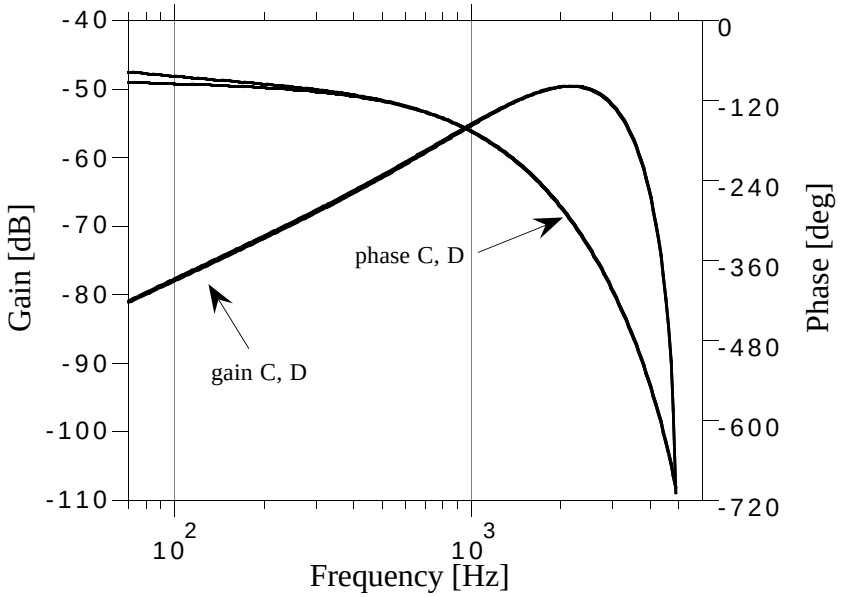

Figure 5: The Bode diagram from the q-grid voltage Δe_q to the d-current Δi_d. The systems C and D are displayed.

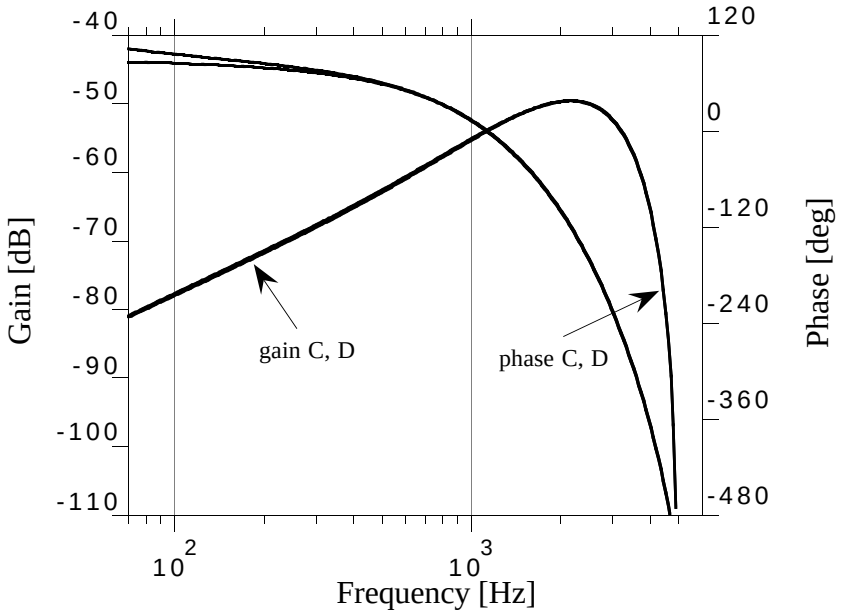

Figure 6: The Bode diagram from the d-grid voltage Δe_d to the q-current Δi_q. The systems C and D are displayed.

C. The Grid Voltage Coupling to the DC-link Current

The transfer function characteristics from the grid voltage components to the DC-link current are shown in Figure 7. The DC-link current characteristics as a function of the grid voltages increase with the frequency and have a maximum at 2.2 kHz. Then the gain decreases rapidly. The gain is higher for the transfer function from Δe_d to Δi_V than for Δe_q to Δi_V.

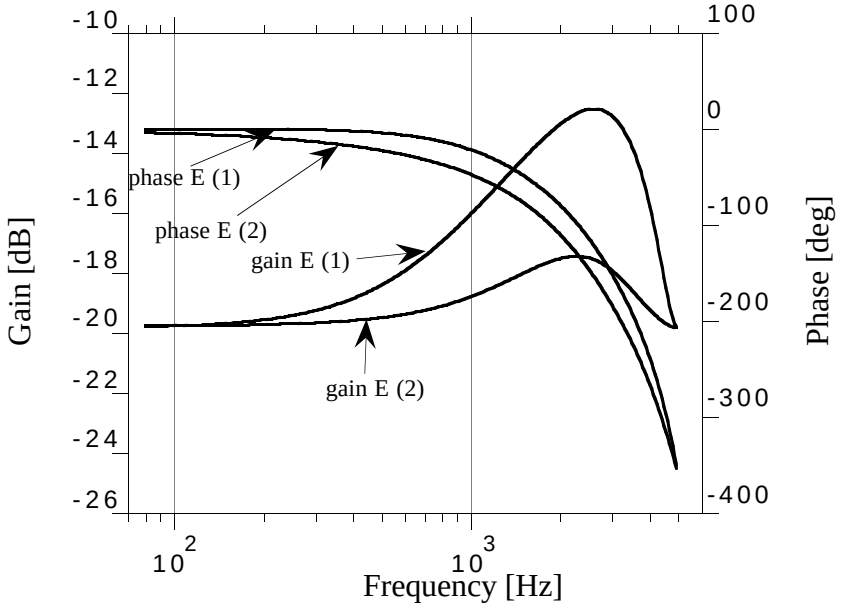

Figure 7: The Bode diagram from the d- and q-grid voltages, Δe_d (marked by 1) and Δe_q (marked by 2) to the DC-link current Δi_V. The system E is displayed.

D. Influence of Parameter Value Variations

In this section, the system response is determined when the controller parameters are misfitted due to an inaccurate determination of the inductance and resistance. The estimated series inductance has an error of ±25 % and the estimated resistance has an error of ±50 %. In Figures 8 to 10, the transfer functions from Δi_d^* to Δi_d and from Δe_d to Δi_d and Δi_q are shown. The gain changes ±6 dB at 300 Hz and ±4.5 dB at 600 Hz for the transfer functions from Δe_d to Δi_q. Further, the gain changes ±2 dB at 300 Hz and ±1.6 dB at 600 Hz for the transfer functions from Δe_d to Δi_d. In both cases, the resistance variations do not influence the results. The gain becomes higher when the estimated inductance is smaller than the correct inductance value. For the transfer functions from Δi_d^* to Δi_d the gain fluctuation becomes ±4 dB.

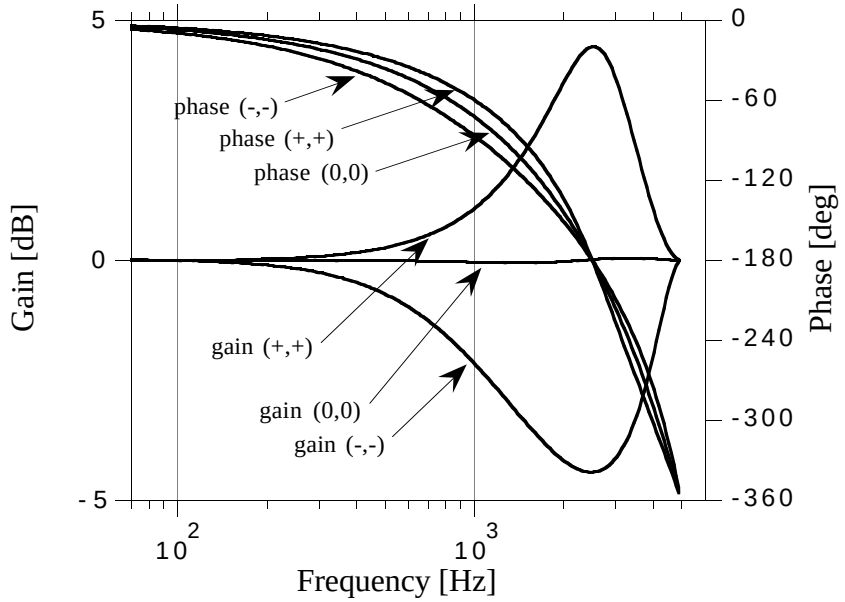

Figure 8: The Bode diagram from the reference value of the d-current Δi_d^* to the d-current Δi_d. The system D is displayed. The (+,+) means higher estimated inductance and higher estimated resistance than the correct value of the series coil.

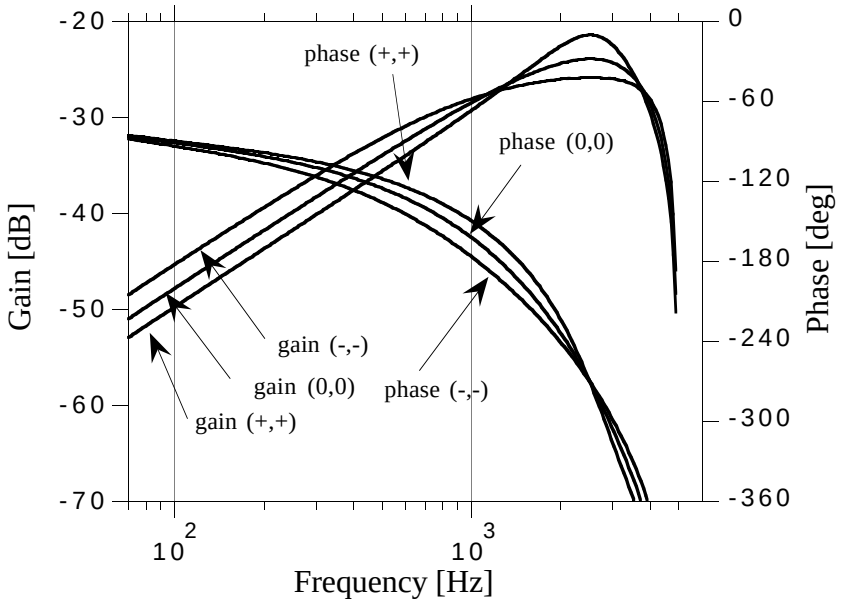

Figure 9: *The Bode diagram from the d-grid voltage Δe_d to the d-current Δi_d. The system D is displayed. The (+,+) means higher estimated inductance and higher estimated resistance than the correct value of the series coil.*

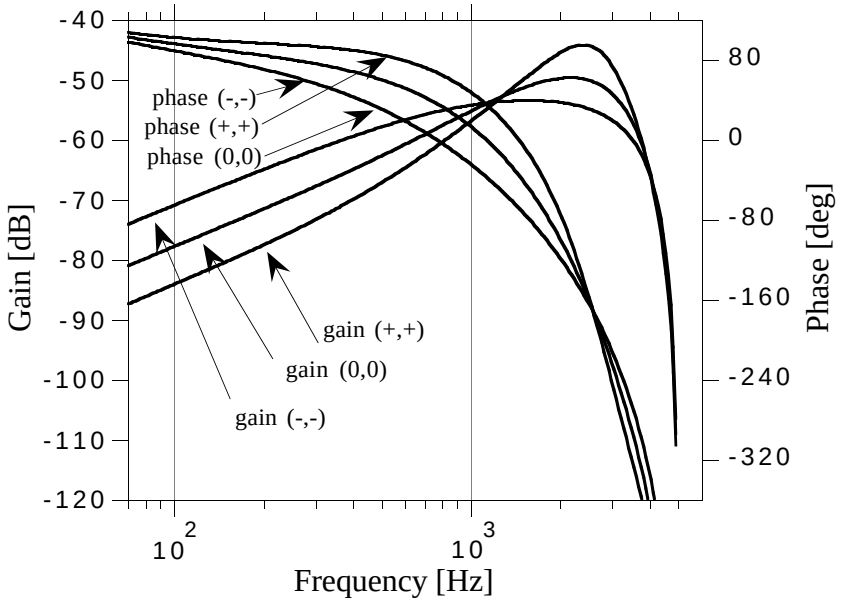

Figure 10: *The Bode diagram from the d-grid voltage Δe_d to the q-current Δi_q. The system D is displayed. The (+,+) means larger estimated inductance and larger estimated resistance than the correct value of the series coil.*

VII. SYSTEM SIMULATION

The complete non-linear model was simulated by using the Matlab/Simulink program in order to verify the linearized frequency responses of the different transfer functions. The simulation model is equal to the system in Figure 1 exept for the PWM-block, which was removed in order to accelerate the simulation. The parameters and operating points of the reference currents are the same as in Table 1.

A. Grid Voltage Harmonics

The phase voltage harmonic components have the same amplitude in all three phases. When the harmonic components are transformed to the *dq*-coordinate system, the frequencies of the components are changed, depending on positive or negative phase sequences. Both the *d*- and *q*-components of the voltage will fluctuate. The voltage fluctuations of the *d*- and *q*-component will be of the same magnitude.

The gain is determined from the phase voltage and the resulting phase current at each harmonic frequency. The voltage harmonic components are listed in Table 3. In Figure 11, the phase voltage and the phase current are shown. The result in Table 3 shows that the gain becomes higher than for the transfer functions from grid voltage harmonic components in *d*- and *q*-direction to the grid current components in *d*- and *q*-direction, for instance Fig. 5. This is because the gain is here composed of both the direct coupling and cross coupling from both *d* and *q*.

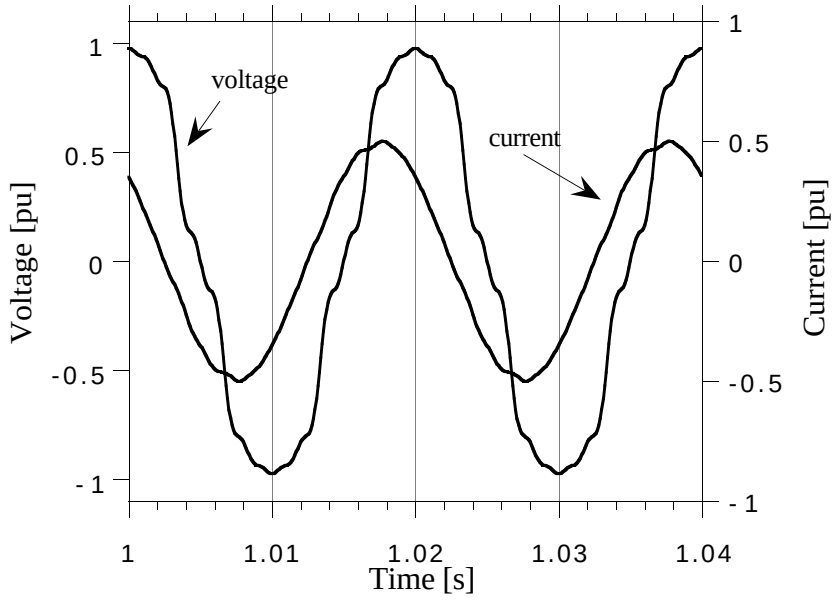

Figure 11: The distorted phase voltage and the resulting phase current.

TABLE 3
THE GAIN OF TRANSFER FUNCTION FROM PHASE VOLTAGE
TO PHASE CURRENT HARMONICS.

Harmonic #	Harmonic level in percent of $e_{1(1)}$	$\lvert i_{1(n)} / e_{1(n)} \rvert$
n=5	7.0	–38 dB
n=7	5.0	–38 dB
n=11	3.2	–32 dB
n=13	2.7	–32 dB

B. Harmonic Fluctuation in d- and q-Components of the Grid Voltage

Simulations were performed to verify the analytical frequency responses from low-frequency disturbances in the *d*- and *q*-components of the grid voltage to the *d*- and *q*-components of grid current. The simulation model was adjusted to inject voltage harmonics in *d*- or *q*-axis of the grid three-phase voltage. The disturbance frequency were altered from 200 to 600 Hz in steps of 100 Hz. The different frequency responses were then determined by frequency analysis. The obtained frequency responses correspond well to the analytical transfer function.

VIII. CONCLUSION

A discrete regulator-controlled VSC connected to the grid is analysed by discrete state equations and by the use of the average switch model method. The controller takes into account the dead-time caused by the calculation time, as well as parameter variations. A linearization at an operating point is performed if the analysed model becomes non-linear.

All transfer functions from the *d*- and *q*- grid voltage components to the *d*- and *q*-current components have the same gain characteristics. The gain of the grid voltages increases when the frequency increases. The gain has a maximum (at 2.2 kHz for the investigated system) and decreases rapidly at higher frequencies. The minimum attenuation is higher for the direct coupling of *d*- and *q*-voltage to *d*- and *q*-current than for the cross coupling. In addition, the influence of parameter variation is analyzed. The attenuation becomes lower when the estimated inductance is smaller than the correct inductance value.

When the phase voltage harmonic components have the same amplitude in all three phases. Both the *d*- and *q*-components of the voltage will fluctuate. The gain becomes higher than for the transfer functions from the grid voltage harmonic components in *d*- and *q*-direction to the grid current components in *d*- and *q*-direction. This is because the gain is composed of both the direct coupling and cross coupling from both *d*- and *q*-components. The gain is still low at low frequencies, resulting in good current control perfomance.

IX. ACKNOWLEDGEMENT

The financial support given by the Swedish National Board for Industrial and Technical Development is gratefully acknowledged.

X. REFERENCES

[1] M. Lindgren, J. Svensson, "Connecting fast switching voltage-source converters to the grid – harmonic distortion and its reduction", IEEE/Stockholm Power Tech Conference, Stockholm, Sweden, June 18-22 1995. Proceedings, vol. "Power Electronics", pp. 191-196.

[2] H. Akagi, "Trends in Active Power Line Conditioners," IEEE Trans. on Power Electronics, Vol. 9, No. 3, pp. 263-268, May 1994.

[3] J. Holtz, "Pulsewidth Modulation for Electronic Power Conversion," Proc. of IEEE, Vol. 82, No. 8, pp. 1194-1214, August 1994.

[4] R. Kagalwala, S. S. Venkata, P. O. Lauritzen, "A Transient Behavioral Model (TBM) for Power Converters," 5th Workshop on Computers in Power Electronics, IEEE Power Electronics Society, Portland USA, 11-14 August, 1996.

[5] J. Ollila, “Analysis of PWM-Converters using Space Vector Theory – Application to a Voltage Source Rectifier,” Tampere University of Technology, Finland, Tampere, Publications 111, 1993.

[6] Naser Abdel-Rahim, John E. Quaicoe, "Small-Signal Model and Analysis of A Multiple Feedback Control Scheme for Three-Phase Voltage-Source UPS Inverters." Power Electronics Specialists Conference (PESC'96), Baveno Italy, 23-27 June, 1996, pp. 188-194.

[7] J. E. Marshall, "Control of time-delay systems." IEE Control Engineering Series; 10. Institution of Electrical Engineers, London and New York, 1979.

[8] K. J. Åström, B. Wittenmark, "Computer-controlled systems." Prentice-Hall International inc., Englewood Cliffs, New Jersey, 1990.

[9] T. Svensson, "On Modulation and Control of Electronic Power Converters." Chalmers University of Technology, Sweden, Technical Report No. 186, 1988.

[10] M. Lindgren, "Feed forward – Time Efficient Control of a Voltage Source Converter Connected to the Grid by Lowpass Filters." Power Electronics Specialists Conference (PESC'95), Atlanta, 18-22 June 1995, Vol. 2, pp. 1028-1032.

XI. ADDRESS OF THE AUTHOR

Jan Svensson
Dept. of Electric Power Engineering
Chalmers University of Technology
412 96 Goteborg, Sweden

PAPER 3B

J. Svensson, "Synchronisation Methods for Grid Connected Voltage Source Converter," Submitted to IEE Proceedings Electric Power Applications.

Synchronisation Methods for Grid-Connected Voltage Source Converters

J. Svensson

Indexing terms: Phase locked loop, Electric power system, Synchronisation, Voltage source converter

Abstract: Four different synchronisation methods for a VSC connected to a three-phase grid are investigated. The methods are adapted for use in a digital controller. The performance of the synchronisation methods is studied by response characteristics of phase-shift steps, frequency steps and low-frequency grid voltage harmonics. The low-pass filtering method can be used only if the frequency of the grid is constant and phase jumps do not occur. If phase jumps occur, the novel space vector filtering method is recommended. The extended space vector filtering method is adapted to handle frequency variations and is also preferred if fast frequency variations occur. This method even has a higher performance than the extended Kalman filter method, in spite of the large number of calculations that must be performed.

LIST OF PRINCIPAL SYMBOLS

$e_{g1},\ e_{g2},\ e_{g3}$	= grid phase voltages
$e_1,\ e_2,\ e_3$	= phase voltages in point of common connection (PCC)
$e_\alpha,\ e_\beta$	= grid voltage in αβ-coordinates in PCC
$e_d,\ e_q$	= grid voltage in dq-coordinates in PCC
$\underline{e} = e_\alpha + je_\beta$	= grid voltage vector in PCC
$i_d,\ i_q$	= grid currents in *dq*-coordinates
$i_\alpha,\ i_\beta$	= grid currents in αβ-coordinates
k	= sample index
k_{ISVF}	= integral gain
k_{PSVF}	= proportional gain
L_g	= short-circuit inductance of the grid
L_S	= series inductance of the grid filter
R_g	= short-circuit resistance of the grid
R_S	= series resistance of the grid filter
T_S	= sample time
$\mathbf{x}$	= state vector
$\mathbf{v}$	= process noise
$\mathbf{w}$	= sensor noise
$\mathbf{A_{SVF}}\ \mathbf{B_{SVF}}\ \mathbf{C_{SVF}}\ \mathbf{D_{SVF}}$	= discrete state equation matrices
$\mathbf{R}(\theta)$	= rotation matrix
$\mathbf{V}$	= process noise covariance matrix
$\mathbf{W}$	= sensor noise covariance matrix
γ	= forgetting factor

θ = transformation angle
$\Delta\theta$ = transformation angle deviation
ω_g = grid angular frequency
$\Delta\omega_g$ = grid angular frequency deviation
^ = estimated value

1 INTRODUCTION

In almost all power electronic equipment connected to the grid, a phase-locked loop (PLL) is used to obtain an accurate synchronisation to the grid. The synchronisation algorithm must cope with the existing electrical environment [1], e.g., with harmonics, voltage sags and commutation notches. Another problem is grid frequency variations. In strong grids, the frequency variations are usually small, but larger frequency variations occur in autonomous grids. Furthermore, the synchronisation must handle measurement noise. An accurate zero voltage crossing detection is essential for the control of grid-commutated converters. Otherwise, the converter system can suffer from poor performance or even instability.

The firing angle unit for thyristor valves uses the zero voltage crossing as a reference; the zero voltage crossing must be accurately detected each half period of the grid [2]. A more demanding application is the grid connection of a forced-commutated voltage source converter (VSC) when vector current control is used [3]. The synchronisation must be updated not just at zero voltage crossings but continuously under the whole period. In this case, a flux-based transformation angle detector (TAD) is used to obtain the rotating dq-coordinate system [3].

The classical synchronisator is an analogue PLL [4], designed around the IC chip 4046. Today, control systems of converters are often implemented in a computer. By using a software solution to the PLL, a flexible and cost effective solution is obtained. The analogue PLL function can be translated into a software PLL function [5], but the low update frequency from zero voltage detection is a disadvantage. Digital filters and controllers can, however, increase performance and make new methods feasible. If the input signal is noisy, a predictive digital filter can be used to find the zero voltage crossings for the PLL [6]. The calculation time is critical for a real time control system, which results in a demand for fast algorithms.

In this paper, four synchronisation methods will be analysed. The complexity of the methods varies from a simple method adapted for stiff-grid applications to the extended Kalman filter (EKF) and a novel space vector filter (SVF), which can handle both phase angle steps and frequency steps. The performance of the synchronisation methods will be analysed based on three criteria: phase shift response, frequency step response and sensitivity to grid voltage harmonics. The maximum allowed frequency change is 1 Hz/s in accordance with the IEC 1800-3. However, a good understanding of the performance is obtained by using frequency step responses.

2 VSC SYSTEM CONNECTED TO WEAK GRID

When a VSC is connected to a weak grid, the voltage at the point of common connection (PCC) will vary and become a function of several variables: the grid voltage behind the

impedance describing the grid, the grid current and the short-circuit parameters of the grid. A step in the power from the VSC (or another user of the grid at the PCC) results in a step change of the voltage vector at the PCC.

The VSC connected to a weak grid and the vector current controller are shown in Fig. 1. The transformation angle $\theta(t)$ is used to transform grid currents and grid voltages at the PCC to the *dq*-coordinate system needed in the vector current controller. The reference voltages from the current controller are transformed back to three-phase values. The synchronisation must have a high performance due to the structure of the vector current controller. A phase shift in the synchronisation will result in steady-state errors, and the cross-coupling current gain will increase. In addition, poor performance or instability can occur if the synchronisation is sensitive to noise or reacts too distinctly to phase steps.

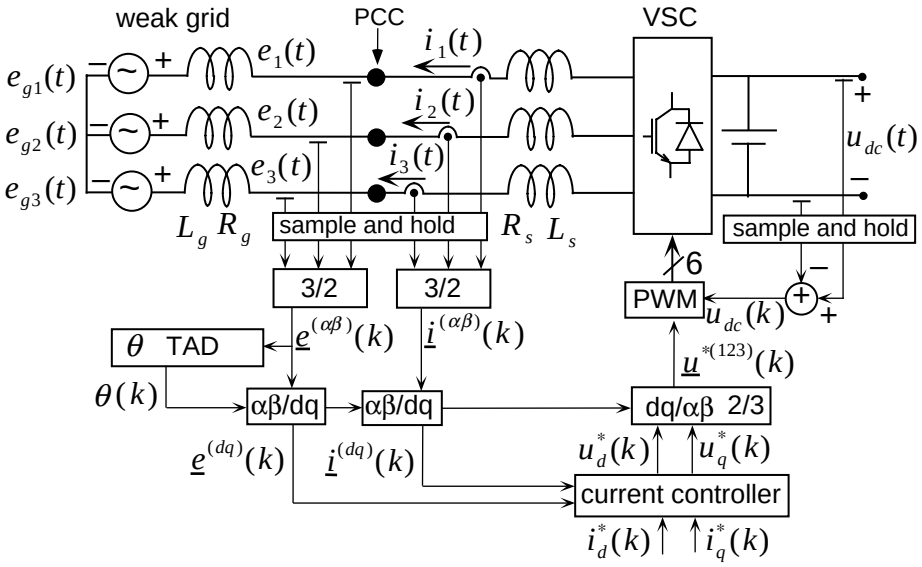

Figure 1: VSC system diagram consisting of the VSC, the grid filter, the weak grid and the vector current controller.

3 TAD BASED ON LOW-PASS FILTERING OF GRID VOLTAGE

A simple method is obtained by low-pass filtering (LP-filtering) the grid voltage vector and the method is denoted by LP-TAD. A first-order Butterworth filter is utilized. The cut-off frequency is tuned to between 0.1 and 25 Hz. The phase lag of a first-order filter depends on the grid frequency and the cut-off frequency. The desired phase lag of 90° occurs at an infinte frequency. The phase lag will, thus, be less than 90° due to the grid frequency of 50 or 60 Hz. The phase lag increases when the cut-off frequency decreases. By using a coordinate transformator, the LP-filtered grid voltage vector can be rotated by an angle $\Delta\theta$ so that the phase lag becomes 90°. Fig. 2 shows a diagram of the LP-TAD.

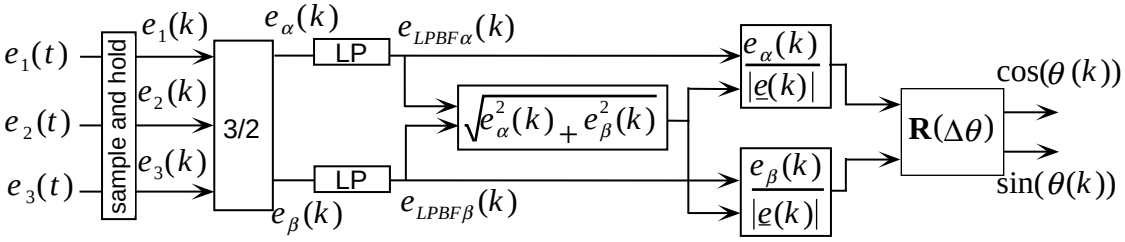

Figure 2: Diagram of the LP-TAD.

Two calculated step responses to a 10° phase-shift in the grid voltage vector are presented in Figs. 3 and 4. The grid frequency is 50 Hz and the cut-off frequency is 0.5 Hz or 5.0 Hz. Coordinate transformation is not used to correct the phase-shift. Different steady-state angle errors, due to different cut-off frequencies, can be observed in Figs. 3 and 4. The phase-shift errors are approximately 1° and 6° for cut-off frequencies 0.5 and 5 Hz, respectively. Unfortunately, the detector characteristics are undamped and oscillate. The damping is increased by a higher cut-off frequency. This behaviour makes the detector unsuitable for applications where phase jumps can occur. In practice, every grid-connected VSC is exposed to grid phase jumps due to short circuits in other nodes of the grid [7]. The LP-TAD is also sensitive to grid frequency deviations.

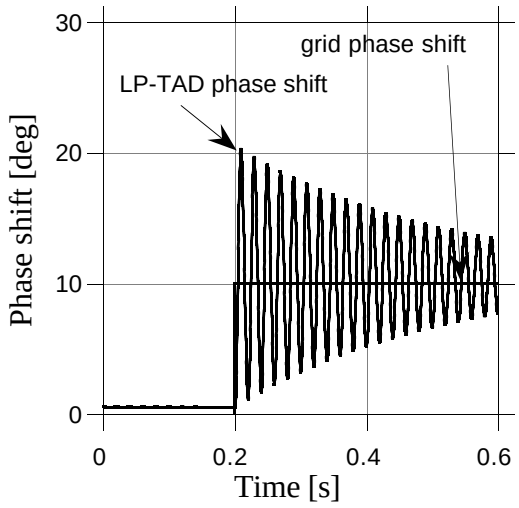

Figure 3: LP-TAD phase shift response to a grid phase shift step. The cut-off frequency is 0.5 Hz.

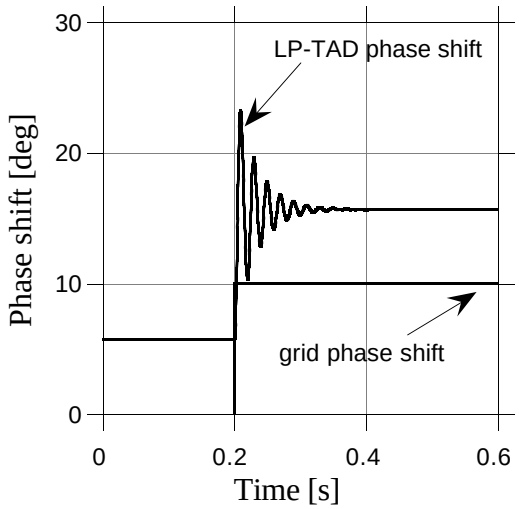

Figure 4: LP-TAD phase shift response to a grid phase shift step. The cut-off frequency is 5 Hz.

4 TAD BASED ON SPACE VECTOR FILTERING FOR CONSTANT GRID FREQUENCY

The novel space vector filter (SVF) is an LP-filter for space vectors; it is based on the fact that the fundamental αβ-components of the grid voltage depend on each other. These voltages can be expressed as a rotating voltage vector with a constant amplitude and constant frequency. The filter has two inputs, $e_\alpha(t)$ and $e_\beta(t)$. The filter uses a model of the grid voltage vector $e_{SVF\alpha} + je_{SVF\beta}$, which is updated with every sample. By assuming a constant sample time and a constant grid frequency, the grid voltage vector of the model can be estimated for the next sample. The value of the forgetting factor γ determines how much influence the grid voltage vector has on the model of the grid voltage. The outputs are $e_{filt\alpha}(t)$ and $e_{filt\beta}(t)$. The filter equations in state variable form become

$$\begin{bmatrix} e_{SVF\alpha}(k+1) \\ e_{SVF\beta}(k+1) \end{bmatrix} = \mathbf{A_{SVF}} \begin{bmatrix} e_{SVF\alpha}(k) \\ e_{SVF\beta}(k) \end{bmatrix} + \mathbf{B_{SVF}} \begin{bmatrix} e_\alpha(k) \\ e_\beta(k) \end{bmatrix} \tag{1}$$

$$\begin{bmatrix} e_{filt\alpha}(k) \\ e_{filt\beta}(k) \end{bmatrix} = \mathbf{C_{SVF}} \begin{bmatrix} e_{SVF\alpha}(k) \\ e_{SVF\beta}(k) \end{bmatrix} + \mathbf{D_{SVF}} \begin{bmatrix} e_\alpha(k) \\ e_\beta(k) \end{bmatrix} \tag{2}$$

where the matrices are given by

$$\mathbf{A_{SVF}} = \gamma \mathbf{R}(\omega_g T_S);\ \mathbf{B_{SVF}} = \begin{bmatrix} 1-\gamma & 0 \\ 0 & 1-\gamma \end{bmatrix};\ \mathbf{C_{SVF}} = \gamma \mathbf{R}(\omega_g T_S);\ \mathbf{D_{SVF}} = \begin{bmatrix} 1-\gamma & 0 \\ 0 & 1-\gamma \end{bmatrix}$$

If the forgetting factor γ = 1, the model has no connection to the inputs of the filter and if the forgetting factor is 0, the output of the filter will be the grid voltage. A scheme of the SVF-TAD is shown in Fig. 5. To determine TAD performance, two tests have been made. The first one is a step-response to a phase-shift of the grid voltage vector. The second test evaluates the influence of grid voltage harmonics on the filter.

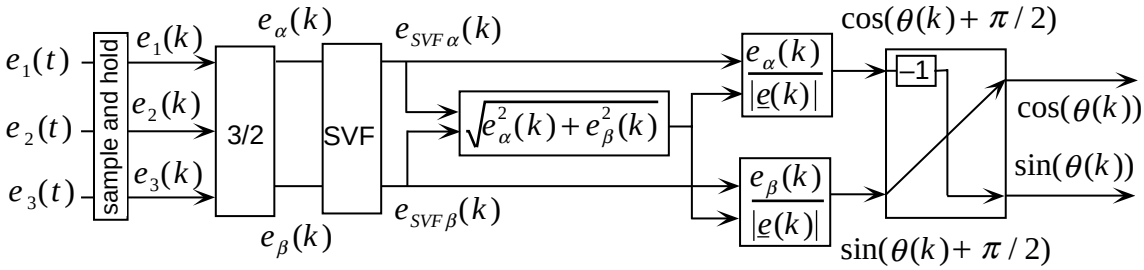

Figure 5: Diagram of the SVF-TAD.

4.1 Phase Shift Step Response

The step response to a 10° phase shift of the grid voltage vector is shown in Fig. 6. The forgetting factor has values between 0.9 and 0.9995. The sample time is 200 µs and the grid frequency is 50 Hz. The SVF-TAD does not introduce any phase shift, and the step response is well damped. A high value of the forgetting factor results in a long settling time, which is preferable because the time constant should be larger than the other time constants in the system.

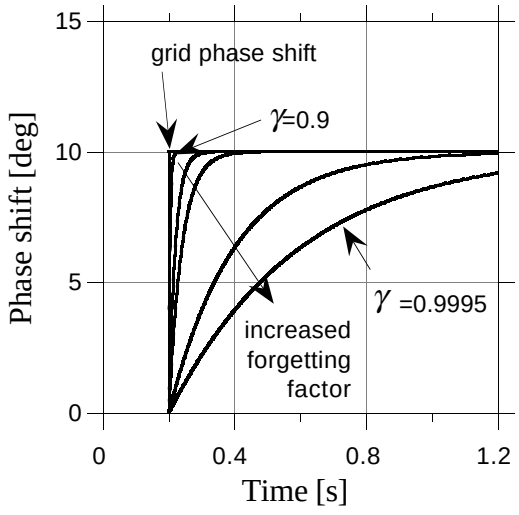

Figure 6: SVF-TAD phase shift responses to a grid phase shift step for different forgetting factors γ.

4.2 The Influence of Grid Voltage Harmonics

The gain of the SVF-TAD for grid voltage harmonics is determined by two simulations performed by injecting a 10 % voltage harmonic component of the 5th or 11th order. The

grid frequency is 50 Hz and the sample time is 200 µs. The gain from the input to the output of the SVF for the harmonic voltage components is displayed in Fig. 7. The forgetting factor varies between 0.9 and 0.999. The gain of the voltage harmonics decreases as the forgetting factor is reduced.

The variance of the grid angle deviation displays how much voltage harmonics affect the SVF. Fig. 8 shows this variance when the forgetting factor varies between 0.9 and 0.999. The variance of the SVF output angle deviation is lower than $0.01^{\circ 2}$ when the forgetting factor is higher than 0.99. The SVF handles the distorted grid successfully. The 5th and 7th voltage harmonics have the same gain factor (and the same is valid for the 11th and 13th harmonics) due to the use of the rotating coordinate system.

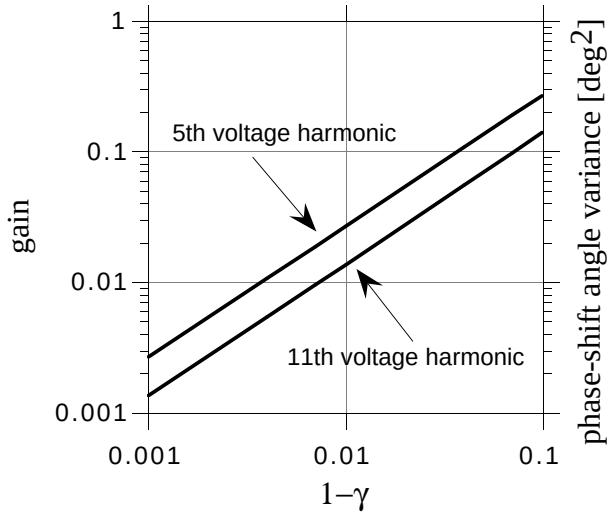

Figure 7: *The gain from the harmonic grid voltage component to the harmonic voltage component after SVF.*

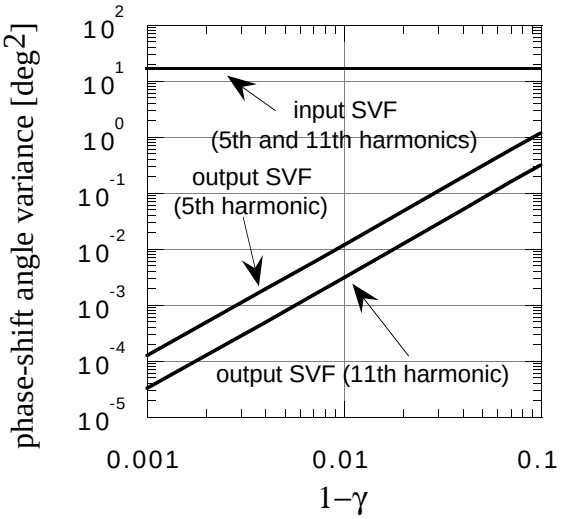

Figure 8: *Variances of the grid phase shift and the SVF-TAD phase shift.*

5 TAD BASED ON SPACE VECTOR FILTERING FOR VARYING GRID FREQUENCY

The SVF-TAD can be adapted to a varying grid frequency and is then called extended SVF-TAD. A phase shift occurs when the grid frequency varies and the forgetting factor of the SVF is high. It is complicated to determine the phase shift directly. However, the phase shift will be proportional to the vector product of the grid voltage vector and the output voltage vector of the SVF for small deviations [8]. If the frequency of the SVF is higher than the grid frequency, the vector product becomes negative. The vector product is called the " Q-vector" referring to the reactive power. To reduce the amplitude-dependence of the Q-vector, the involved voltage vectors are normalized. The Q-vector is fed to a discrete PI-regulator, which is connected to the SVF, as shown in Fig. 9. The PI-regulator output is the estimated frequency deviation. The estimated frequency is the sum of the rated frequency and the estimated frequency deviation.

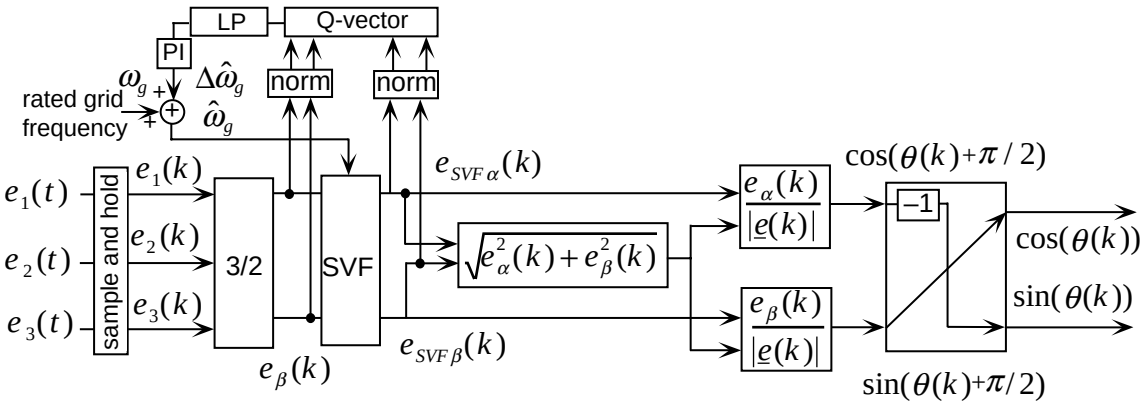

Figure 9: Diagram of the extended SVF-TAD.

Compared with the basic SVF-TAD, the proposed non-linear filter for fluctuating frequency is difficult to analyse. Several parameters must be determined to get a good filter performance: the forgetting factor γ as well as the proportional gain k_{PSVF} and the integrating gain k_{ISVF} of the discrete PI-regulator. To minimise the influence of the voltage harmonics on the grid, a 150 Hz first-order LP-filter is placed between the Q-vector block and the discrete PI-regulator.

The problem of tuning the discrete PI-regulator is the conflict between frequency tracking and sensitivity to voltage harmonics. Another problem is the parallel operation of the frequency regulator and the SVF. If the phase displacement is large, the frequency regulator responds to a frequency error. To reduce this problem, the frequency regulator is tuned to respond slowly. The time constant of the PI-regulator is set to one grid period.

Two simulations are presented in the following: the phase-shift step response and the frequency step response. The simulation parameters, which have been selected by an iterative process to decouple the SVF and the frequency regulator, are listed in Table 1.

TABLE 1
PARAMETERS OF EXTENDED SVF-TAD.

T_S = 200 µs	k_{PSVF} = –4.0
γ = 0.99	k_{ISVF} = –0.04

5.1 Phase Shift Step Response

At the simulation time 0.2 s, the grid voltage vector makes a positive phase shift step of 10°. Fig. 10 shows the phase shift of the extended SVF-TAD. The estimated grid frequency deviation is shown in Fig. 11. The phase shift out from the extended SVF-TAD has an overshoot when the estimated grid frequency deviation increases. This overshoot is caused by the integrating part of the PI-regulator; the integrated part cannot decrease to zero immediately. The estimated grid frequency deviation responds by a step of 0.11 Hz, after which it decreases monotonously to zero.

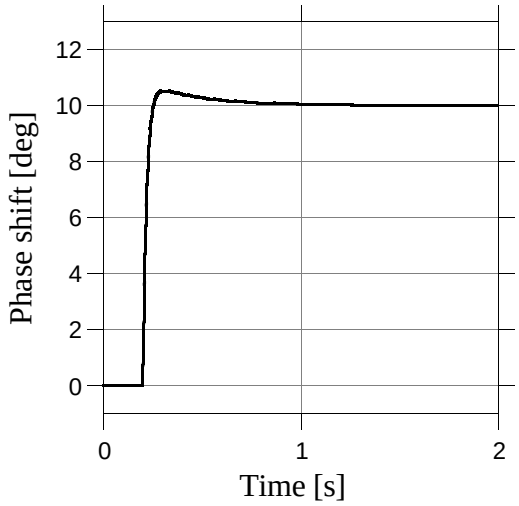

Figure 10: Extended SVF-TAD phase shift response to a grid phase shift step. The phase shift step is 10° at 0.2 s.

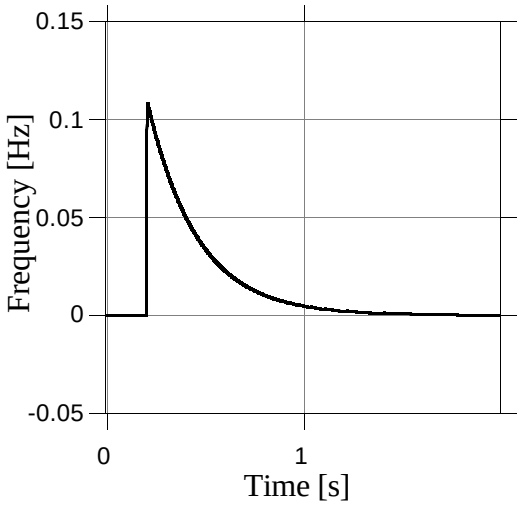

Figure 11: Extended SVF-TAD frequency deviation response to a grid phase shift step. The phase shift step is 10° at 0.2 s.

5.2 Frequency Step Response

The simulation results of a frequency step from 50.0 Hz to 52.5 Hz at 0.2 s are examined. The step and the estimated grid frequency deviation are shown in Fig. 12, and the phase shift of the extended SVF-TAD due to the frequency step is shown in Fig. 13. Due to the slow frequency regulator, the phase shift becomes –14° before it is decreased by the frequency regulator. The phase shift of the extended SVF-TAD tracks the real grid phase shift smoothly without any overshoots. By choosing a faster frequency regulator, the maximum phase shift will decrease, however, the frequency regulator will be more sensitive to the harmonics of the grid voltage, as well.

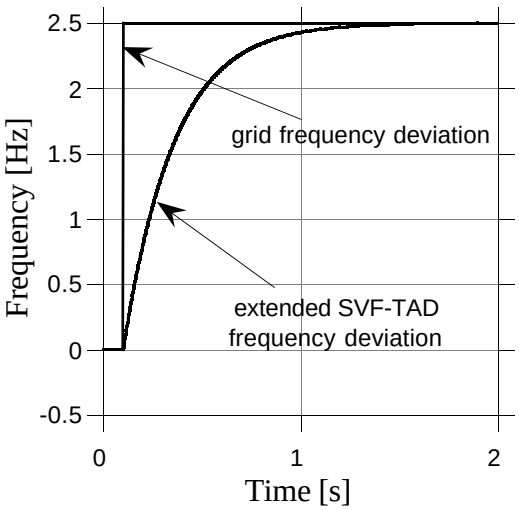

Figure 12: Extended SVF-TAD frequency deviation response to a grid frequency deviation step. The grid frequency steps from 50.0 Hz to 52.5 Hz at 0.2 s.

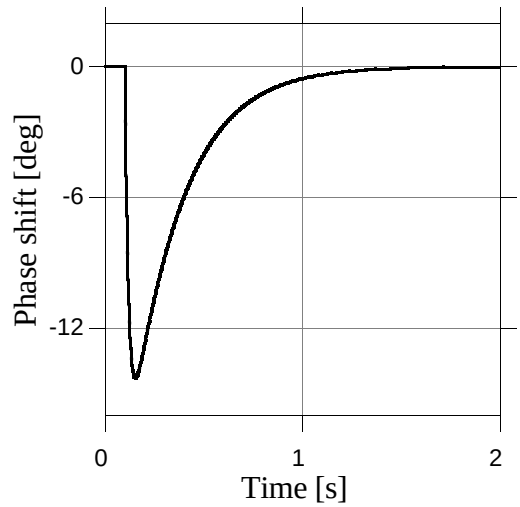

Figure 13: Extended SVF-TAD phase shift response to a grid frequency step. The grid frequency steps from 50.0 Hz to 52.5 Hz at 0.2 s.

5.3 The Influence of Grid Voltage Harmonics

The influence of grid voltage harmonics on the extended SVF-TAD is minor when the frequency regulator parameters are chosen so that the regulator responds slowly. The variance of the grid voltage angle fluctuation is $16.46°^2$, when a 10 % 5th voltage harmonic component is injected to the grid. The filtered variance is $0.012°^2$, i.e., the influence of voltage harmonics has been practically eliminated.

6 TAD BASED ON EXTENDED KALMAN FILTER

The extended Kalman filter (EKF) used as a TAD (EKF-TAD) tracks the amplitude, frequency, and the grid voltage angle instantaneously. The EKF is extensively used in power electronic applications to estimate parameters and variables in drive systems. In grid applications, the EKF has been used, for instance, to detect grid voltage harmonics [9,10] and to fault relaying [11]. The use of the EKF as a grid synchroniser is not a common application.

6.1 State Equation Model of the Grid Voltage

The state vector contains three elements: the amplitude, the angle and the frequency of the grid voltage vector, i.e., $\mathbf{x}(k) = [e_q(k)\ \theta(k)\ \omega_g(k)]^T$. The voltage model of the grid in αβ-coordinate system becomes

$$\mathbf{x}(k+1) = \begin{bmatrix} 1 & 0 & 0 \\ 0 & 1 & T_S \\ 0 & 0 & 1 \end{bmatrix} \mathbf{x}(k) + \mathbf{v}(k) \tag{3}$$

$$\begin{bmatrix} e_\alpha(k) \\ e_\beta(k) \end{bmatrix} = \begin{bmatrix} x_1(k)\cos\left(x_2(k)\right) \\ x_1(k)\sin\left(x_2(k)\right) \end{bmatrix} + \mathbf{w}(k) \tag{4}$$

where **v** and **w** are the process noise and sensor noise, respectively. The state equation is non-linear. The EKF [12] is used to estimate the states of the grid in the model above. To change the performance of the filter, the sample time as well as the process and sensor noise covariance matrices are altered.

6.2 Simulations of the EKF-TAD

In the following, the results of two simulations will be presented: the phase shift step response and the frequency step response. The grid voltage amplitude $e_q(t)$ has a constant value of 400 V and the grid frequency $\omega_g(t)$ is 100π rad/s. The sample time is 100 μs. The process and measure covariance matrices are set to

$$\mathbf{V} = \begin{bmatrix} 0.0400 & 0 & 0 \\ 0 & 0.0006 & 0 \\ 0 & 0 & 0.0314 \end{bmatrix} \qquad \mathbf{W} = \begin{bmatrix} 4000 & 0 \\ 0 & 4000 \end{bmatrix}$$

by using the trial and error method. The initial state vector is

$$\hat{\mathbf{x}}(0) = \left[1.1e_q \;\; 0 \;\; 1.1\omega_g\right]^T$$

6.3 Frequency Step Response

The frequency deviation and the phase-shift responses of the EKF-TAD to a grid frequency step are analysed by means of a frequency step from 50 Hz to 52.5 Hz at 0.2 s. The grid frequency step and the estimated frequency deviation are shown in Fig. 14. The estimated frequency deviation response has an overshoot of 0.2 Hz but is well damped. The phase shift of the EKF-TAD due to the frequency step is shown in Fig. 15. The phase shift decreases to –22° before it starts to increase. The phase shift settles to 0° after a small overshoot of 1°.

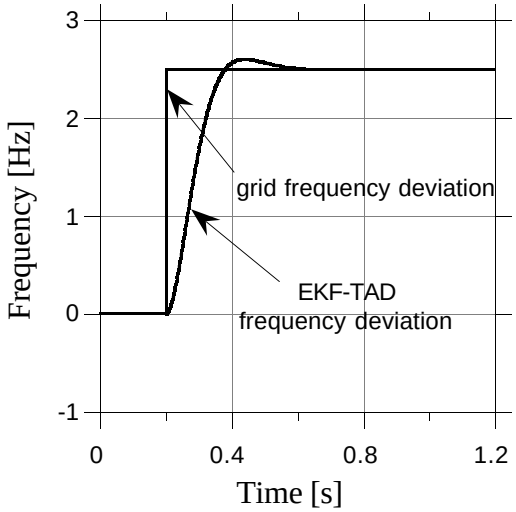

Figure 14: EKF-TAD frequency deviation response to a grid frequency deviation step. The grid frequency steps from 50.0 Hz to 52.5 Hz at 0.2 s.

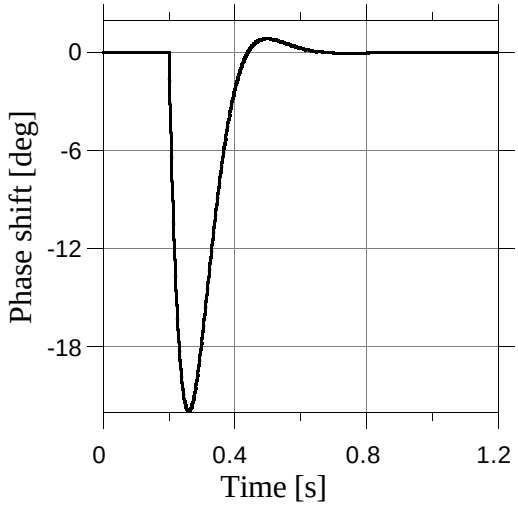

Figure 15: EKF-TAD phase shift response to a grid frequency step. The grid frequency steps from 50.0 Hz to 52.5 Hz at 0.2 s.

6.4 Phase Shift Step Response

The phase shift step response of the estimated grid frequency and of the phase shift of the EKF-TAD are analysed by means of a positive phase shift of 10° at 0.2 seconds. The EKF-TAD phase shift response to a grid phase shift step, and the step, are shown in Fig. 16. The EKF-TAD frequency deviation is shown in Fig. 17. The phase shift step response of the EKF-TAD has an overshoot of 20 % but is well damped. The frequency deviation increases to a maximum of 0.23 Hz before it decreases to 0 Hz.

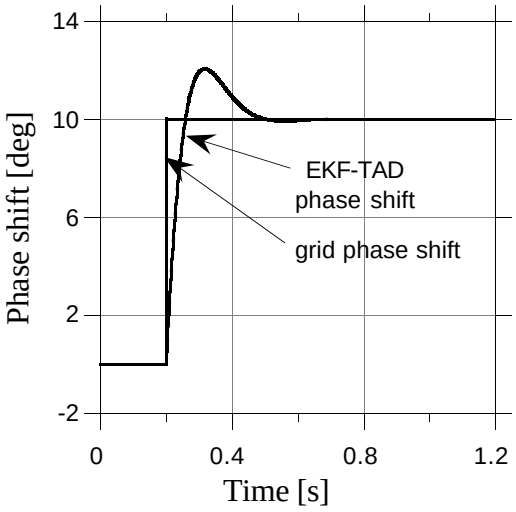

Figure 16: EKF-TAD phase shift response to a grid phase shift step. The phase shift step is 10° at 0.2 s.

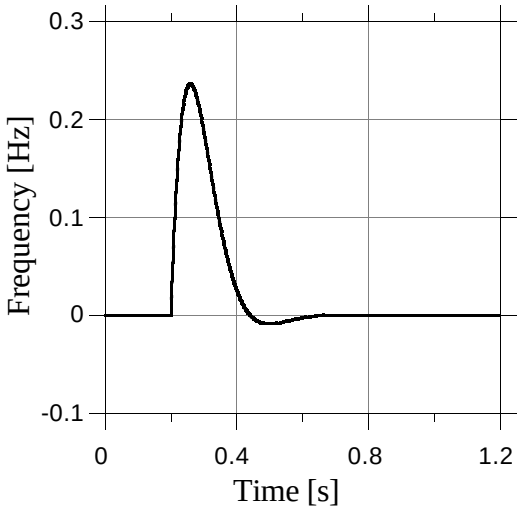

Figure 17: EKF-TAD frequency deviation response to a grid phase shift step. The phase shift step is 10° at 0.2 s.

6.5 Influence of Grid Voltage Harmonics

The influence of grid voltage harmonics on the EKF-TAD is small when the frequency regulator parameters are chosen so that the regulator responds slowly to variations. For a 10 % 5th voltage harmonic component injected into the grid voltage, the variance of the grid voltage angle fluctuation is $16.46^{\circ 2}$. The variance of the phase shift of the EKF-TAD is $0.013^{\circ 2}$, which is negligible.

6.6 Simulation Experience from the EKF-TAD

The EKF estimates the frequency, the angle and the amplitude successfully. Depending on what kind of disturbances occur in the grid, the weighting matrices must be changed so that the EKF operates adequately. The bandwidth of the estimated states decreases if the grid voltage vector is noisy. Low-frequency harmonics have frequencies near or in the active frequency band of the system, which requires larger weighting matrice elements to reduce the noise. The EKF-TAD tracks the amplitude and frequency steps with an overshoot response. One problem of using the EKF is finding the optimal weighting matrices **V** and **W**. The method used was based on trial and error; other weighting matrices **V** and **W** might have resulted in a slightly better performance of the system. Another drawback is the calculation time of the EKF algorithm. If a high sample frequency is required, problems will be encountered due to the extensive time consumption of the EKF-algorithm.

7 IMPLEMENTATION

The TAD algorithms have been implemented in an experimental system. The system consists of a control system, a VSC connected to the grid and interface circuits for measurements and control signals. The controller is implemented in a TMS320C30 DSP using 40 MHz clock frequency. The algorithms are written in C. At every sample, the main interrupt function calls the synchronisation function. In Table 2, the execution time is shown for the 4 synchronisation functions. Three of them were implemented in the

DSP. A three-phase system was created to simulate the phase jumps and frequency steps. The implemented TADs operate as expected from the foregoing analysis. The calculation time of the EKF-TAD algorithm was estimated due to extensive calculation time.

TABLE 2
EXECUTION TIME OF TAD ALGORITHMS.

TAD type	Time
LP-TAD	10.0 µs
SVF-TAD	9.6 µs
extended SVF-TAD	25 µs
EKF-TAD	75 µs

8 CONCLUSION

Four synchronisation methods with different complexities have been analysed. The synchronisation methods for a VSC connected to a weak grid are compared with using phase and frequency steps and fluctuations. Furthermore, the immunity to low-frequency voltage harmonics in the grid is addressed.

The TAD based on low-pass Butterworth filtering of grid voltage works adequately in a distorted grid; problems occur when phase shifts and frequency variations are introduced. The algorithm is highly time-efficient.

The basic SVF-TAD for a fixed and known grid frequency can deal with phase-shift steps and works adequately in distorted grids. The method has a short execution time and is well suited to the synchronisation of VSCs to distorted grids where phase jumps can occur.

The extended SVF-TAD also handles frequency variations and frequency steps. The performance of the method is almost equal to that of the basic SVF-TAD. The voltage distortion attenuation is slightly lower than that of the basic SVF-TAD, and the phase-shift step response has an overshoot of approximately 5 %. The method is suited to weak grids with phase jumps and voltage distortion. Furthermore, the method can be used in autonomous grids, where frequency variations occur. The execution time is longer in comparison to the basic SVF-TAD, but is still acceptably low.

The EKF-TAD can operate in a weak grid where the frequency and the phase shift step and fluctuate. Grid voltage distortion is well attenuated. Compared with the extended SVF-TAD, the EKF-TAD has a lower performance, even if the sample time is shorter. The EKF-algorithm results in a long execution time and, thus, is not suited to high sample frequencies.

9 REFERENCES

[1] *Voltage Characteristics of Electricity Supplied by Public Distribution Systems*, European Standard EN50160, CENELEC, 1994.

[2] R. Weidenbrug, F. P. Dawson, R. Bonert, "New Synchronization Method for Thyristor Power Converters to Weak AC-Systems," *IEEE Transactions on Industrial Electronics*, Vol. 40, No. 5, October 1993, pp. 505-511.

[3] J. Svensson, "Inclusion of Dead-Time and Parameter Variations in VSC Modelling for Predicting Responses of Grid Voltage Harmonics." *7th European Conference on Power Electronics and Applications (EPE'97)*, Trondheim, Norway, 8-10 September 1997. Proceedings, Vol. 3, pp. 216-221.

[4] G.-C. Hsieh, J. C. Hung, "Phase-Locked Loop Techniques — A Survey," *IEEE Transactions on Industrial Electronics*, Vol. 43, No. 6, October 1996, pp. 609-615.

[5] A. A. El-Amawy, A. Mirbod, "An Efficient Software-Controlled PLL for Low-Frequency Application," *IEEE Transactions on Industrial Electronics*, Vol. 35, No. 2, May 1988, pp. 341-344.

[6] O. Vainio, S. J. Ovaska, "Noise Reduction in Zero Crossing Detection by Predictive Digital Filtering," *IEEE Transactions on Industrial Electronics*, Vol. 42, No. 1, February 1995, pp. 55-62.

[7] M. H. J. Bollen, "Fast Assessment Methods for Voltage Sags in Distribution Systems," *IEEE Transactions on Industry Applications*, Vol. 32, No. 6, November/December 1996, pp. 1414-1423.

[8] G. H. Jung, G. C. Cho, S. W. Hong, G. H. Cho, "DSP Based Control of High Power Static VAR Compensator Using Novel Vector Product Phase Locked Loop." *27th Annual IEEE Power Electronics Specialists Conference (PESC'97)*, June 23-27,1996, Baveno, Italy, pp. 238-243.

[9] H. Ma, A. A. Girgis, "Identification and Tracking of Harmonic Sources in a Power System Using a Kalman Filter," *IEEE/PES Winter Meeting*, Januari 21-25, 1996, Baltimore, MD., 96WM086-9PWRD.

[10] A. A. Girgis, W. B. Chang, E. B. Makram, "A Digital Recursive Measurement Scheme for On-line Tracking of Power System Harmonics," *IEEE Transactions on Power Delivery*, Vol. 6, No. 3, July 1991, pp. 1153-1160.

[11] Y. V. V. S. Murty, W. J. Smolinski, "A Kalman Filter Based Digital Percentage Differential and Ground Fault Relay for a 3-Phase Power Transformer," *IEEE Transactions on Power Delivery*, Vol. 5, No. 3, July 1990, pp. 1299-1306.

[12] T. Söderström, *Discrete-time Stochastic Systems— Estimation & Control*, Cambridge, Prentice Hall International (UK), 1994.

PAPER 3C

J. Svensson, M. Lindgren, "Influence of Non-linearities on the Frequency Response of a Grid-Connected Vector-Controlled VSC," submitted to IEEE Transactions on Industrial Electronics.

Influence of Non-linearities on the Frequency Response of a Grid-Connected Vector-Controlled VSC

Jan Svensson Michael Lindgren

Abstract- In this paper, the small-signal performance of different vector controllers for grid connected voltage source converters is investigated. In the VSC literature, losses in the grid filter as well as nonlinearities due to blanking time and non-ideal valves are usually not modelled in the evaluation of the performance of control principles. A method is implemented for compensating for nonlinearities due to blanking-time and non-ideal valves. Furthermore, the influence of the compensation principle on the performance of traditional dead-beat controllers is shown in measured frequency responses. Valve compensation reduces the cross-coupling gain. In addition, the direct-coupling gain is improved. To show the influence of non-linearities, measured frequency responses are compared with responses from analytical models. At high frequencies, the frequency-dependent losses in the line filter must be taken into account to predict the dynamic performance correctly.

I. INTRODUCTION

The discrete-time vector current controller with a sub-oscillating PWM uses a constant switching frequency and harmonics appear at distinct frequencies [1]. This type of controller is sensitive to parameter variations and the non-linearities of semiconductor valves. In steady state and for slowly varying reference values, an integration term in the controller allows some parameter variations and errors due to non-ideal valves. By using feed-forward compensation for parameter variations and errors due to valve non-linearities, the system is able to track the reference values with a higher accuracy. This has been investigated for adjustable-speed drives [2]. Furthermore, cross-coupling and non-linear gain may occur due to the uniform sampling and non-ideal PWM [3]. In vector current control systems, the cross-coupling should be low. If the current reference value changes dynamically, a tracking error will occur. In converters connected to the AC grid, it is important to take the total system non-linearities into consideration. In addition to the static characteristics, the dynamics of the system and its control should be studied.

In this paper, the performance of a discrete-time current controller using a sub-oscillating PWM for a grid-connected VSC is investigated. Small-signal frequency responses from grid current references to grid currents are determined at an operating point. The system is modelled on an analytical discrete state-space equation and on the use of the average switch model (ASM) technique [4]. The uniform sampling phenomenon is avoided by choosing a sufficiently high sampling frequency. The controller model takes into account the delay-time of one sample due to computational calculation time. A compensation function has been introduced to reduce the influence of the valves both in steady state and dynamically. Comparisons of two analytically obtained frequency responses and measured frequency responses are presented. In the first analytical model, the grid filter has constant parameters. In the latter model, frequency-dependent losses of the filter,

obtained from measurements, are taken into account. Experimental results are presented for P and PI controllers with and without compensation.

II. SYSTEM CONFIGURATION

The system configuration is shown in Figure 1. The diagram contains a VSC, a grid filter and a controller. The controller tracks reference active current $i_q^*(t)$ and reference reactive current $i_d^*(t)$. Grid currents and grid voltages are sampled and transformed into the two-axis αβ-coordinate system and then into the rotating *dq*-coordinate system. The *d*-axis of the *dq*-frame is synchronized with the grid flux vector. The reference voltage vector from the controller is transformed into the three-phase system. To take full advantage of the dc-link voltage $u_{dc}(t)$, triplen harmonics are added to the reference voltage values in the block OPT. The last step in controlling the VSC is to transform the reference voltages into a pulse width pattern in the block PWM. The resistance and the inductance of the grid filter are denoted by R_s and L_s, respectively. The phase voltages and currents of the grid are denoted by $e_1(t)$, $e_2(t)$ and $e_3(t)$ and $i_1(t)$, $i_2(t)$ and $i_3(t)$, respectively. The phase voltages of the VSC are denoted by $u_1(t)$, $u_2(t)$ and $u_3(t)$.

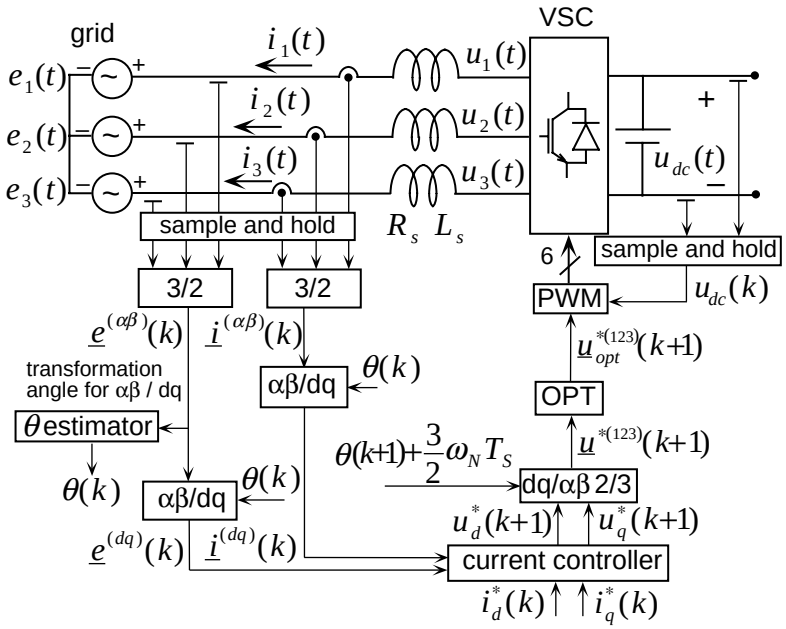

Figure 1: Overview of the system which contains the VSC, the grid filter and the controller.

The experimental system consists of a VSC with IGBT valves (Toshiba MG400Q1US41 1200V, 400A) and a TMS320C30 control computer. The characteristic parameters of the system are displayed in Table 1. The sample frequency is equal to the switching frequency f_{sw}.

TABLE I

CHARACTERISTIC PARAMETERS OF THE SYSTEM.

L_S =0.071 pu	E=1.0 pu	ω_{grid}=100π rad/s	f_{sw}=6000 Hz
R_S=0.012 pu	u_{dc}=1.5 pu	T_S=166.7 μs	

The grid filter consists of three inductors, one for each phase. The 50 Hz values of the series resistance and inductance of the coil are used in the current controller. The iron core of the inductors is made of 0.5 mm non-oriented laminations, and the core has an air-gap. When the frequency increases, the I^2R losses increase due to the skin effect, but the iron losses dominate due to increased eddy-current and hysteresis losses. If the inductor is modelled on a resistance and an inductance in series, these parameters vary, according to measurements, as shown in Figure 2. When the frequency increases from 50 Hz to 1 kHz, the resistance increases to 41 times the 50 Hz value, and the inductance decreases to 78 % of the 50 Hz value.

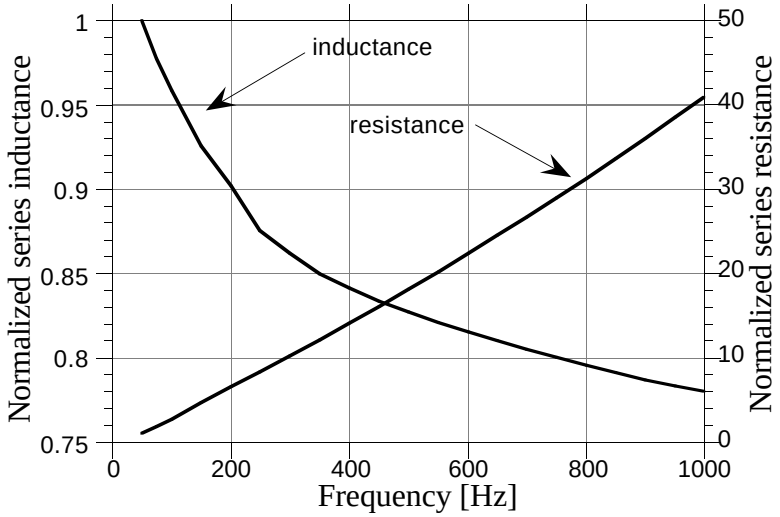

Figure 2: Measured grid filter inductance and resistance as a function of frequency. The values are normalized to 50 Hz values.

III. VSC AND GRID MODELS

The VSC and the grid are modelled as three-phase voltage sources, and the grid filter is placed between these sources. The continuous-time state equation for the grid filter in the *dq*-coordinate system is

$$\frac{d}{dt}\begin{bmatrix} i_d(t) \\ i_q(t) \end{bmatrix} = \mathbf{A}\begin{bmatrix} i_d(t) \\ i_q(t) \end{bmatrix} + \mathbf{B_u}\begin{bmatrix} u_d(t) \\ u_q(t) \end{bmatrix} + \mathbf{B_e}\begin{bmatrix} e_d(t) \\ e_q(t) \end{bmatrix} \tag{1}$$

where the matrices are given by

$$\mathbf{A} = \begin{bmatrix} -\frac{R_s}{L_s} & \omega_g \\ -\omega_g & -\frac{R_s}{L_s} \end{bmatrix} \qquad \mathbf{B_u} = \begin{bmatrix} \frac{1}{L_s} & 0 \\ 0 & \frac{1}{L_s} \end{bmatrix} \qquad \mathbf{B_e} = \begin{bmatrix} -\frac{1}{L_s} & 0 \\ 0 & -\frac{1}{L_s} \end{bmatrix}$$

The vector current controller operates in discrete time. To model the closed-loop system, the grid model is transformed into a zero-order held sampled system with the sample time T_s. The state equation is

$$\begin{bmatrix} i_d(k+1) \\ i_q(k+1) \end{bmatrix} = \mathbf{F}\begin{bmatrix} i_d(k) \\ i_q(k) \end{bmatrix} + \mathbf{G_u}\begin{bmatrix} u_d(k) \\ u_q(k) \end{bmatrix} + \mathbf{G_e}\begin{bmatrix} e_d(k) \\ e_q(k) \end{bmatrix} \tag{2}$$

where the matrices are

$$\mathbf{F} = e^{\mathbf{A}T_S}$$
$$\mathbf{G_u} = -\mathbf{G_e} = \int_0^{T_S} e^{\mathbf{A}\tau} d\tau \mathbf{B_u} \tag{3}$$

The VSC is modelled on the ASM method and is assumed to provide the requested voltage vector in the *dq*-frame. Ideal valves that commutate according to the PWM pattern are assumed. The influence of the blanking time between switching valves and the on-state voltage drops in the valves is neglected. Errors due to variations of the grid voltage angle during the sample interval are ignored.

It is common in literature that grid filter parameters and the valve parameters are assumed to be constant. In this study, two different inductor models are used. In the first model, the inductors have a constant inductance and resistance. In the second one, the influence of the losses on the equivalent series resistance and inductance is taken into account. For all models, the voltage reference values from the controller must be unsaturated.

IV. Controller and Closed-Loop System Equations

A. The P-controller

The P-controller presented here has partially been adopted from [6]. Equation (1) can be rewritten as

$$u_d(t) = e_d(t) + R_r i_d(t) - \omega_N L_r i_q(t) + L_r \frac{d}{dt} i_d(t) \tag{4}$$

$$u_q(t) = e_q(t) + R_r i_q(t) + \omega_N L_r i_d(t) + L_r \frac{d}{dt} i_q(t) \tag{5}$$

where the inductance and the resistance of the series coil are denoted by subscript *r* to emphasize that the parameters of the controller can differ from real values. The mean voltages for the sample period *k* to *k*+1 are derived by integrating (4) and (5) from kT_S to $(k+1)T_S$ and dividing by T_S. Dead-beat control is used. During one sample period, the current variations are assumed to be linear and the grid voltage components constant. The output reference voltage is delayed in one sample due to computational calculation time. A time delay compensation term is included in the dead-beat controller to avoid current oscillations. The controller equations are

$$u_d^*(k+1) = e_d(k) + R_r i_d(k) - \frac{\omega_N L_r}{2}\left(i_q^*(k) + i_q(k)\right) + k_P\left(i_d^*(k) - i_d(k)\right) - \Delta u_d(k) \tag{6}$$

$$u_q^*(k+1) = e_q(k) + R_r i_q(k) + \frac{\omega_N L_r}{2}\left(i_d^*(k) + i_d(k)\right) + k_P\left(i_q^*(k) - i_q(k)\right) - \Delta u_q(k) \tag{7}$$

where the gain for the dead-beat control is

$$k_P = \frac{L_r}{T_s} + \frac{R_r}{2} \tag{8}$$

The compensation terms for one sample time delay [5] are

$$\Delta u_d(k) = k_p\left(i_d^*(k-1) - i_d(k-1)\right) - \Delta u_d(k-1) \tag{9}$$

$$\Delta u_q(k) = k_p\left(i_q^*(k-1) - i_q(k-1)\right) - \Delta u_q(k-1) \tag{10}$$

The closed-loop state equation with the P-controller can be written in matrix form as

$$\begin{bmatrix} i_d(k+1) \\ i_q(k+1) \\ u_d^*(k+1) \\ u_q^*(k+1) \\ \Delta u_d(k+1) \\ \Delta u_q(k+1) \end{bmatrix} = \mathbf{F_{CLP}} \begin{bmatrix} i_d(k) \\ i_q(k) \\ u_d^*(k) \\ u_q^*(k) \\ \Delta u_d(k) \\ \Delta u_q(k) \end{bmatrix} + \mathbf{G_{CLP}} \begin{bmatrix} i_d^*(k) \\ i_q^*(k) \\ e_d(k) \\ e_q(k) \end{bmatrix} \tag{11}$$

B. The PI-controller

The PI-controller is introduced to remove static errors. The errors are caused by non-linearities, noisy measurements and non-ideal components. When using dead-beat control, it takes two samples before the grid currents are equal to the reference values of the current. The equations of the PI-controller can be written as

$$u_d^*(k+1) = e_d(k) + R_r i_d(k) - \frac{\omega_N L_r}{2}\left(i_q^*(k) + i_q(k)\right) + k_P\left(i_d^*(k) - i_d(k)\right) + \Delta u_{Id}(k) - \Delta u_d(k) \tag{12}$$

$$u_q^*(k+1) = e_q(k) + R_r i_q(k) + \frac{\omega_N L_r}{2}\left(i_d^*(k) + i_d(k)\right) + k_P\left(i_q^*(k) - i_q(k)\right) + \Delta u_{Iq}(k) - \Delta u_q(k) \tag{13}$$

The compensation terms are the same as for the P-controller. The integration term of the PI-controller is a sum of the current errors for all the old samples and can be written as

$$\begin{bmatrix} \Delta u_{Id}(k+1) \\ \Delta u_{Iq}(k+1) \end{bmatrix} = \begin{bmatrix} \Delta u_{Id}(k) \\ \Delta u_{Iq}(k) \end{bmatrix} + k_I \begin{bmatrix} i_d^*(k-2) \\ i_q^*(k-2) \end{bmatrix} - k_I \begin{bmatrix} i_d(k) \\ i_q(k) \end{bmatrix} \tag{14}$$

where the integration constant is defined by $k_I = T_S k_P R_r / L_r$. The closed-loop state equation with the PI-controller becomes

$$\mathbf{x}(k+1) = \mathbf{F_{CLPI}}\mathbf{x}(k) + \mathbf{G_{CLPI}}\left[i_d^*(k)\ i_q^*(k)\ e_d(k)\ e_q(k)\right]^T \tag{15}$$

where the state vector $\mathbf{x}(k)$ has 12 states.

V. System Linearization at an Operating Point

A small-signal analysis is generally performed by analysing the linearized system around an operating point. Perturbations around the operating point are denoted by Δ. In this paper, a linear model of the system is used. However, due to non-linearities in the PWM and the non-linear grid-filter parameters, the result is assumed to be valid only at the operating point.

The operating point of the system is determined by the reference values of grid currents, grid voltages and the DC-link voltage. When using a PI-controller, grid currents become equal to their reference values in steady state. The controller output becomes

$$\begin{aligned} u_{d0}^* &= e_{d0} + R_r i_{d0} - \omega_N L_r i_{q0}^* \\ u_{q0}^* &= e_{q0} + R_r i_{q0} + \omega_N L_r i_{d0}^* \end{aligned} \tag{16}$$

where the operating point is denoted by the subscript 0. The output voltage of the converter is equal to the reference voltage of the converter. The steady-state grid current is

$$\begin{bmatrix} i_{d0} \\ i_{q0} \end{bmatrix} = (I - \mathbf{F})^{-1}\left(\mathbf{G_u} \begin{bmatrix} u_{d0} \\ u_{q0} \end{bmatrix} + \mathbf{G_e} \begin{bmatrix} e_{d0} \\ e_{q0} \end{bmatrix} \right) \tag{17}$$

VI. VALVE COMPENSATION FUNCTION

To reduce the influence of the non-idealities caused by the PWM and the valves, a valve compensation function for the valve parameters has been developed. Nonlinearities occur due to two different phenomena: blanking time and on-state voltage drop. To avoid short-circuiting the dc-link, each commutation is divided into two steps. First, the conducting valve is turned off. After the blanking time, the other valve in the phase leg is turned on. If the transistor is conducting in the valve that is turned off, the diode in the valve that is to be turned on starts to conduct as soon as the transistor is turned off. Thus, the switching time instant is not influenced by the blanking time. If the sign of the current is not changed, the next commutation will be delayed by the blanking time since a commutation from a diode to a transistor occurs. Consequently, the average phase voltage deviates from that requested by the PWM modulator. The influence of blanking time and on-state voltage drop can be reduced by adding compensation voltages Δu^* to the reference phase voltages u^*, i.e., by introducing a valve compensation function. The equations for the compensation for phase 1 are

$$\Delta u^*_{1,Tb}(k) = \text{sign}\big(i_1(k)\big) T_b / T_S \tag{18}$$

$$u^*_{1,comp}(k) = \Delta u^*_{1,Tb}(k) + D_1 u_{onT1} + \big(1 - D_1\big) u_{onD2} + u^*_1(k) \tag{19}$$

$$u^*_{1,comp}(k) = \Delta u^*_{1,Tb}(k) - \big(1 - D_1\big) u_{onT2} - D_1 u_{onD1} + u^*_1(k) \tag{20}$$

Blanking time and sampling time are denoted by T_b and T_S. The phase 1 duty ratio is $D_1 = 2u^*_1 / u_{dc}$. Transistor and diode voltage drops are denoted by u_{onT} and u_{onD}. These voltage drops have been measured and are displayed in Table 2. The voltage drops consist of a constant term u_0 and a current-dependent term $R_{on} i$. As discussed above, the compensation is only valid when the current is positive or negative under a whole sample period. When the amplitude of the phase current sample is smaller than the amplitude of the current ripple, the valve compensation is not included.

TABLE II
MEASURED PARAMETERS FOR THE VALVE COMPENSATION FUNCTION.

u_{0T}=1.08 V	u_{0D}=1.05 V	T_S=166.7 μs
R_{onT}=12 mΩ	R_{onD} =10 mΩ	T_b=1.4 μs

Equation (18) compensates only for blanking time. Equations (19) and (20) compensate also for the voltage drop across the valves in the on-state, for positive and negative phase currents, respectively. These equations do not consider the delay from the gating of the transistor to the actual switching.

VII. Analytical and Experimental Frequency Response Analysis

The frequency responses (around the operating point i_{d0}^{*}=0.22 pu and i_{q0}^{*}=–0.67 pu) were both measured and calculated by means of the analytical models. Four different controllers were used in the experimental investigation. They are denoted by the following symbols:

M(p) P-controller without valve compensation function
M(pi) PI-controller without valve compensation function
M(p,c) P-controller with valve compensation function
M(pi,c) PI-controller with valve compensation function

Theoretical frequency responses were obtained for four models, all without compensation functions:

A(p) P-controller with constant grid filter parameters
A(pi) PI-controller with constant grid filter parameters
B(p) P-controller with frequency-dependent grid filter parameters
B(pi) PI-controller with frequency-dependent grid filter parameters

In the measurements, a sinusoidal small-signal current Δi^{*} of 0.1 pu was added to one of the reference currents at the operating point. Measurements were performed at 27 different frequencies between 10 Hz and 1200 Hz. The reference currents as well as the *d*- and *q*-currents were sampled. In the analysis of the measured results, the FFT-algorithm was used to evaluate the amplitude gain and phase shift between the sinusoidal reference current Δi_{d}^{*} or Δi_{q}^{*} and the measured currents Δi_{d} and Δi_{q}.

A. Direct Coupling in q-direction

As shown in Fig. 3, the theoretical gain of the controllers A(·) from Δi_{q}^{*} to Δi_{q} is approximately 0 dB over the whole frequency span. The measured gain of the controllers M(·) is close to 0 dB at low frequencies. When the frequency increases above approximately 400 Hz, the gain of all the controllers increases. At 1 kHz, the gain is approximately 1 dB. The measured gain can be predicted by including the frequency-dependent grid filter parameters according to models B(·). The gain characteristics are very similar for all controller types. The analytical models A(·) give a slightly larger phase lag than the measured one, but the analytical models B(·) track the measured phase correctly.

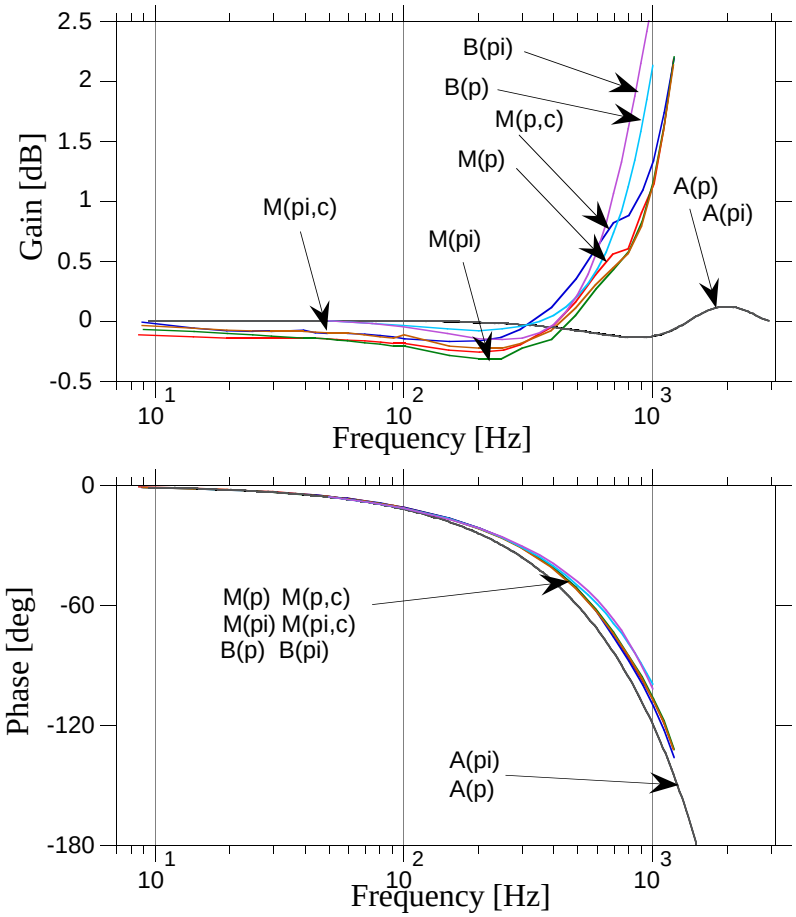

Figure 3: The Bode diagram for the reference q-*current* Δi_q^* *to the* q-*current* Δi_q.

B. Cross-coupling from q-direction to d-direction

As shown in Fig. 4, the theoretical gains of the controllers A(·) from Δi_q^* to Δi_d are low at low frequencies. The gain increases with frequency and reaches a maximum of –25 dB at 1.8 kHz. Compared with the direct-coupled transfer function (TF) from Δi_q^* to Δi_q, the gains and phase-shifts of the cross-coupling TFs have slightly different characteristics. At low frequencies from 10 to 40 Hz, the measured gain of model M(p) is higher than the gain of M(pi); –40 dB compared to –45 dB. At higher frequencies, the gains increase with frequency and converge. The gains of the compensated models M(p,c) and M(pi,c) are lower and have a minimum of –70 dB at 55 Hz. From 55 Hz and upwards, the gain increases and at 1.2 kHz, the gain is –20 dB. Valve compensation decreases the cross-coupling gain. The theoretical gains of the controllers B(·) are slightly higher than those of the controllers A(·) but lower than the measured gains. Phase displacement when using valve compensation results in a phase-shift change from 0° to 180° at 55 Hz.

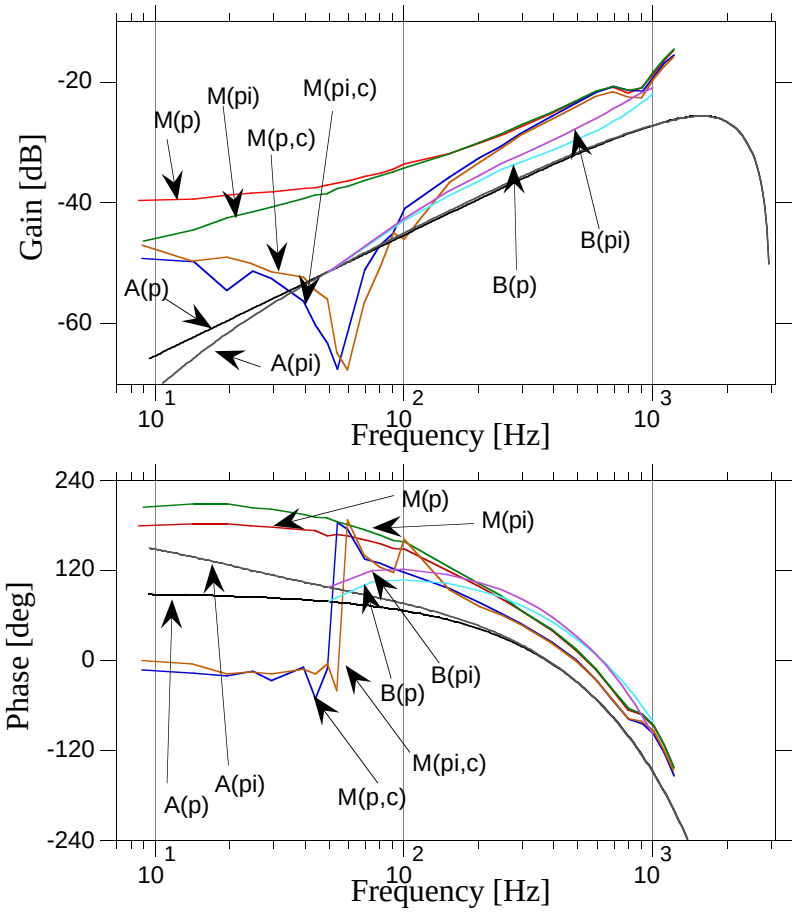

Figure 4: The Bode diagram for the reference q-*current* Δi_q^* *to the* d-*current* Δi_d.

C. Direct Coupling in d-direction

According to Fig. 5, the gain of the TF Δi_d^* to Δi_d is close to 0 dB for the theoretical system A(·). The measured gain characteristics can be divided into two groups: with and without valve compensation; the integration term does not affect the performance. Without valve compensation, the gains are constant, approximately –0.3 dB, up to 750 Hz where the gains drop down to a minimum of –0.8 dB at 900 Hz before increasing again. At 1200 Hz, the gains are 1.0 dB. With valve compensation, the gains of the transfer functions M(p,c) and M(pi,c) are approximately 0 dB for frequencies up to 750 Hz. Above 750 Hz, the gains are similar both with and without compensation. The gains of the theoretical TFs B(p) and B(pi) do not have a gain dip at 900 Hz, but the gain is 0 dB and starts to increase at a frequency of 500 Hz. The phase-shifts of the measured frequency responses follow the theoretical phase-shifts B(p), B(pi), which have a smaller phase lag than the models A(p) and A(pi).

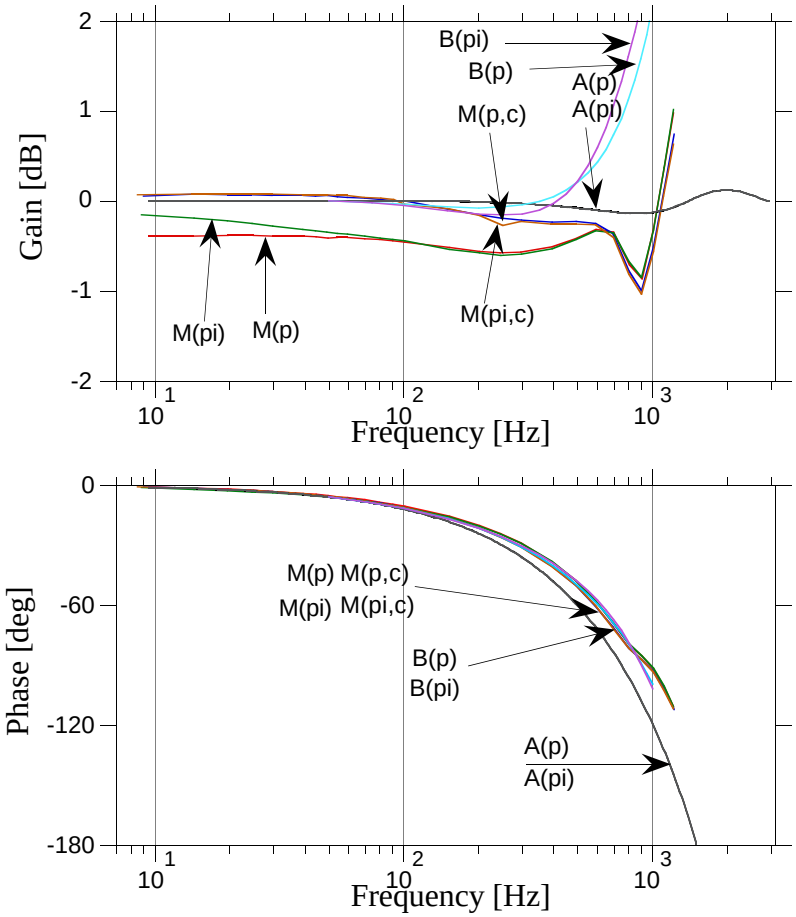

Figure 5: The Bode diagram for the reference d-*current* Δi_d^* *to the* d-*current* Δi_d.

D. Cross-coupling from d-direction to q-direction

The theoretical TFs A(p) and A(pi) from Δi_d^* to Δi_q have a low gain at low frequencies, as shown in Fig. 6. The gain increases with frequency and reaches a maximum of –26 dB at 2 kHz. The measured gains can be divided into two groups: with and without valve compensation; the integration term does not influence the gain. When using valve compensation, the gain is almost constant (–34 dB) up to 100 Hz, which can be compared with –30 dB without compensation. From approximately 150 Hz, the gain characteristics are the same both with and without valve compensation. At 1200 Hz, the gain amplitudes are –12 dB. The gains of the analytical TFs B(p) and B(pi) are higher than the gains of the TFs A(p) and A(pi) but lower than the measured gains.

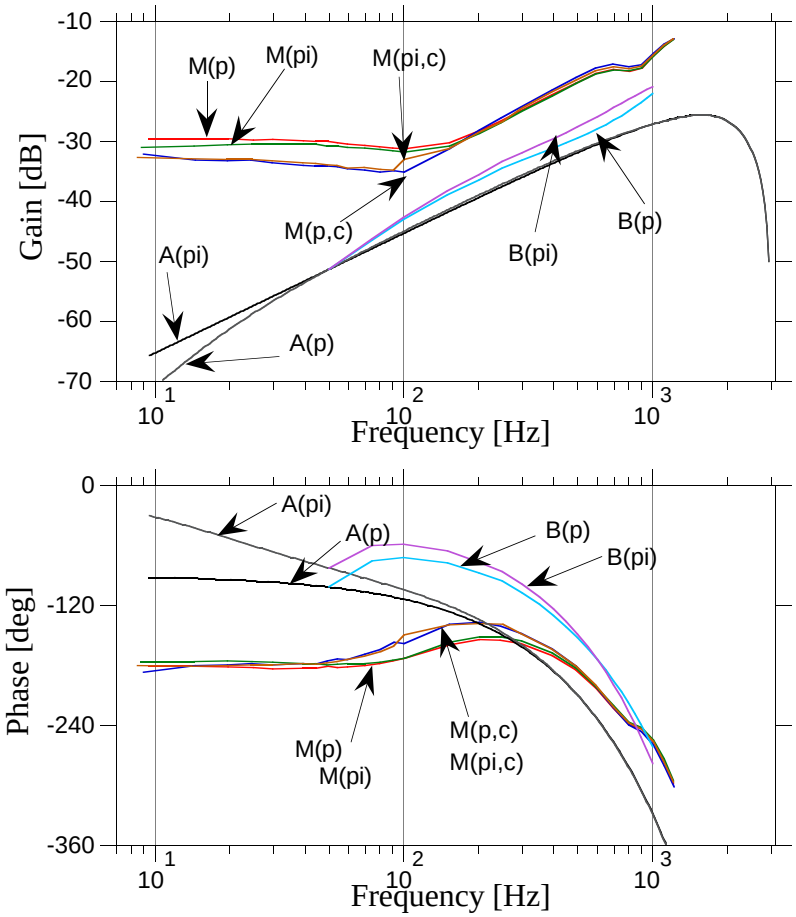

Figure 6: The Bode diagram for the reference d-*current* Δi_d^* *to the* q-*current* Δi_q.

VIII. Summary of Transfer Function Analysis

A. Low-frequency Responses

The valve compensation function can be used to obtain the correct steady-state values of the *d*- and *q*-currents. The compensation acts as a feedforward term whereas an integration term can be characterized as a feedback term. When analysing the TFs, it is clear that valve compensation does not influence the gain at low frequencies for direct coupling in the *q*-direction. But for direct coupling in the *d*-direction, valve compensation improves gain characteristics. Valve compensation reduces the gain by approximately 10 dB in the cross-coupled TF from the reference *q*-current to the *d*-current. Valve compensation has a much smaller influence on the cross-coupled TF from the reference *d*-current to the *q*-current.

B. High-frequency Responses

At high frequencies, from approximately 500 Hz and upwards, the influence of coil parameter variations with frequency dominates over the influence of the valves. It is, thus, difficult to evaluate the performance of the valve compensation function. For the directly-coupled TFs, the gain increases with frequency. For the cross-coupled TFs, a deviation occurs between theoretical and measured gains. However, the actual measured cross-coupled currents are small and reach the noise level of the system.

IX. CONCLUSION

In this paper, the current frequency response of a grid-connected VSC using a vector current controller is investigated to determine the performance of different current controllers. The measured transfer functions show that the steady-state performance is improved by adding a valve compensation function to the controller. The valve compensation should be used because the cross-coupling gain is reduced at low frequencies and the direct-coupling gain is closer to one. The integration part of the controller has a minor influence on the dynamic performance. The compensation function reduces the coupling especially from the *q*-direction to the *d*-direction. At high frequencies, i.e., from 500 Hz and upwards, frequency response is affected by frequency dependent losses in the grid filter of the set-up investigated: gain and cross-coupling increase in all measured transfer functions. This can partly be predicted by using a frequency-dependent model of the grid filter.

X. REFERENCES

[1] J. Holtz, "Pulsewidth Modulation for Electronic Power Conversion," *Proc. of IEEE*, Vol. 82, No. 8, pp. 1194-1214, August 1994.

[2] J. K. Pedersen, F. Blaabjerg, J. W. Jensen, P. Thogersen, "An Ideal PWM-VSI Inverter with Feedforward and Feedback Compensation," *5th European Conference on Power Electronics and Applications (EPE'93)*, Brighton, England, 13-16 September 1993, pp. 501-507.

[3] S. Hiti, D. Boroyevich, "Small-Signal Modeling of Three-Phase PWM Modulators," *Power Electronics Specialists Conference (PESC'96)*, Baveno Italy, 23-27 June, 1996, pp. 550-555.

[4] R. Kagalwala, S. S. Venkata, P. O. Lauritzen, "A Transient Behavioral Model (TBM) for Power Converters," *5th Workshop on Computers in Power Electronics*, IEEE Power Electronics Society, Portland USA, 11-14 August, 1996.

[5] M. Lindgren, "Feed forward – Time Efficient Control of a Voltage Source Converter Connected to the Grid by Lowpass Filters." *Power Electronics Specialists Conference (PESC'95)*, Atlanta, USA, 18-22 June 1995, Vol. 2, pp. 1028-1032.

[6] J. Svensson, "Inclusion of Dead-Time and Parameter Variations in VSC Modelling for Predicting Responses of Grid Voltage Harmonics." *7th European Conference on Power Electronics and Applications (EPE'97)*, Trondheim, Norway, 8-10 September 1997, Proceedings, Vol. 3, pp. 216-221.

PAPER 4

M. Lindgren, J. Svensson, "Connecting Fast Switching Voltage-source Converters to the Grid — Harmonic Distortion and its Reduction," *IEEE/Stockholm Power Tech Conference*, Stockholm, Sweden, June 18-22 1995. Proceedings, Vol. "Power Electronics", pp. 191-196.

Connecting Fast Switching Voltage-source Converters to the Grid — Harmonic Distortion and its Reduction

Michael Lindgren M. Sc. Jan Svensson M. Sc.

Department of Electrical Machines and Power Electronics
Chalmers University of Technology
S-412 96 Gothenburg, Sweden

Abstract: In this paper, harmonic distortion of fast switching pulse width modulated (PWM) converters connected to the grid is addressed. The origin of harmonic distortion and methods to reduce it are presented. Due to high voltage derivatives, Electro Magnetic Interference (EMI) and insulation stress on the transformer connected to the converter occur. To reduce the distortion, a third order LCL-filter is proposed. It is compared with a first order L-filter. A major advantage of the LCL-filter compared with the L-filter is that the switching frequency of the converter can be significantly decreased. This facilitates reduction of the switching speed of the semiconductor valves, such a step reduces voltage derivatives. In addition, if the plant is to be used for Static Var Compensation (SVC), the system cost can be decreased.

I. INTRODUCTION

In converter systems based on fast switching semiconductors, PWM is adopted. In this case, the order of the harmonics injected to the grid can be affected by a proper choice of switching frequency. However, harmonics are still present.

To obtain a sinusoidal current, filters are used. If the converter is connected to the grid by a transformer, the leakage inductance provides filtering. However, to obtain a low current harmonic distortion, the switching frequency has to be set very high, (above 10 kHz). To facilitate this switching frequency, the power semiconductors have to be rapidly switched. This is a drawback since fast switching gives rise to high voltage derivatives in the converter output voltage. High voltage derivatives give rise to electro magnetic interference, (EMI). In addition, if the converter is connected to the transformer by a long cable, the insulation stress is further increased due to reflections [1].

An alternative solution to reduce both voltage- and current harmonic distortion is to use a low-pass LCL-filter [2]. A major advantage of the LCL-filter compared with the L-filter is that a low current harmonic distortion can be obtained at low switching frequencies. This increases the efficiency of the converter and reduces the high frequency distortion caused by the switching of the semiconductors. It is also an advantage in high power applications where it is hard to reach switching frequencies above a few kHz.

II. ORIGIN OF HARMONICS

In power converters, the semiconductors are used as controlled switches. The component current and voltage are high simultaneously during switching only. This is the principle of PWM. A commonly proposed principle to connect a voltage source converter (VSC) to the utility grid is illustrated in Fig. 1. The resistive parts have been neglected. *L* is the

filter inductance and L' the equivalent inductance of the grid. The voltages u_{1a}, u_{1b} and u_{1c} are the phase voltages of the converter. The voltages u_{2a}, u_{2b} and u_{2c} are the phase voltages in the so called point of common connection, (PCC). The result of the PWM is displayed in Fig. 2. The fundamental converter phase voltage, u_{1a}, is equal to the phase voltage of the grid, u_{2a}. Consequently, the fundamental current is zero. As displayed, a harmonic current occurs due to the PWM. The switching frequency is 1 kHz and the grid frequency is 50 Hz.

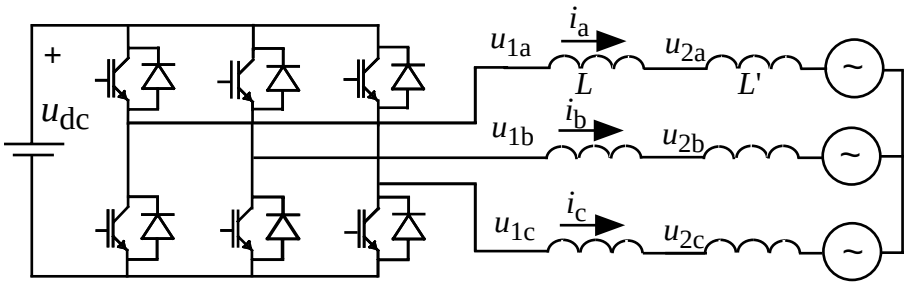

Figure 1: VSC connected to the grid by L-filter.

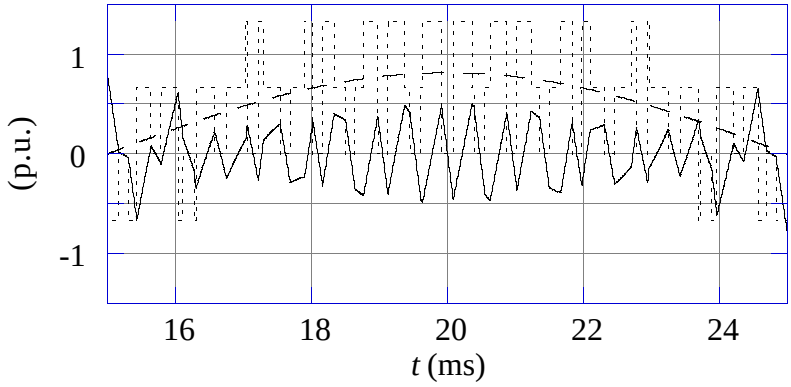

Figure 2: Converter phase voltage (dotted), grid phase voltage (dashed) and resulting phase current (solid).

A. Low and Medium Frequency Harmonics

The harmonic content of the converter output voltage can cause current and voltage harmonic distortion. If an L-filter is used, the voltage harmonic distortion in the point of common connection is determined by

$$\frac{u_2(\mathrm{n})}{u_1(\mathrm{n})} = \frac{L'}{L'+L} \tag{1}$$

This relation is valid below approximately 15 kHz. As well known, the equivalent inductance depends on the short circuit power of the grid. The equivalent reactance of the grid at the low voltage side of the transformer is

$$x_{L_2'} = \left(\frac{u_{\mathrm{lo}}{}^2}{S_{\mathrm{KN}}}\right) \tag{2}$$

where u_{lo} is the nominal low voltage of the transformer and S_{KN} is the short circuit power of the grid. The base impedance

$$z_{\text{base}} = \left(\frac{{u_{\text{lo}}}^2}{S_{\text{NT}}}\right) \tag{3}$$

where S_{NT} is the rated power of the transformer is used. Thus, the equivalent reactance in p.u. is

$$x_{\text{L}_{2'}} = \left(\frac{S_{\text{NT}}}{S_{\text{KN}}}\right) \tag{4}$$

Usually the short circuit power is above 50 MVA. In a converter system installation based on fast switching semiconductors, the power is limited to about 1 MVA. This would give an equivalent grid reactance of 0.02 p.u. Assumed the converter voltage harmonic distortion in Fig. 3, the maximum voltage harmonic distortion is 5.7 %.

In Fig. 3, the ideal harmonic phase voltage spectra of a commonly proposed PWM method, 3rd harmonic injection PWM, is presented. The dc-voltage is 1.5*U*, where *U* is the grid line to line voltage. *U* is defined as 1 p.u. The modulation index, *M* is one. *M* is defined by

$$M = \frac{u(1)}{u(1)_{\text{max}}} \tag{5}$$

where $u(1)_{\text{max}}$ is the maximum fundamental converter phase voltage. As presented in [3], the voltage harmonics of the lowest frequency occur at frequencies

$$f_{1,2} = (p \pm 2\text{n}_1) \tag{6}$$

where *p* is the frequency ratio defined as

$$p = \frac{f_{\text{mod}}}{f_1} \tag{7}$$

and $\text{n}_1 = 1,2,3$. Further on, the modulation frequency and fundamental frequency are denoted f_{mod} and f_1. As displayed in Fig. 3, there are also voltage harmonics at frequencies close to multiples of *p*. The corresponding current harmonic spectra is presented in Fig. 4. The current harmonic distortion is determined by

$$\frac{i_{\text{n}}}{u_{1\text{n}}} = \frac{1}{\text{n}\omega_1(L' + L)} \tag{8}$$

where $\omega_1 = 2\pi f_1$ rad/s. The inductive reactance of the filter, x_{L}, is 0.05 p.u. The grid inductance, *L'*, is assumed to be zero (very high ratio of the grid short circuit power and the rated power of the transformer). As displayed, the high order converter phase voltage harmonics are efficiently attenuated.

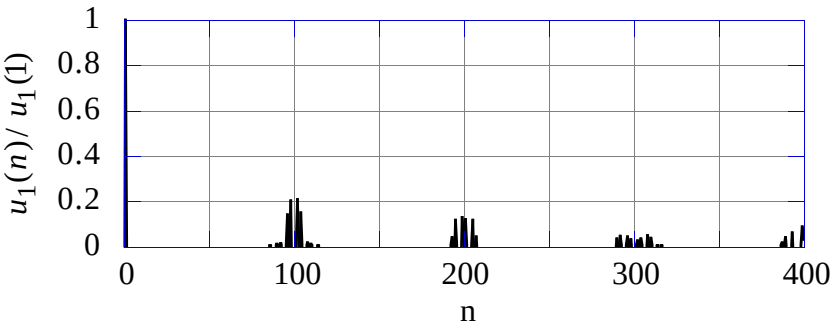

Figure 3: Ideal harmonic phase voltage spectra of 3rd harmonic injection PWM, p= 100 and u_{dc}= 1.5 p.u.

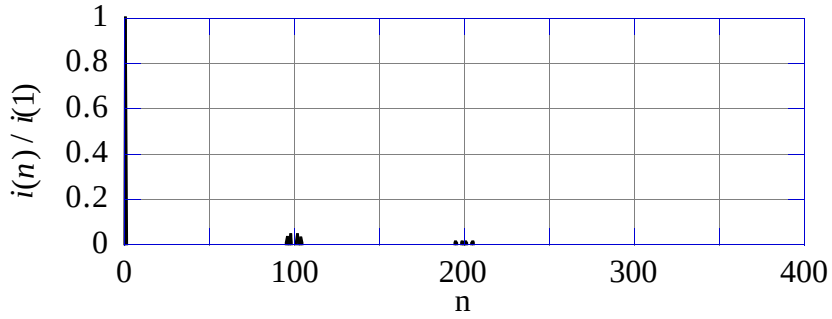

Figure 4: Ideal harmonic current spectra of 3rd harmonic injection PWM. L-filter, x_L= 0.05 p.u., p= 100 and u_{dc}= 1.5 p.u.

Ideally no low order harmonics should occur. In a real system, low order harmonics may occur due to dc-voltage fluctuations and non ideal switching. In Fig. 5, the voltage spectra of an IGBT converter is presented. An analogue Quasine modulator is used and the switching frequency is 4.9 kHz. The properties of Quasine modulation are described in [3]. As displayed, no low order harmonics occur. This is obtained if the commutation time is small in comparison to the period time of the PWM. This usually applies to IGBT converters.

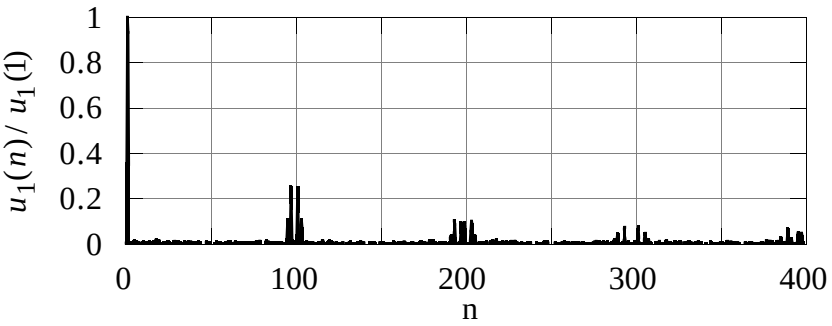

Figure 5: Measured harmonic phase voltage spectra of an IGBT converter, M= 1.

The amplitude of the voltage harmonics in the converter output depends on the ratio of the dc-voltage and the fundamental output voltage. It is thus important to use a PWM-method that can deliver as high output voltage as possible. The method 3rd harmonic injection

PWM provides a maximum fundamental line to line voltage of $u_{dc} / \sqrt{2}$ V. Thus, at steady state a dc-voltage of $\sqrt{2}\ U$ is sufficient. However, to obtain high band width the dc-voltage has to be set higher. As presented in [4], the requested dc-voltage depends on the inductance of the grid-filter. The dc-voltage is usually not set above 2*U*.

The dc-voltage influence on current harmonic distortion is displayed in Fig. 6. The current is presented in the rotating *dq*-frame and an L-filter is used. In this frame, a fundamental current is represented as a dot. Consequently, each deviation from the point (0,1) corresponds to a harmonic current. As illustrated, the quadrature ripple is strongly dependent on the dc-voltage. Since quadrature ripple gives rise to active power ripple, the dc-voltage should be set as low as possible. This is also an advantage since the voltage derivative is reduced.

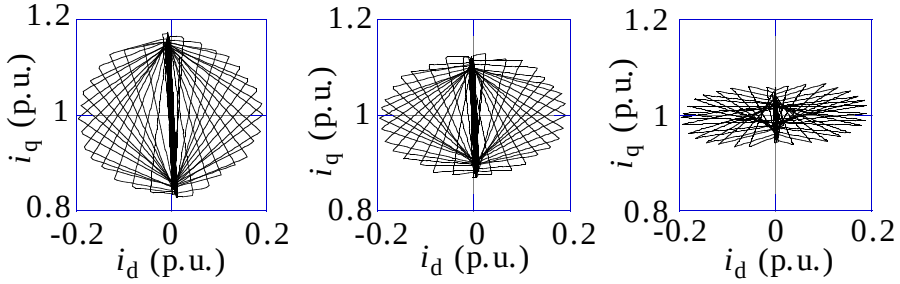

Figure 6: Current vectors at different dc-voltages. i_d is the direct and i_q the quadrature current. u_{dc}= 2.5 p.u. (left), u_{dc}= 2 p.u. (middle) and u_{dc}= 1.5 p.u. (right). L-filter with p= 100 and x_L= 0.05 p.u.

B. Harmonic Distortion above 100 kHz

Harmonic distortion at frequencies above 100 kHz occur due to high voltage derivatives in the converter output voltage. The voltage derivatives give rise to insulation stress and electro magnetic interference (EMI). EMI occur due to each switching and is proportional to the switching frequency. In commercial converters, voltage derivatives are usually limited to reduce these phenomena. Reduction is obtained by slower switching of the semiconductors. Unfortunately, this increases the switching losses. An alternative method often addressed in papers [5] is to perform zero voltage switching (ZVS). Such a step also facilitates increased switching frequency since the switching losses are considerably reduced. Disadvantages are that the dc-link of the converter becomes complex and expensive and the control more advanced.

If long cables are used, reflections may occur at the load connected to the converter. Such reflections are avoided if the voltage pulse rise time is much longer than the wave travelling time on the cable between the converter and the load. In Fig. 7, the equivalent circuit of the converter, cable and the load is displayed.

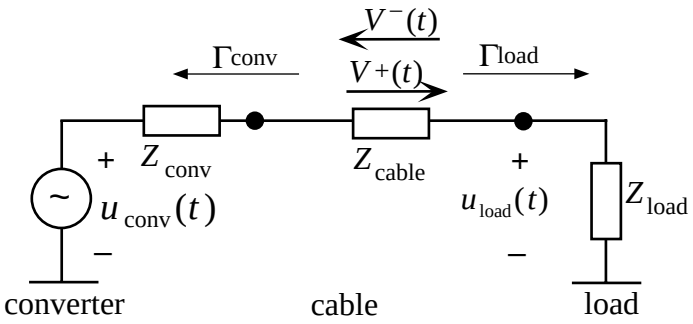

Figure 7: Equivalent circuit of converter, cable and load.

The load reflection coefficient is

$$\Gamma_{load} = \frac{Z_{load} - Z_{cable}}{Z_{load} + Z_{cable}} = \frac{V^-}{V^+} \tag{9}$$

Z_{load} and Z_{conv} denotes the wave impedance of the load and the converter. Z_{cable} is the characteristic impedance of the cable. If the cable is open the Z_{load} is infinite yielding Γ_{load} is 1. The impedance Z_{conv} is almost zero, thus Γ_{conv} is –1. The reflection coefficient is approximately the same for an inductor, induction motor or a transformer. The voltage at a specific point at the cable, for example at the load, can be divided into two travelling voltage waves, V^+ and V^- according to

$$u_{load} = V^+(t) + V^-(t) \tag{10}$$

At each switching of a semiconductor, a voltage travelling wave V^+ occurs. The amplitude of the wave is u_{dc}. Due to the reflection at the load, the load voltage is amplified. The reflected wave changes sign at the converter, thus, after twice the wave travelling time between the load and the converter, τ, the load voltage will start to decrease. The maximum load voltage, $2u_{dc}$ is obtained if the wave travelling time is equal to twice the rise time of the converter voltage. The travelling voltage wave is damped out due to cable losses.

To verify that the combination long cables and fast switching semiconductors give rise to voltage stress on the load connected to the converter, measurements have been carried out. In Fig. 8 a positive line to line voltage pulse at the terminal of the converter is shown. As displayed in Fig. 8, the voltage pulse rise time is approximately 0.35 μs. In Fig. 9, Fig. 10 and Fig. 11, the voltage pulses using open cable and installed motor are displayed at cable length 5, 20 and 32 meters. The wave travelling times are 0.03 μs (5 meter), 0.13 μs (20 meter), 0.20 μs (32 meter).

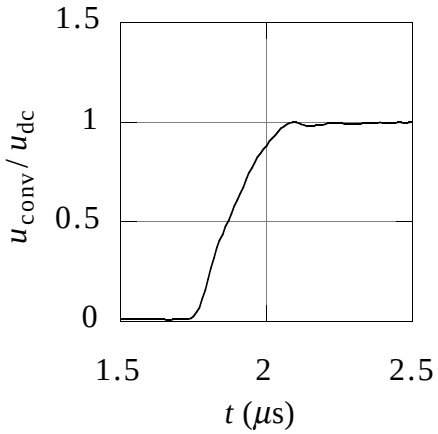

Figure 8: Line to line voltage pulse directly at converter terminals.

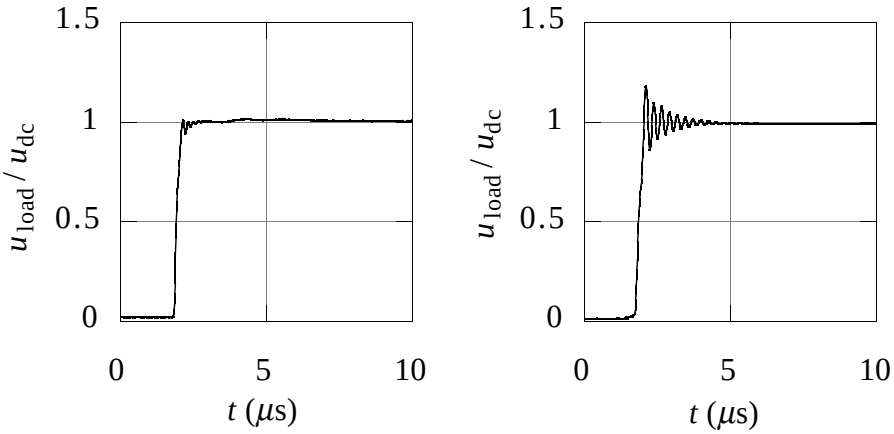

Figure 9: Line to line voltage pulse using a 5 meter cable. Open cable (left) and at machine terminals (right).

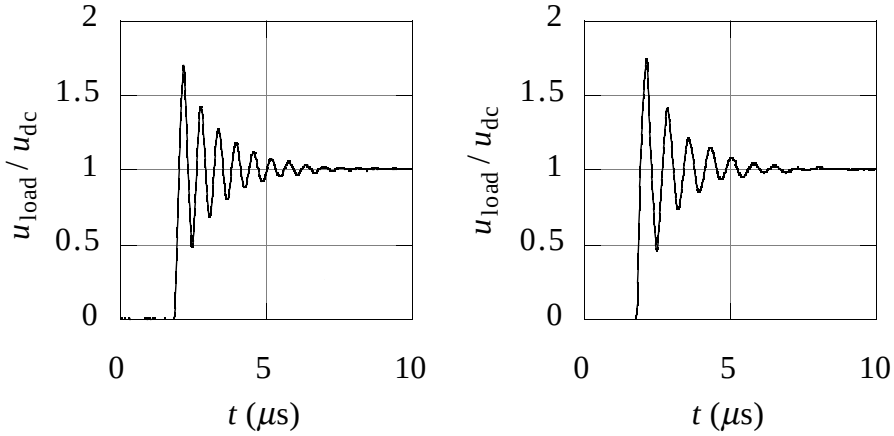

Figure 10: Line to line voltage pulse using a 20 meter cable. Open cable (left) and at machine terminals (right).

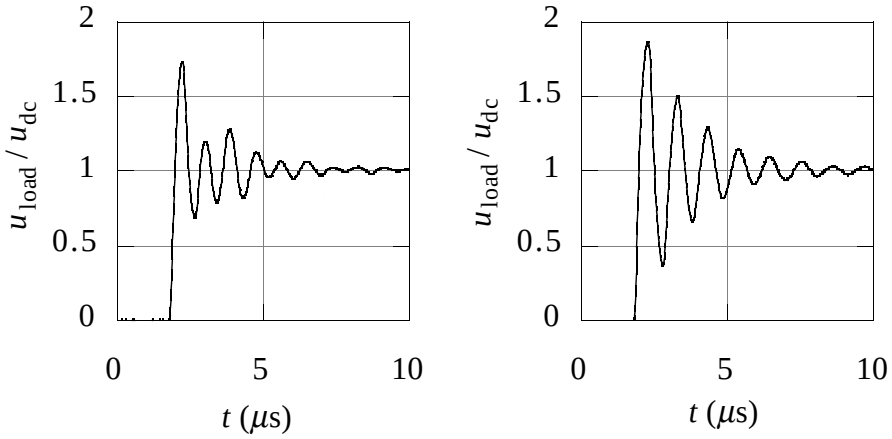

Figure 11: Line to line voltage pulse using a 32 meter cable. Open cable (left) and at machine terminals (right).

In the open cable case, the period time of the resonance frequency corresponds to the wave travelling time. As displayed, the resonance frequency of the load voltage is decreased when the motor is connected compared with an open cable. With motor installed, the reflection occur in the stator winding. This results in increased wave travelling time, thus a lower resonance frequency compared with open cable. The wave velocity is 160 m/µs. The critical cable length is 28 meters, at this length, the peak overvoltage occurs.

III. FILTERING HARMONICS

Filters are used to reduce the harmonic content of the current injected to the grid. In this section, the L- and the LCL-filter are compared from a filtering point of view. Since the grid always provides inductance, a regular LC-filter becomes an LCL-filter. The configurations are displayed in Fig. 12. As illustrated in Fig. 13, in the LCL-filter case at the resonance frequency, a peak occurs in the transfer function. To assure that the converter does not supply harmonics at the resonance frequency, the PWM has to be accurate.

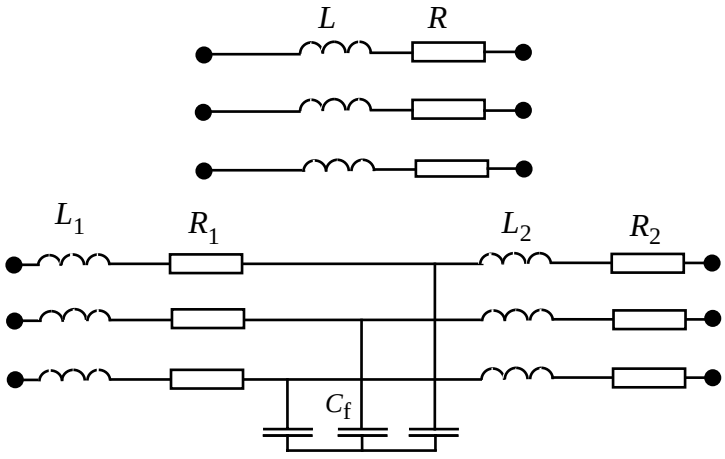

Figure 12: L- and LCL-filter scheme.

In the filters, separate inductors or the transformer leakage inductance can be used. Advantages of including a transformer is that it facilitates supplying non symmetrical loads demanding a zero order current and that it supplies galvanic insulation. If a transformer is included, the inductive reactance is fixed in the range of 4-6 %, here it is assumed to be 5%.

The attenuation of the LCL-filter is determined by the resonance frequency

$$f_{\text{res}} = \frac{1}{2\pi}\sqrt{\frac{L_1 + L_2}{L_1 L_2 C_{\text{f}}}} \tag{11}$$

In Fig. 13, the L- and the LCL-filter attenuation of harmonic distortion is illustrated. The objective is to obtain an attenuation of 20 dB. The total inductive reactance of the L- and LCL-filter are assumed to be 0.075 p.u. The equivalent inductance of the grid is assumed to be a part of the inductance L and L_2 respectively. The capacitive reactance is 10 p.u., thus 0.1 p.u. reactive current is produced by the filter capacitors. If the plant is to be used for SVC, this total cost is decreased compared with switched reactive power. The capacitors should be set to fulfill the average demand for reactive power.

The cross over frequency of the filter is 1258 Hz. As displayed, an attenuation of 20 dB is obtained at frequencies of 7 kHz for the L-filter and 2.4 kHz for the LCL-filter. Consequently, the requested switching frequency is 7 kHz with the L-filter and 2.4 kHz with the LCL-filter. Using these parameters gives the grid current vectors displayed in Fig. 14. In applications where dynamic performance is requested, the voltage has to be set above 1.5 p.u. Here it is assumed to be 2 p.u.

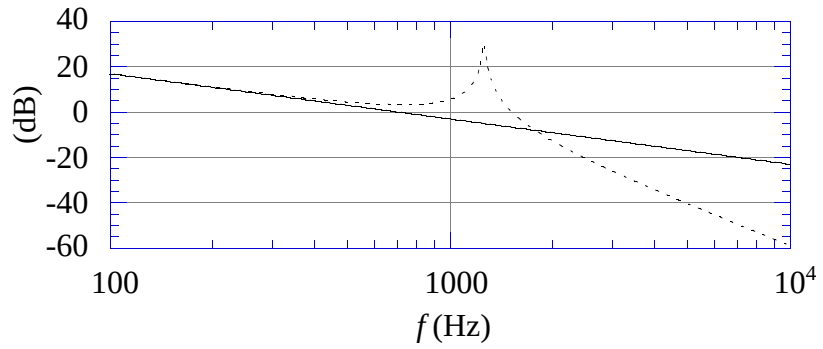

Figure 13: Transfer function from converter phase voltage to line current. L-filter (solid) and LCL-filter (dotted).

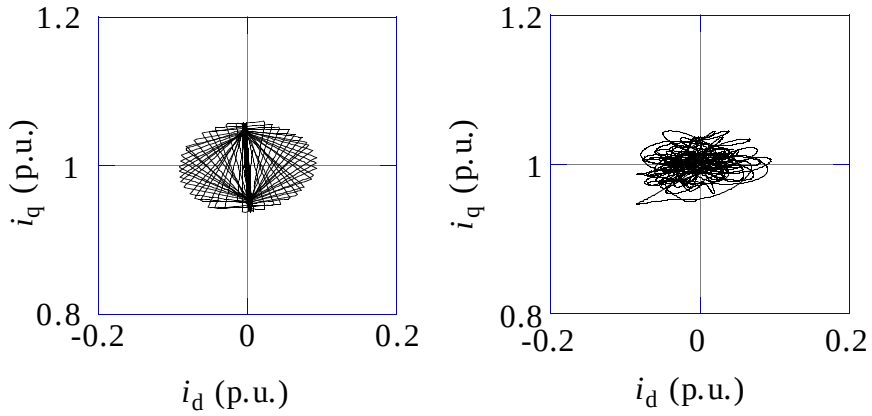

Figure 14: Current vectors. L-filter p= 140 (left) and LCL-filter with p= 48 (right).

IV. CONCLUSIONS

Harmonic distortion of fast switching converters is presented. The voltage harmonic distortion in the point of common connection is usually very low. This applies if the converter rated power is low compared with the short circuit power of the grid. If a standard transformer is used for filtering, to obtain sufficiently low current harmonic distortion, the switching frequency has to be set high. This is a drawback since very fast switching is the origin of high voltage derivatives. The voltage derivatives give rise to high frequency harmonic distortion and insulation stress on the load connected to the converter. Reflections measured at the terminal of an induction motor are presented.

To obtain low current- and voltage harmonic distortion at low switching frequencies, a third order low pass filter is proposed. The required switching frequency decreases from 7 kHz with the regular transformer, to 2.4 kHz with the low-pass filter. In addition, if the reactive power produced by the filter capacitors is requested, the cost of the plant can be decreased. This is due to the fact that the converter rated power can be decreased and its efficiency increased due to reduced switching losses. When the switching frequency is decreased, slower switching of the semiconductor valves can be performed. This is a major advantage since the EMI due to voltage derivatives and switching frequency is reduced.

V. REFERENCES

[1] T. F. Lowery and D. W. Petro, “Application Considerations for PWM Inverter-Fed Low-Voltage Induction Motors,” IEEE Trans. on Industry Application, vol. 30, pp. 286-293, 1994.

[2] J. Ollila, “A PWM rectifier without current measurement,” EPE Journal, vol. 44, pp. 14-19, 1994.

[3] K. Thorborg, Power Electronics -in Theory and Practice. Lund: Stundentlitteratur, 1993.

[4] M. B. Lindgren, “Feed forward- time efficient control of a Voltage source Converter connected to the grid by lowpass filters,” presented at PESC, Atlanta, 1995.

[5] K. Yurugi, H. Yonemori, and M. Nakaogi, “Next generation zero-voltage soft switched PWM three phase Ac-Dc active power converter,” presented at TELESCON, Berlin, 1994.